AD-A078 733 ROYAL AIRCRAFT ESTABLISHMENT FARNBOROUGH (ENGLAND) F/G 9/1
INFLUENCE OF THE ENVIRONMENTAL CONDITIONS ON A QUARTZ RESONATOR--ETC(U)
MAY 78 M VALDOIS
UNCLASSIFIED RAE-LIBRARY TRANS-1897 DRIC-BR-70941 NL

1 OF 2
AD A078733

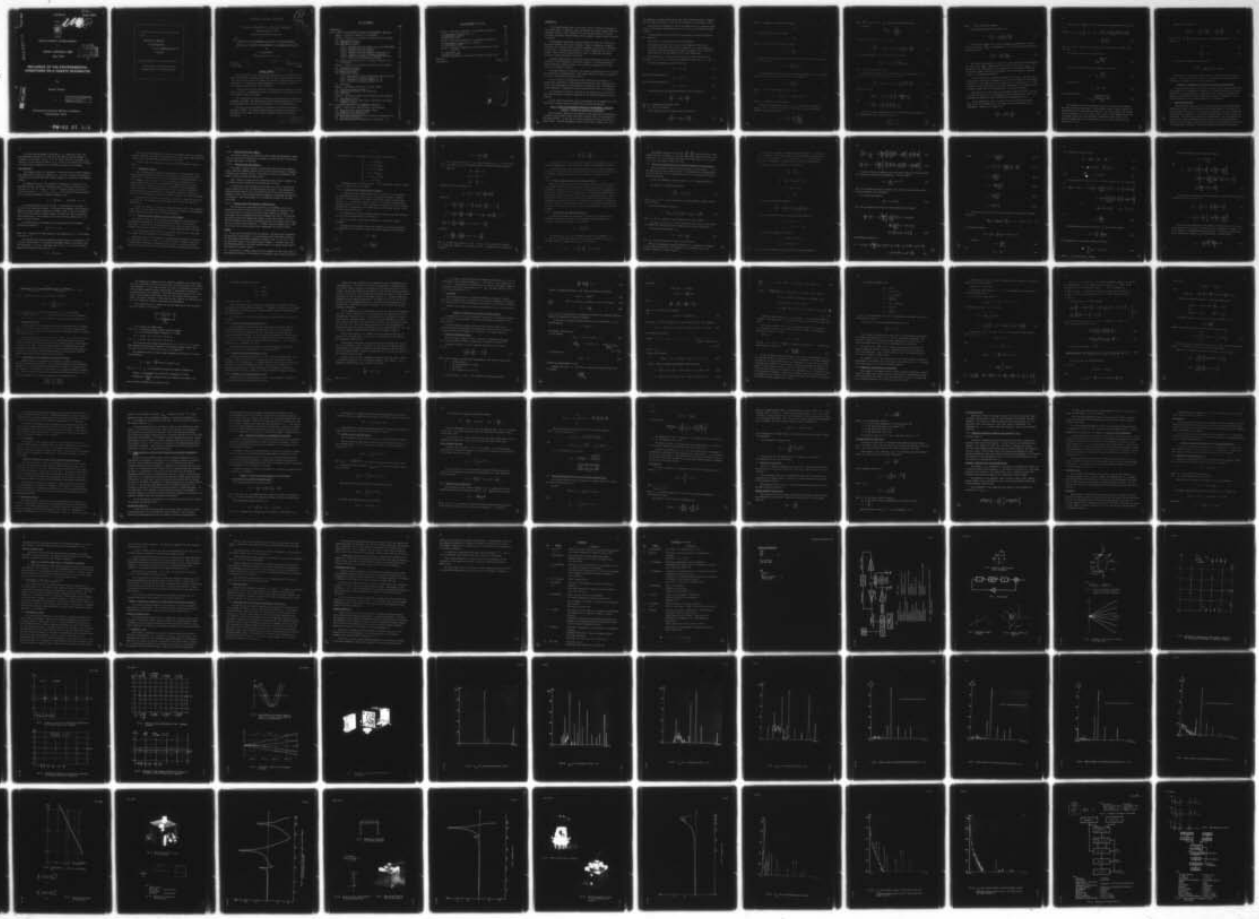

ROYAL AIRCRAFT ESTABLISHMENT

*

Library Translation 1897

May 1978

INFLUENCE OF THE ENVIRONMENTAL CONDITIONS ON A QUARTZ RESONATOR

by

Michel Valdois

*

Procurement Executive, Ministry of Defence
Farnborough, Hants

Translations in this series are available from:

THE R.A.E. LIBRARY
Q.4 BUILDING
R.A.E. FARNBOROUGH
HANTS

New translations are announced monthly in:

"LIST OF R.A.E. TECHNICAL REPORTS, TRANSLATIONS and BIBLIOGRAPHIES"

UDC 621.373 : 621.3-493 : 621.317.361

ROYAL AIRCRAFT ESTABLISHMENT

Library Translation 1897

Received for printing 23 May 1978

(6) INFLUENCE OF THE ENVIRONMENTAL CONDITIONS ON A QUARTZ RESONATOR

(INFLUENCE DES CONDITIONS D'ENVIRONNEMENT SUR UN RÉSONATEUR À QUARTZ).

by

(10) Michel/Valdois

ONERA Technical Note 225 (1974)

(12) 115

(14) RAE-LIBRARY TRANS-1897

Translator
W.F. Fielding

Translation editor
J. Wright

(11) May 78

AUTHOR'S SUMMARY

Quartz oscillators, used for aerospace applications, are subjected to very severe environmental conditions, particularly as far as accelerations and vibrations, which can be periodic or random, are concerned. The main effect of these disturbances is to modify the natural frequency of the resonator and thus to cause frequency instabilities in the oscillator.

In this paper the quartz resonator is studied both by itself, as a passive element placed in a transmitting circuit, and installed in an oscillator, which is its normal condition of usage.

The accelerations to which the resonators were subjected were steady state, sinusoidal or random. The orientation of the acceleration relative to the quartz crystallographic axis, as well as its direction, are of prime importance.

The same tests were performed on oscillators containing the resonators previously studied. The results confirm the part played by the resonator in the degradation of the stability of a quartz oscillator subjected to external disturbances.

LIST OF CONTENTS

LIST OF CONTENTS (concluded)

INTRODUCTION

The primary standard used at the present time for frequency measurement is the caesium clock. In general, atomic oscillators are used as primary frequency standards. However, recent progress into the long-term stability of quartz oscillators has given them performances which approach, closely, those of quantum oscillators.

Time-frequency systems have numerous applications such as for aerial and maritime navigation, anticollision systems, flights in formation, navigation satellites, all of which require frequency standards to be fitted to terrestrial or spacecraft. The necessary conditions of volume, weight and, also, price, allied to their excellent characteristics, lead to a preference for quartz oscillators rather than atomic oscillators.

Aerospace applications of quartz oscillators necessitate the study of the influence of the environment on oscillator stability. The main disturbances, accelerations and vibrations, modify the oscillator characteristics by their effects on the quartz resonator.

This paper begins by referring to the general, nonlinear theory of an elastic body subjected to a predeformation. This theory allows us to give an interpretation of the experimental phenomena observed.

The first part of the experimental study deals with the influence of steady-state, sinusoidal or random accelerations applied to the resonator alone. In all cases a disturbance of the resonator frequency was seen. The problem of crystal suspension is approached from the very particular case of two supports.

The second part is devoted to the use of the resonator in an oscillation loop. The oscillator so formed is subjected to the same disturbances as was the resonator.

All the results confirm the role of the resonator in the degradation of the stability of a quartz oscillator subjected to external disturbances.

Part 1 - STUDY OF THE RESONATOR SUBJECTED TO ENVIRONMENTAL CONDITIONS

Chapter 1 Theoretical aspects of the phenomena

The acceleration applied to the resonator caused prestreses and predeformations due to the internal forces and surface stresses (these latter being due to the fixing points). In the case of a steady acceleration these prestresses are purely static. From the mathematical point of view this is almost true, also,

the sinusoidal or random accelerations since their maximum frequencies (5000 Hz) are still small with respect to the natural frequency of the resonator (5 MHz).

This problem is analogous to that of the application of an external, static stress to the crystal, as mentioned by P.C.Y. Lee[1] or to the problem of thermal stresses.

In this study we use the nonlinear relationships for quartz developed by R.N. Thurston[2].

Three states of the crystal will be distinguished:-

- the natural state where the crystal is not subjected to any force.
- the initial state where the crystal is subjected to a static prestress.
- the final state where a dynamic deformation, assumed to be of infinitely-small amplitude, is superimposed on the static deformation.

The coordinates of a point in the crystal in its three states will be defined by a_i, x_i and X_i, and the corresponding densities by ρ_0, $\bar{\rho}$ and ρ.

The static displacement can be defined as:-

$$\bar{u}_i = x_i - a_i \,. \tag{1}$$

The dynamic displacement as:-

$$u_i = X_i - x_i \tag{2}$$

and the total displacement as:-

$$U_i = X_i - a_i \,. \tag{3}$$

In the final state the equilibrium equation can be written as:-

$$\rho \frac{\partial^2 U_i}{\partial t^2} = F_i(X_\ell) + \frac{\partial T_{ij}}{\partial X_j} \tag{4}$$

where F_i represents the internal forces
and T_{ij} the total stresses.

In the natural state this equation can be written as:-

$$\rho_0 \frac{\partial^2 U_i}{\partial t^2} = JF_i(X_\ell) + \frac{\partial P_{ij}}{\partial a_j} \tag{5}$$

where J represents the Jacobien determinant

$$J = \frac{\rho_0}{\rho} \quad .$$

In the same way we can also introduce

$$\bar{J} = \frac{\rho_0}{\bar{\rho}} \tag{6}$$

and P_{ij} is the first Piola-Kirchhoff tensor

$$P_{ij} = \frac{\partial X_j}{\partial a_r} t_{jr} \tag{7}$$

t_{ij} represents the thermodynamic tensions which can be related to the stresses T_{ij} by the equation

$$t_{sr} = J \frac{\partial a_s}{\partial X_i} \frac{\partial a_r}{\partial X_j} T_{ij} \ . \tag{8}$$

The thermodynamic tensions have considerable magnitudes since it is through them that the normal elastic coefficients are introduced.

$$t_{ij} = \left(\frac{\partial \phi}{\partial \eta_{ij}} \right)_S \tag{9}$$

where ϕ is the initial energy per unit volume

and

$$t_{ij} = C_{ijk\ell} \eta_{k\ell} + \tfrac{1}{2} C_{ijk\ell mn} \eta_{k\ell} \eta_{mn} + \ldots \tag{10}$$

where $\eta_{k\ell}$ represents the deformations.

The first Piola-Kirchhoff tensor P_{ij} is a function of the gradients $\partial X_k / \partial a_m$ only. It can also be written in the form of a series development limited to the first two terms:-

$$P_{ij} = \overline{P_{ij}} + \frac{\partial u_k}{\partial a_m} \frac{\partial \overline{P_{ij}}}{\partial \left(\frac{\partial x_k}{\partial a_m} \right)} \tag{11}$$

where $\overline{P_{ij}}$ is the value of P_{ij} expressed in the initial state.

If we let

$$\overline{\overline{A_{ikjm}}} = \frac{\partial \overline{P_{ij}}}{\partial \left(\frac{\partial x_k}{\partial a_m} \right)} , \tag{12}$$

the equilibrium equation (5), can be written

$$\rho_0 \frac{\partial^2 u_i}{\partial t^2} = J F_i(X_\ell) - \bar{J} F_i(x_\ell) + \frac{\partial}{\partial a_j} \left(A_{ikjm} \frac{\partial u_k}{\partial a_m} \right) \tag{13}$$

and by putting equation (7) into equation (12) we have:-

$$\overline{\overline{A_{ikjm}}} = \delta_{ik} t_{jm} + \frac{\partial x_i}{\partial a_p} \frac{\partial x_k}{\partial a_q} C_{jpmq} \tag{14}$$

where δ_{ik} is the Kronecker symbol.

The equilibrium equation (13) is expressed in the natural state. It is of interest to express it in the initial state as:-

$$\bar{\rho} \frac{\partial^2 u_i}{\partial t^2} = \frac{\bar{\rho}}{\rho} F_i(X_\ell) - F_i(x_\ell) + \frac{\partial}{\partial x_s} \left(\overline{\overline{B_{iskr}}} \frac{\partial u_k}{\partial x_r} \right) \tag{15}$$

where we have let:-

$$\overline{\overline{B_{iskr}}} = \delta_{ik} \overline{T_{sr}} + \overline{\overline{C_{iskr}}} \left[1 + \frac{C_{jpmquv}}{C_{jpmq}} \bar{\eta}_{uv} \right] \tag{16}$$

and

$$\overline{\overline{C_{iskr}}} = \frac{J}{\bar{J}} \frac{\partial x_i}{\partial a_j} \frac{\partial x_s}{\partial a_p} \frac{\partial x_k}{\partial a_m} \frac{\partial x_r}{\partial a_q} C_{jpmq} . \tag{17}$$

In the case under consideration, we can consider that the accelerations are independent of the deformations and hence:

$$F_i(X_\ell) = \rho \Gamma \tag{18}$$

$$F_i(x_\ell) = \bar{\rho} \Gamma \tag{19}$$

where Γ is the acceleration applied,

The equilibrium equation then reduces to:-

$$\bar{\rho} \frac{\partial^2 u_i}{\partial t^2} = \frac{\partial}{\partial x_s} \left(\overline{B_{iskr}} \frac{\partial u_k}{\partial x_r} \right) . \tag{20}$$

A particularly simple case is that of homogeneous deformation. In this case the coefficient $\overline{B_{iskr}}$ is independent of x_s and the equilibrium equation can be written as:-

$$\bar{\rho} \frac{\partial^2 u_i}{\partial t^2} = \overline{B_{iskr}} \frac{\partial^2 u_k}{\partial x_s \partial x_r} . \tag{21}$$

This equation is analagous to that for a linear system with predeformation. The coefficients $\overline{B_{iskr}}$ simply replace the elastic coefficients C_{iskr}. The advantage is that this equation is of a general form and can thus be applied to any elastic model subjected to prestresses due to acceleration to external forces or to temperature gradients[3].

It is now possible to consider the problem in two parts. The first part is the study of the static deformation alone. Since the amplitude of the dynamic deformation is very small (and this is always true, at least in part) it can be considered to have no influence on the static deformation. This latter can then be studied using a two- or three-dimensional linear model as needed.

The second part is the study of the dynamic deformation itself. This can be treated with the aid of a one-dimensional model using equations (20) or (21) depending upon whether the static deformation is homogeneous or not.

Let us consider the case of a quartz plate cut along AT vibrating in shear across the thickness and let us assume the static deformation to be homogeneous. Equation (21) reduces to:-

$$\bar{\rho} \frac{\partial^2 u_1}{\partial t^2} = \overline{B_{1212}} \frac{\partial^2 u_1}{\partial x_2^2} . \tag{22}$$

The coefficient $\overline{B_{12\,12}}$ can be expressed by using equations (16) and (17) as:-

$$\bar{J}\,\overline{B_{12\,12}} = \bar{J}\,\bar{T}_2 + C_{66}\left[1 + 2\bar{S}_1 + 2\bar{S}_2 + \frac{C_{661}\bar{S}_1 + C_{662}\bar{S}_2 + C_{663}\bar{S}_3 + C_{664}\bar{S}_4}{C_{66}} + 2\,\frac{C_{56}}{C_{66}}\,\frac{\partial u_2}{\partial a_3}\right] \tag{23}$$

where $\bar{S}_j$ and $\bar{T}_2$ define the deformations and static forces in single index notation.

The vibration frequency can be written as:-

$$f = \frac{1}{2\bar{e}}\sqrt{\frac{\overline{B_{12\,12}}}{\bar{\rho}}} \quad . \tag{24}$$

When there is no prestress, the frequency is equal to:-

$$f_0 = \frac{1}{2e_0}\sqrt{\frac{C_{66}}{\rho_0}} \quad . \tag{25}$$

We also have:-

$$\bar{e} = e_0(1 + \bar{S}_2) \tag{26}$$

from which we obtain:-

$$f = f_0\sqrt{\frac{\bar{J}\,\overline{B_{12\,12}}\,(1 - 2\bar{S}_2)}{C_{66}}} \quad . \tag{27}$$

The resonators used have electrodes fitted at the centres of the plates. The plate can then be considered to vibrate mainly about its centre, and of the distribution of forces and static deformations, only their values at the centre need be considered. It can be shown, easily, that if these deformations are due to internal forces and if the resonator is symmetrical with respect to its principle planes (Fig 6), the deformations $\bar{S}_1$, $\bar{S}_2$ and $\bar{S}_3$ are zero at the centre, as is $\bar{T}_{22}$ [4].

Equation (23) reduces to:-

$$\bar{J}\,\overline{B_{12\,12}} = C_{66}\left(1 + \frac{C_{664}\bar{S}_4}{C_{66}} + 2\,\frac{C_{56}}{C_{66}}\,\frac{\partial\bar{u}_2}{\partial a_3}\right) \tag{28}$$

and since $\bar{S}_4$ and $\frac{\partial\bar{u}_2}{\partial a_3}$ are proportional to the applied acceleration Γ, we can write:-

$$\bar{S}_4 = k_1\Gamma \tag{29}$$

$$\frac{\partial\bar{u}_2}{\partial a_3} = k_2\Gamma \quad . \tag{30}$$

The relative frequency variation is then:-

$$\frac{f - f_0}{f_0} = \frac{1}{2C_{66}}\,(C_{664}k_1 + 2C_{56}k_2)\Gamma \quad . \tag{31}$$

This follows a linear law and shows that its origin is due to the effects of shear. It also explains why a change in the direction of the acceleration Γ produces a sign change in the frequency variation[5].

Chapter 2 Influence of a constant acceleration on the resonator

The acceleration applied to the quartz crystal produces internal forces and hence surface forces through the intermediary of reactions caused at the crystal supports[6,7] by the fixing points. These forces lead to static deformations of the quartz which modify its elastic properties and also its dimensions. This causes a variation in the natural frequency of the resonator.

2.I Measurement principle

When the quartz crystal is at its resonant frequency, the phase difference between the current in the resonator and the voltage applied to its terminals is zero (provided that the effect of the parallel capacitance C_0 and the parasitic capacitances are negligible). Any frequency change leads to a phase change, and vice versa. The principle of the method of measurement is that of detecting this phase change, using a phasemeter which gives out a dc voltage proportional to the phase. This voltage is used to servo the synthesiser, externally, by means of its interpolation oscillator. The quartz crystal is excited at its resonant

frequency by the synthesiser. However, when the natural frequency of the quartz is altered the corresponding phase change, which is detected, allows the synthesiser to be servoed to a new value for the quartz resonant frequency. The frequency variations can be measured directly by using the synthesiser interpolation oscillator. The phase changes can also be recorded graphically on a graph-plotter.

2.II Experimental equipment

A centrifuge was used to provide the continuous acceleration, allowing up to 100 g (g is the unit of acceleration) to be applied to the crystal. Because of the mechanical strengths of the quartz crystal supports the tests carried out were limited to 50 g in most cases.

The test equipment is shown schematically in Fig 1. The quartz crystal was excited by means of the synthesiser too close to its resonant frequency. The level could be adjusted with an attenuator. The power amplifier had a very low output impedance, of 1 Ω, and provided a voltage which was practically constant at the quartz crystal terminals regardless of the current. The resistance R allowed the current in the quartz crystal to be measured; its value was about 50 Ω. At the resonant frequency, the designed resistance of the quartz was of the order of several tens of ohms. The crystal was placed in a chamber thermostatically-controlled at the temperature of its inversion point. The temperature stability of this chamber was within $0.01^{\circ}C$ per hour.

This experimental equipment also allows the parameters of the quartz crystal to be measured. At resonance, the phase difference between A and B is zero, the voltage V_B is a maximum and the impedance of the quartz crystal is equal to the resistance of its equivalent circuit (Fig 2).

Measurement of the bandwidth at 3 dB gives the values of the quadrilateral frequencies f_1 and f_2. The selectivity coefficient, Q, can be written as:-

$$Q = \frac{f_0}{f_2 - f_1} \quad \text{or} \quad Q = \frac{L_1\omega_0}{R_1 + R} \quad .$$

Now

$$Q_0 = \frac{L_1\omega_0}{R_1}$$

and hence

$$Q_0 = Q \frac{R_1 + R}{R} \tag{32}$$

$$L_1 = \frac{R_1 + R}{2\pi(f_2 - f_1)} \tag{33}$$

$$C_1 = \frac{1}{L_1 \omega_0^2} \quad . \tag{34}$$

C_0 is the interelectrode capacity and can be measured directly when the quartz is at a distance from its resonant frequency. The parallel frequency can also be used to calculate C_0 :-

$$C_0 = C_1 \frac{f_s}{2(f_p - f_s)} \tag{35}$$

where f_s is the series frequency ($f_s \triangleq f_r$).

When the acceleration is applied, the interelectrode capacity C_0 can vary with crystal deformation. This variation can be related to that of the quartz frequency.

If we let C_0 be the capacity for which the series frequency is:-

$$f_0 = \frac{1}{2\pi\sqrt{L_1 C_1}} \left(1 + \frac{R_1^2 C_0}{2L_1}\right) \tag{36}$$

and $C_0' = C_0 + \gamma$ be the capacity for which we have:-

$$f_0' = \frac{1}{2\pi\sqrt{L_1 C_1}} \left(1 + \frac{R_1^2 C_0'}{2L_1}\right) \tag{37}$$

a new value of the series frequency for a given acceleration.

LT
1987

$\delta f_0 = f_0' - f_0$ is related to $\gamma = C_0' - C_0$ by the equation:-

$$\gamma = 4\pi \frac{L_1\sqrt{L_1 C_1}}{L_1^2} \delta f_0 \quad . \tag{38}$$

To satisfy the experimental variations of f_0 (some tens of Hz), the corresponding variations of C_0 must be of the order of several hundreds or thousands of picofarads. Now C_0 is of the order of several picofarads. Consequently, we can exclude the effect of C_0 as far as the variation in frequency of a quartz crystal subjected to a continuous acceleration is concerned.

Servo principle

This equipment (Fig 3) is designed to achieve the quartz resonant frequency very rapidly and to follow the changes in it. For that, we used the synthesiser interpolation oscillator which had a linear response as a function of the applied voltage.

The modulation slope of the synthesised frequency is a function of the modulation pulsing. We chose a frequency range of ±10 Hz for a voltage of ±5 V, and hence for $\Delta f = Sv$ we have $S = 2$ Hz/v. The time-constant of the interpolation oscillator is $\tau = 1/2\pi f_c$, where f_c is the cut-off frequency relative to the synthesiser modulation frequency defined at 3 dB.

$$f_c = 100 \text{ kHz}, \qquad \text{from which } \tau = 2 \mu s.$$

The phasemeter gives out a dc voltage v proportional to the phase Φ measured at the resonator terminals. To measure the phasemeter time-constant we applied a reference signal (5 MHz from an atomic clock) to one of the channels and to the other channel a frequency signal, initially the same but capable of being varied slowly. The variation in the output voltage, proportional to the phase, is shown in Fig 4.

The operation of the phasemeter can be represented by the following differential equation[8]:-

$$R'C'v' + v = K\phi \tag{39}$$

where $R'C'$ represents the time-constant of the apparatus and v is the signal, a function of ϕ.

The frequency for which the phasemeter output signal is attenuated by 3 dB is equal to about 500 Hz. The different measurement ranges for the phase cause the coefficient K to vary. The range used, $\pm 6^o$ for $v = \pm 0.5$ V is the most sensitive and determines the value of K.

$$K = \frac{15}{\pi} \text{ V/rd} .$$

The servo system evidently does not make an automatic search of the quartz resonant frequency. This must be searched for by a slow, manual sweep, which is coupled to the apparatus when the servo-field is entered.

At this stage, the transitory states are only attributable to those of quartz.

2.III Experimental results

The accelerations were applied systematically for all positions of the quartz crystal (along the ox'y'z' axes) with respect to the direction of the acceleration. The tests were carried out with different mountings having 2, 3, 4 or 5 supports for the crystal. Fig 5 represents the resonator in its crystallographic axes ox'y'z'. We indicate the slightly convex face of the crystal, which is a plano-convex lens of 15 mm diameter and of thicknesses 1 mm and 1.65 mm. All the resonators used were cut in the AT form, which is the one most used for the production of ultrastable oscillators. Moreover, this cut has the advantage of being only slightly sensitive to thermal variations.

The plane face of the quartz crystal is in the x'oz' plane and the convex face along oy'. The supports were fixed immaterially in the z'oy' and z'ox planes (Fig 6).

In Fig 6 the figures in circles on each of the arrows refer to the synthesis curves (Fig 7) of the frequency variation obtained in each case. The experimental curves, which follow, carry the same reference numbers.

2.III.1 Resonator with two supports (No.01, No.5048 ENSCMB)

The curves of Figs 8,9 and 10 represent the frequency variations when the acceleration applied was in 24 different positions relative to the crystal. With respect to each of the two senses defined by one axis, the quartz crystal occupies four positions, displaced by 90^{o}, in a plane perpendicular to this axis.

It is established that the frequency variations always have the same sign for a given direction and sense of the acceleration.

When the sense of the acceleration is changed, whilst keeping its direction the same (cases 1 and 2, or 3 and 4, or 5 and 6 of Fig 6) a change in the sense of the frequency variation is noticed and in all cases it can be stated, definitely, that this variation is directly proportional to the applied acceleration.

2.III.2 Resonator with three supports

This quartz crystal, in a metal box, and of industrial manufacture, shows (Fig 11) curves of the variations in frequency of which the main characteristic is their high degree of linearity.

2.III.3 Resonator with four supports

This quartz crystal, No.5057, specially made and held by four supports, shows a behaviour somewhat different as far as the relative values of frequency variations are concerned (Fig 12). This effect is due to the increase in the number of quartz crystal attachment points.

Fig 13 shows the results from an industrial quartz crystal, supported at four points, which we subjected to an acceleration of 100 g.

It would appear that the behaviour was similar to that of the previous quartz crystal up to 50 g, but differed above that value. The linearity disappeared and the shape of the curve between 50 and 100 g can be attributed to nonlinear effects. The different points correspond to increasing excitations of the resonator. There would appear to be no behaviour peculiar to the large excitations.

2.III.4 Resonator with five supports. No.5065 (Fig 14)

This resonator was constructed specially at the ENSCMB piezoelectric laboratory in order to study the action of a large number of supports as well as the influence of the positions at which these supports are attached. It would appear that the frequency inversion disappears for the oy' axis and that the relative values are changed with respect to the first results. All the available evidence shows that the anchorage points of the supports play a large part in the quartz crystal behaviour. It seems, from this example, that a careful choice in their positioning can give compensation for certain effects.

Remarks

(1) In the case of resonators with two supports - the type least disturbed by the presence of fixing points - it was noticeable that acceleration along the ox axis produced the smallest frequency variation. Now ox (or ox') is the only axis which keeps to the original crystal symmetry. It seems, then, that the disturbance effect is the least sensitive when it is applied along a particular axis of the quartz crystal.

(2) In the case of a quartz crystal with two supports, we take a mean value of the frequency variations. The variation is reasonably linear, and we can write:-

$$\Delta f = k\Gamma$$

and the values of k for curves 1 to 6 of Figs 8, 9 and 10 are:-

$$k_1 = -3 \times 10^{-3} \text{ Hz/g}$$
$$k_2 = 4.4 \times 10^{-3} \text{ Hz/g}$$
$$k_3 = -1.2 \times 10^{-3} \text{ Hz/g}$$
$$k_4 = 1.2 \times 10^{-3} \text{ Hz/g}$$
$$k_5 = -1.6 \times 10^{-3} \text{ Hz/g}$$
$$k_6 = 2 \times 10^{-3} \text{ Hz/g} .$$

The maximum value of the coefficient k was obtained for a quartz crystal with five supports and was 0.04 Hz/g.

2.III.5 Variation of the anti-resonance frequency

In order to provide a better definition of the quartz crystal behaviour, the same measurements were carried out on the parallel frequency. However, this is not very pronounced for a quartz crystal with a small interelectrode capacity C_0 . By placing a capacity of about 10 picofarads in parallel with the quartz crystal, the anti-resonance frequency is brought close to the resonant frequency and, in particular, the minimum current in the quartz crystal is then much more easily displaceable.

The variations in the anti-resonance frequency maintain the same characteristics as those found previously for resonance.

Figs 8, 9, 10 and 11 show these variations for the quartz crystals considered.

By using the relationships between the resonance (ω_0) and anti-resonance (ω_a) frequencies it is possible to check that these frequencies are identical.

If

$$\omega_0^2 = \frac{1}{L_1 C_1}$$

and

$$\omega_a^2 = \frac{C_0 + C_1}{L_1 C_0 C_1}$$

LT 1897 we have

$$\omega_a \# \omega_0 \left(1 + \frac{C_1}{2C_0}\right). \tag{40}$$

Let ω_a' be the new value of ω_a during acceleration. ω_a' is of the form $\omega_a^*(1 + \delta_a)$, where ω_a^* is the constant value of the anti-resonance frequency.

Similarly:-

$$\omega_0' = \omega_0^*(1 + \delta_0)$$

$$C_1' = C_1^*(1 + \eta)$$

$$C_0' = C_0^*(1 + \gamma)$$

and equation (40) is equivalent to:-

$$\omega_a' \# \omega_0^*(1 + \delta_0)\left(1 + \frac{C_1^*}{2C_0^*}\frac{1 + \eta}{1 + \gamma}\right)$$

and hence:-

$$\omega_a' \# \omega_0^*\left[1 + \frac{C_1^*}{2C_0^*}(1 + \eta - \gamma)\right] + \omega_0^*\delta_0\left[1 + \frac{C_1^*}{2C_0^*}(1 + \eta - \gamma)\right]$$

$$\omega_a' \# \omega_0^*\left(1 + \frac{C_1^*}{2C_0^*}\right) + \omega_0^*\frac{C_1^*}{2C_0^*}(\eta - \gamma) + \omega_0^*\delta_0 + \omega_0^*\delta_0\frac{C_1^*}{2C_0^*}(1 + \eta - \gamma)$$

$$\omega_a^*\delta_a^* \# \omega_0^*\left[\delta_0 + \frac{C_1^*}{2C_0^*}\left[(\eta - \gamma) + \delta_0(1 + \eta - \gamma)\right]\right]$$

from which

$$\delta_a \# \frac{\omega_0^*}{\omega_a^*}\left[\delta_0 + \frac{C_1^*}{2C_0^*}\left[(\eta - \gamma)(1 + \delta_0) + \delta_0\right]\right] .$$

Now δ_0 is small with respect to 1 and η and γ are very small with respect to δ_0 and also $C_1^*/2C_0^*$ is of the order of 10^{-4}. Consequently it is justifiable to write:-

$$\delta_a \# \frac{\omega_0^*}{\omega_a^*} \delta_0 \left[1 + \frac{C_1^*}{2C_0^*} \right] \quad . \tag{41}$$

It can be seen that δ_a is practically equal to the variation δ_0 of the resonant frequency and so this calculation confirms the experimental results.

All the variations in the resonant and anti-resonance frequencies show that the effect of the acceleration on the quartz crystal is to cause a translation of the 'current in the quartz crystal' curve as well as of the phase curve (Fig 15).

2.III.6 Effect of hysteresis of the frequency variation

When the acceleration decreases the frequency does not go back to the same values which it had when the increasing acceleration was applied. No complete explanation for this is given here, but it is comparable with the phenomena shown when a field is applied[9]. It is probably due to a progressive disappearance of the stresses caused by the memory effect of the crystalline structure. When the acceleration is zero once more, the difference between the initial and final frequencies can reach 0.1 Hz and it is possible for the variation to change sign during the course of the deceleration (Fig 16). It often takes several tens of seconds for the resonator to return to within one hundredth of 1 Hz of its initial frequency.

2.III.7 Variation in the designed resistance

In order to determine the equivalent resistance of the resonator it is sufficient to measure the voltage at the terminals, when the resonator is excited at its resonant frequency. We then have:

$$R_1 = \frac{V_A - V_B}{V_B} R \quad .$$

The voltages V_A and V_B are measured by means of a phasemeter. If ΔV_A and ΔV_B are the variations of these voltages, respectively, then ΔR_1, the variation in the designed resistance, is such that:-

$$\Delta R_1 > 0 \quad \text{if} \quad \frac{\Delta V_A}{V_A} > \frac{\Delta V_B}{V_B} \quad \text{and vice versa.}$$

Measurements show that in all cases $\frac{\Delta V_A}{V_A} > \frac{\Delta V_B}{V_B}$, and from this it can be deduced that the resistance R_1 decreases as the acceleration increases. The variation in R_1 is not always very linear and a mean value for it is about 0.5 Ω (for a resistance of 100 Ω) at 50 g.

2.IV Effects of nonlinearities in a resonator subjected to an acceleration

This calculation is limited to the case where the acceleration Γ is in the same direction as the shear vibration. The model used is one-dimensional. The aim of this section is to explain the effect of the curvature noticed for large accelerations.

We use the fundamental equations (Refs.10, 11, 12) amongst which are:-

- the equation for dynamic equilibrium

$$\rho \frac{\partial^2 u_i}{\partial t^2} = \text{div } T_j + F_i \qquad (42)$$

where u_i, T_j and F_i are, respectively, the displacements, stresses and the internal forces.

- the force-deformation equation:

$$T_i = C^E_{ij} S_j + \frac{1}{6} C_{ijk\ell} S_j S_k S_\ell - e_{mi} E_m + r_{ij} \frac{\partial S_j}{\partial t} \qquad (43)$$

where S_j and E_m represent the deformations and electric fields.

C_{ij}, $C_{ijk\ell}$, e_{mi} and r_{ij} are the 2nd and 4th order elastic coefficients, the piezoelectric coefficients and the damping coefficients, respectively.

- the electrical displacement D_n

$$D_n = e_{nj} S_j + \varepsilon_{mn} E_m \qquad (44)$$

where ε_{mn} is the coefficient of electrical polarisation.

We used the mathematical models developed by J.J. Gagnepain[13] and applied by him to the determination of the influence of a continuous field on the resonant frequency of a quartz crystal[14]. LT 1897

In the case of a plate cut along AT , with thickness e , of infinite lateral dimensions, vibrating in shear across the thickness, the deformation reduces to S_6 , the stress to T_6 and the field E_2 is applied along oy . We shall neglect the damping r_{ij} which does not cause any nonlinearities.

Equations (42), (43) and (44) can be written:-

$$\rho \frac{\partial^2 u}{\partial t^2} = \frac{dT_6}{dy} + \rho\Gamma \tag{45}$$

$$T_6 = C_{66}^E S_6 + \frac{1}{6} C_{6666} S_6^3 - e_{26} E_2 \tag{46}$$

$$D_2 = e_{26} S_6 + \varepsilon_{22} E_2 \tag{47}$$

$$S_6 = \frac{\partial u}{\partial y} \ . \tag{48}$$

We can obtain the propagation equation:-

$$\rho \frac{\partial^2 u}{\partial t^2} = C_{66}^D \frac{\partial^2 u}{\partial y^2} + \frac{1}{2} C_{6666}^D \left(\frac{\partial u}{\partial y}\right)^2 \frac{\partial^2 u}{\partial y^2} + \rho\Gamma \tag{49}$$

to which are associated the two following limiting conditions:-

$$u = 0 \quad \text{for} \quad y = 0 \tag{50}$$

$$T_6 = 0 \quad \text{for} \quad y = \pm \frac{e}{2} \ . \tag{51}$$

If we take a solution of the form:-

$$u = U_0(y) + A(y) \cos \omega t \tag{52}$$

$$D_2 = D_0 + M_0 \cos \omega t \tag{53}$$

LT
1897 and put this into equation (49) we obtain the following equations:-

$$\frac{d^2U_0}{dy^2} + \rho \frac{\Gamma}{C^D_{66}} = -\frac{1}{2}\frac{C^D_{6666}}{C^D_{66}}\left\{\frac{d^2U_0}{dy^2}\left[\left(\frac{dU_0}{dy}\right)^2 + \frac{1}{2}\left(\frac{dA}{dy}\right)^2\right] + \frac{d^2A}{dy^2}\frac{dU_0}{dy}\frac{dA}{dy}\right\} \tag{54}$$

$$\frac{d^2A}{dy^2} + \frac{\omega^2}{c^2}A = -\frac{1}{2}\frac{C^D_{6666}}{C^D_{66}}\left[2\frac{d^2U_0}{dy^2}\frac{dU_0}{dy}\frac{dA}{dy} + \frac{d^2A}{dy^2}\left(\frac{dU_0}{dy}\right)^2 + \frac{3}{4}\frac{d^2A}{dy^2}\left(\frac{dA}{dy}\right)^2\right] . \tag{55}$$

In each of these two equations the second term is small and allows solutions to be obtained by successive approximations. Thus we obtain:-

$$U_0 = \frac{\rho\Gamma}{2C^D_{66}}(\pm ey - y^2) \tag{56}$$

which is the general solution for equation (54) without the second term, and is accurate enough for this calculation.

In the same way we have:-

$$A(y) = a \sin \frac{\omega}{c} y \tag{57}$$

and if we put equations (56) and (57) into equation (55) we obtain:-

$$\begin{aligned}\frac{d^2A}{dy^2} + \frac{\omega^2}{c^2}A = -\frac{1}{2}\frac{C^D_{6666}}{C^D_{66}}\Bigg[&-\left(\frac{\rho\Gamma}{C^D_{66}}\right)^2 \frac{a\omega}{c}(\pm e - 2y)\cos\frac{\omega}{c}y \\ &- \frac{a\omega^2}{c^2}\left(\frac{\rho\Gamma}{2C^D_{66}}\right)^2(\pm e - 2y)^2 \sin\frac{\omega}{c}y \\ &- \frac{3}{4}a^3\frac{\omega^4}{c^4}\sin\frac{\omega}{c}y\cos^2\frac{\omega}{c}y\Bigg]\end{aligned} \tag{58}$$

whose general solution is:-

$$\begin{aligned}A = a\sin\frac{\omega}{c}y - \frac{1}{2}\frac{C^D_{6666}}{C^D_{66}}\Big(&\alpha_1 y\sin\frac{\omega y}{c} + \alpha_2 y\cos\frac{\omega y}{c} + \alpha_3 y^2\sin\frac{\omega y}{c} + \alpha_4 y^2\cos\frac{\omega y}{c} \\ &+ \alpha_5 y^3\cos\frac{\omega y}{c} + \alpha_6\sin e\frac{\omega y}{c}\Big)\end{aligned} \tag{59}$$

LT
1897

where

$$\alpha_1 = \mp \frac{3}{4}\left(\frac{\rho\Gamma}{C^D_{66}}\right)^2 ae \tag{60-1}$$

$$\alpha_2 = \frac{3}{32} a^3 \frac{\omega^3}{c^3} + a\left(\frac{\rho\Gamma}{C^D_{66}}\right)^2 \left(\frac{c}{4\omega} - \frac{e^2\omega}{8c}\right) \tag{60-2}$$

$$\alpha_3 = \frac{a}{4}\left(\frac{\rho\Gamma}{C^D_{66}}\right)^2 \tag{60-3}$$

$$\alpha_4 = \pm \frac{ae\omega}{4c}\left(\frac{\rho\Gamma}{C^D_{66}}\right)^2 \tag{60-4}$$

$$\alpha_5 = \frac{a\omega}{6c}\left(\frac{\rho\Gamma}{C^D_{66}}\right)^2 \tag{60-5}$$

$$\alpha_6 = \frac{3}{128} a^3 \frac{\omega^2}{c^2} \quad . \tag{60-6}$$

The application of the second limiting condition leads to the following equation:-

$$C^D_{66} S_6 + \frac{1}{6} C^D_{6666} S_6^3 - \frac{e_{26}}{\varepsilon_{22}} D_2 = 0 \qquad \text{for } y = \pm \tfrac{1}{2}e \tag{61}$$

and from this we have:-

$$S_6 = \frac{\partial u}{\partial y} = \frac{\partial}{\partial y}\left[U_0(y) + A(y)\cos \omega t\right] \quad .$$

If we put

$$\alpha = \frac{e_{26}}{C^D_{66}\varepsilon_{22}} \tag{62}$$

LT
1897

and

$$S_6 = \alpha D_2 \, , \tag{63}$$

we can obtain, by identification:-

$$\alpha M_0 - 3D_0^2 M_0 \beta - \frac{3}{4} M_0^3 \beta = \frac{dA}{dy} \pm \frac{e}{2} \tag{64}$$

$$\alpha D_0 - [illegible] - \frac{3}{2} \beta D_0 M_0^2 = \frac{dU_0}{dy} \left(\pm \frac{e}{2} \right) = 0 \tag{65}$$

where

$$\beta = \frac{1}{6} C^D_{6666} \alpha^3 \quad . \tag{66}$$

By using equations (59) and (60-1) to (60-6) equation (64) can be expressed as:-

$$\alpha M_0 - 3D_0^2 M_0 \beta - \frac{3}{4} \beta M_0^3 = a \cos \frac{\omega e}{2c} \left\{ \frac{\omega}{c} - H \left(\frac{\rho \Gamma}{C^D_{66}} \right)^2 \left[\mp \frac{3}{16} \frac{\omega}{c} e^3 \pm \frac{1}{4} e^2 \frac{\omega}{c} \right] - \frac{3}{32} Ha^2 \frac{\omega^3}{c^3} \right\}$$

$$+ a \sin \frac{\omega e}{2c} H \left[\left(\frac{\rho \Gamma}{C^D_{66}} \right)^2 \left(\frac{e}{2} \pm \frac{e^4}{96} \frac{\omega^2}{c^2} \right) + \frac{3}{128} ea^2 \frac{\omega^4}{c^4} \right]$$

$$+ \frac{9}{128} a^3 \frac{\omega^3}{c^3} \cos \frac{3\omega e}{2c} \qquad \text{for } y = \pm \frac{1}{2} e \tag{67}$$

with

$$H = \frac{1}{2} \frac{C^D_{6666}}{C^D_{66}} \quad . \tag{68}$$

The conditions which affect the field E_2 must then be applied:-

$$E_2 = \frac{D_2}{\varepsilon_{22}} - \frac{e_{26}}{\varepsilon_{22}} \frac{\partial u}{\partial y} \quad . \tag{69}$$

By integrating over the crystal thickness we obtain:-

$$\int_{-\frac{1}{2}e}^{\frac{1}{2}e} E_2 dy = V_0 \cos \omega t \tag{70}$$

where V_0 is the exciting ac voltage.

After identification, two new equations appear:-

$$D_0 - e_{26} \frac{e}{8} \frac{\rho\Gamma}{C^D_{66}} = 0 \tag{71}$$

and

$$V_0 = \frac{e}{\varepsilon_{22}} M_0 - \frac{e_{26}}{\varepsilon_{22}} \left\{ a \sin \frac{\omega e}{2c} \left[2 + \frac{5}{16} \frac{C^D_{6666}}{C^D_{66}} e^2 \left(\frac{\rho\Gamma}{C^D_{66}} \right)^2 \right] \right.$$

$$- \frac{a}{2} \frac{C^D_{6666}}{C^D_{66}} \cos \frac{\omega e}{2c} \left[\left(\frac{\rho\Gamma}{C^D_{66}} \right)^2 \left(\frac{\omega e^3}{24c} + \frac{ec}{4\omega} \right) + \frac{3}{32} ea^2 \frac{\omega^3}{c^3} \right]$$

$$\left. - \frac{3}{128} \frac{C^D_{6666}}{C^D_{66}} a^3 \frac{\omega^2}{c^2} \sin \frac{3\omega e}{2c} \right\} . \tag{72}$$

By taking into account the orders of magnitude of the different coefficients, equations (67) and (72) reduce to:-

$$\alpha M_0 = a \left(n \frac{\omega}{c} \frac{\pi}{2} \delta - \frac{3}{256} \frac{C^D_{6666}}{C^D_{66}} ea^2 \frac{\omega^4}{c^4} \right) \tag{73}$$

$$V_0 = \frac{e}{\varepsilon_{22}} M_0 - \frac{e_{26}}{\varepsilon_{22}} a \left[2 + \frac{5}{16} \frac{C^D_{6666}}{C^D_{66}} e^2 \left(\frac{\rho\Gamma}{C^D_{66}} \right)^2 \right] . \tag{74}$$

Since we are not interested in the absence of isochronism, that is to say in the influence of the level of oscillation on the frequency, the terms in a^3 can be neglected. The dependence of the frequency on the applied acceleration will be obtained by letting V_0 tend towards zero. We then obtain:-

$$\delta_0 = - \frac{10}{16\pi^2} \frac{e_{26}^2 e^2}{\varepsilon_{22}} \frac{C^D_{6666}}{C^{D\,4}_{66}} (\rho\Gamma)^2 \tag{75}$$

where δ_0 represents the relative error between the excitation frequency and the natural frequency of the resonator, and n the range used in the vibration (here n = 5).

δ_0 is clearly a quadratic function of the acceleration.

Chapter 3 Influence of a sinusoidal vibration on the resonator

The problem of vibrations is different from the previous one in the sense that it introduces dynamic deformations of the crystal and hence a low-frequency modulation of the resonator natural frequency.

3.I Measurement principle

The method used consists of detecting the frequency variations by means of the corresponding phase fluctuations in the current through the resonator. For that, a spectral analysis is carried out on the output signal from the phasemeter. Since the phase fluctuations are random, it is possible to extract from this noise the harmonic components in direct relation to the sinusoidal disturbance.

3.II Experimental equipment

The experimental equipment is almost the same as that used for steady accelerations, but the manipulations were carried out without the frequency servo-loop. In this case we used the voltage output from the phasemeter connected across the terminals of the quartz crystal. This voltage was recorded on an FM tape recorder then analysed on a programmable analyser controlled by a computer. The accuracy of the analysis depended upon the frequency range chosen. To give an idea of the order of magnitude, the incremental accuracy was 1 Hz for a 500 Hz range of analysis. The analysis dynamic was 50 dB and each of the spectrum graphs was accompanied by a table showing the frequency and amplitude of each line with respect to a reference signal.

3.III Method of analysis

It is possible to analyse a certain frequency range in real time thanks to compression of the signal in time and which also allows the time taken for analysis to be 'accelerated'.

The analysis is carried out in an analogue matter but on the other hand the signal acceleration is achieved by the use of numerical techniques (shift register, acoustic delay line).

To explain the principle of this analyser, the real acceleration mode is replaced by a symbolic acceleration mode. Suppose that a portion of a signal $x(t)$ of duration Δt is recorded with a writing speed v on a magnetic

tape-loop. The signal can then be read-off by means of a read-out head mounted on an arm and turning at a speed $V = \alpha v$ ($\alpha \gg 1$). The signal $x_a^i(t)$ read during the first revolution of the read-out head will be the accelerated signal and:-

$$x_a^i(t) = x(\alpha t)$$

where α is the acceleration ratio.

If we put

$$X(\nu) = TFx(t)$$

where TF is the Fourier transform
then we have:-

$$X_a^i(\nu) = TFx_a^i(t)$$

$$= \int_0^{\Delta t/\alpha} x(\alpha t) e^{-2\pi j \nu t} dt$$

$$= \frac{1}{\alpha} X(\nu/\alpha) \quad . \tag{76}$$

Thus the spectral spread of a period of an accelerated signal and that of the initial signal are in the ratio α. In order to obtain the spectrum of the signal $x(t)$ within the frequency range (B,NB) by means of N equidistant filtering points, and with a resolution $B = 1/\Delta t$, it is sufficient to analyse $X_a(\nu)$ with a filter of resolution αB.

Again, the filter and the associated detection system have a response time of $\frac{1}{\alpha B} = \frac{\Delta t}{\alpha}$ which, for signal analysis, allows the use of a sliding filter F whose central frequency ν_F takes, successively, the values αB, $2\alpha B$ ... $N\alpha B$ at the time instants of $0, \frac{\Delta t}{\alpha}$ ... $\frac{(N-1)}{\alpha} \Delta t$.

The analysis time $T = N \frac{\Delta t}{\alpha}$ is equal to the signal duration in $N = \alpha$, and the system operates as if the signal $x(t)$, of duration Δt, had been analysed by N filter points. In reality, the signal $x(t)$ is applied continuously to the analyser input, which gives out an elementary spectrum $|X^k(\nu_j)|$, ($j = 1$ to N), the spectrum obtained during the kth analysis sequence. This spectrum passes through a quadratic circuit and then its mean value over a frequency range is found.

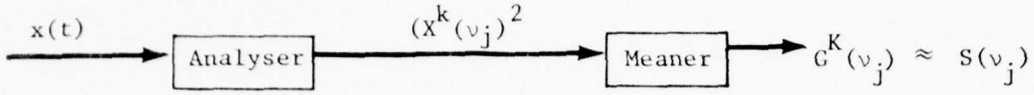

$G^K(\nu_j)$ spectral function is thus related to $|X^k(\nu_j)|^2$ by

$$G^K(\nu_j) = \frac{1}{K} \sum_{k=1}^{K} |X^k(\nu_j)|^2 \qquad (77)$$

$S(\nu)$, the power spectral density associated with $x(t)$ is such that $S(\nu) \# \lambda E\left[|X^k(\nu)|\right]$ where λ is a scaling constant peculiar to the apparatus.

Hence $G^K(\nu_j)$ is a correct estimate of the power spectral density $S(\nu)$.

3.IV Experimental results

We have applied to the resonators sinusoidal vibrations within a frequency range of 10 to 5000 Hz and from several g to 40 g. The quartz crystals were placed in a specially-constructed, thermostatically-controlled chamber to undergo the vibrations (Fig 17).

The resonators used could form different sources, thus enabling the testing of quartz crystals having two, three, four or five support points. For low-frequency external vibrations the effect of the supports is due to their moments of inertia. Only those resonators manufactured by the ENSCMB laboratory were subjected to the highest accelerations. The quartz crystals with two supports formed part of the normal laboratory manufacture but those with four and five supports were manufactured especially for this study.

3.IV.1 Manipulation of the frequency servo with closed loop

Although frequency servoing was not necessary, a series of tests was carried out under these conditions. The vibration frequencies were chosen spontaneously at any suitable values, but different from those of the sector and of its harmonics. Fig 18 shows the fluctuations in the natural frequency of quartz, $S_{\Delta f_0}$, when the quartz crystal does not undergo any disturbance and Figs 19 to 21 show the fluctuations for exciting frequencies and accelerations of:-

32 Hz, 3 g Fig 19
60 Hz, 3 g Fig 20
87 Hz, 3 g Fig 21.

The appearance of harmonics of the vibration frequency can be seen, which can only be explained as due to the servo loop. With the loop open, the harmonic peaks disappear. In fact, when the loop is closed, the synthesiser is guided by a voltage whose harmonic content (fluctuations in the resonator frequency) is regenerated within the synthesiser. Each spectrum shows the presence of a large peak of fixed frequency (particularly Fig 18). This arises from the mixing between the natural frequency of the quartz crystal, shown by the synthesiser and the 5 MHz calibration frequency which guides the synthesiser.

This remark allows us to deduce the relative amplitude of the disturbance peak with respect to the carrier.

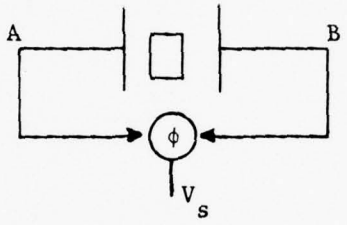

If we consider the scheme above,

where ω_0 is the quartz crystal resonant angular frequency

ω_r is the reference angular frequency = $2\pi \times 5$ MHz.

At A we have $V_A = V_1 \sin \omega_0 t + V_1' \sin \omega_r t$

and at B we have $V_B = V_2 \sin \omega_0 t + V_2' \sin \omega_r t$.

The resonators have a quality coefficient of 1.5×10^6 to 2×10^6 and the 5MHz component is practically nonexistent at the quartz crystal output, since this plays the role of a filter, and so V_2' can be neglected.

The phasemeter gives an output voltage comparable with that from a 4-diode ring demodulator.

$$V_s = V_A V_B = \frac{V_1 V_2}{2} \cos \Delta\omega t + g(2\omega_0 \omega r + \omega_0)$$

where $\Delta\omega = \omega_r - \omega_0$ is the difference between the angular frequencies:

$g(2\omega_0 \omega r + \omega_0)$ represents the terms with a frequency of 10 MHz.

Consequently, $\dfrac{V_1 - V_2}{\frac{V_1' V_2}{2}}$ represents the ratio between the voltage at the quartz crystal terminals and the parasitic peak.

The values currently in use are:-

$$V_1 = 20 \text{ mV}$$

$$V_2 = 10 \text{ mV}$$

$$V'_1 = 500 \ \mu\text{V}$$

which give a ratio of 72 dB.

Since the analysis gives the error, in dB, between the parasitic frequency peak and that of the disturbing frequency, it is simple to obtain the ratio between the amplitude of the quartz crystal resonant frequency and that of the external, disturbing vibration.

As in the case of the steady accelerations, three particular cases will be considered.

3.IV.2 Direction of vibration parallel to ox

This arrangement is such the natural vibration of the crystal and the disturbing vibrations are in the same direction. Figs 19 to 21 show that the effect of the vibration diminishes as the frequency increases and that the acceleration remains constant. In the case where the frequency is fixed and the acceleration varies, the amplitude of the peak increases with the acceleration, as Figs 22 to 24 show, where the acceleration has the values of 2 g, 4 g and 8 g, respectively, at a frequency of 30 Hz.

These results are the same whether the external vibration is directed along the +ox' axis or along the -ox' axis of the crystal.

3.IV.3 Direction of vibration parallel to oy'

In this configuration the two faces of the crystal are perpendicular to the vibration. Again, the position of one particular face with respect to the disturbance is of no importance. It appears, however, that in this position the resonator is much less disturbed than in the previous case. Moreover, for increasing acceleration at a fixed frequency, the disturbance is practically unchanged (Figs 25 and 26). However, it decreases when the frequency increases.

3.IV.4 Direction of vibration parallel to oz'

This position gives results which are in all ways comparable to those for the first case and the conclusions are the same.

Besides the phase information, the phasemeter gives a measurement of the signal amplitude. It provides a dc voltage, proportional to the amplitude of the observed signal, and whose fluctuations are represented by those of the dc voltage. We have proceeded with the analysis of this voltage without being able to detect the presence of the disturbing peak, which has led us to think that the phenomenon seen for the whole of the quartz crystals is a frequency modulation phenomenon without amplitude modulation. Referring to Fig 15, we see that the external vibration phenomenon operates on the phase curve and produces a displacement of the external disturbance frequency. This confirms the frequency modulation phenomenon.

Fig 27 summarises all the measurements carried out. Each curve represents the ratio $A\Omega/A_0$ in dB, that is to say the ratio of the amplitude of the disturbing peak, of frequency $\Omega/2\pi$, to the amplitude of vibration of the quartz crystal at its resonant frequency. The effect of the disturbance increases as the frequency drops and as the acceleration increases. The positions for which the ox' and oz' axes of the quartz crystal are vertical (designated by vertical positions) give larger disturbances than are obtained when the oy' axis is vertical (shown by the horizontal position of the quartz crystal).

The vertical position oz' appears to be more sensitive than the ox' position for low frequencies. This is due to the influence of the supports, which disappears above 100 Hz.

Technological limitations in the exciter did not allow more than 4 g, at 10 Hz, to be applied. Also, the dynamics of the analyses (50 dB) has limited the researches to disturbance frequencies greater than 500 Hz and for which the effect is extremely small. However, we shall show that they show up clearly in the oscillator phase spectrum.

We have tried to obtain a mathematical description of the curves relative to the vertical position ox' by using the method of least squares. In an orthogonal reference they can be written in the form:-

$$\frac{A_{\Omega_i}}{A_0} = a_i \Gamma^3 + b_i \Gamma \qquad (78)$$

LT 1897

where $a_i \ll b_i$.

Ω_i is fixed for each curve and Fig 28 shows the variations in a_i and b_i as functions of the vibration frequency Ω. The slope of this straight line is f^{-2} $f = \frac{\Omega}{2\pi}$. Consequently, the variation of the resultant disturbance amplitude undergone by the quartz crystal obeys a $1/f^2$ law. The same results are true for the vertical position oz'.

3.V Conclusions

Whilst being subjected to a sinusoidal vibration, the quartz resonator gives out a frequency which is modulated by the vibration frequency. The modulation increases as the vibration frequency drops and as the acceleration increases.

Finally, the position of the crystal determines the size of the disturbance effect.

Chapter 4 Vibration of the quartz resonator supports

The behaviour of the quartz resonator is modified by its supporting elements which, by their natural resonance, can induce considerable disturbances in the quartz crystal.

We shall examine the quartz crystal with two supports, which is the traditional method of manufacture, by considering, successively, the transverse bending vibrations and the symmetrical vibrations of an arched structure.

4.I Transverse bending vibrations

The model used is shown in Fig 29. The mass M represents the quartz crystal and the support housing is animated by a sinusoidal vibration[15,16].

The general equation for free transverse vibrations of a bar can be written:-

$$\frac{\partial^2}{\partial x^2}\left[EI\,\frac{\partial^2 y}{\partial x^2}\right] = -\rho S\,\frac{\partial^2 y}{\partial t^2} \qquad (76)$$

where $y(x,t)$ defines the transverse displacement of the centre of the section

E = Young's modulus

I = the bending moment of inertia

ρ = the density

S = the cross-section of the bar.

In the case where E and I are constants, the equation becomes:-

$$\frac{\partial^2 y}{\partial t^2} + \frac{EI}{\rho S}\frac{\partial^4 y}{\partial x^4} = 0 \quad . \tag{77}$$

The use of normalised functions $Y(x)$ gives a solution of the form:-

$$y(x,t) = Y(x)e^{i\Omega t} \tag{78}$$

where $$Y(x) = a\cosh \alpha x + b \sinh \alpha x + c \cos \alpha x + d \sin \alpha x \tag{79}$$

with

$$\alpha^4 = \Omega^2 \frac{\rho S}{EI} \tag{80}$$

a, b, c and d are constants of integration defined by the limiting conditions imposed by the methods of fixing the supports.

In our case, the support housing was excited at the pulse-rate Ω by a forced-vibration

$$y = A \sin \Omega t \quad .$$

The limiting conditions are:-

- at the housing

$$v(o,t) = A \sin \Omega t \rightarrow Y(0) = A \tag{81}$$

$$\left(\frac{\partial y}{\partial x}\right)_{x=0} = 0 \rightarrow Y'(0) = 0 \qquad \text{for} \begin{cases} a + c = A \\ \alpha(b + d) = 0 \\ \alpha \neq 0 \end{cases} \qquad \ldots\ldots \tag{82}$$

- at the free end

$$Y''(L) = 0 \tag{83}$$

because the flexing moment is zero.

However, the force $T = -EIY'''(x)$ is equal to the inertial force due to the mass

$$-M\left(\frac{\partial^2 y}{\partial t^2}\right)_{x=L}$$

and hence

$$EIY'''(L) = -M\Omega^2 Y(L)$$

$$Y'''(L) = -\frac{M\Omega^2}{EI} Y(L) \quad .$$

Now:-

$$\frac{M\Omega^2}{EI} = \frac{M\alpha^4}{\rho S} = \frac{M\alpha^4 L}{\rho SL} = \frac{M}{m}\alpha^4 L$$

where m is the mass of the lamina

and

$$Y'''(L) = -\frac{M}{m}\alpha^4 L Y(L) \quad . \tag{84}$$

By putting $\mu = M/m$ and taking into account equation (82), $Y(x)$ becomes:-

$$Y(x) = a(\cosh \alpha x - \cos \alpha x) + b(\sinh \alpha x - \sin \alpha x) + A \cos \alpha x \tag{85}$$

and equation (84) gives:-

$$a(\sinh \lambda - \sin \lambda) + b(\cosh \lambda + \cos \lambda) + A \sin \lambda = \mu\lambda [a(\cosh \lambda - \cos \lambda) + b(\sinh \lambda - \sin \lambda) + A \cos \lambda]$$

..... (86)

where $\lambda = \alpha L$,

Equation (83) becomes:-

$$a(\cosh \lambda + \cos \lambda) + b(\sinh \lambda + \sin \lambda) - A \cos \lambda = 0 \tag{87}$$

a and b can be calculated from equations (86) and (87):-

$$a = \frac{A}{\Delta} [2\mu\lambda \cos \lambda \sinh \lambda + \sin \lambda \sinh \lambda + \cos \lambda \cosh \lambda + 1] \tag{88}$$

$$b = \frac{A}{\Delta} [+ 2\mu\lambda \cos \lambda \cosh \lambda + \cos \lambda \sinh \lambda + \cosh \lambda \sin \lambda] \tag{89}$$

where $\Delta = \mu\lambda(\sin\lambda\cosh\lambda - \cos\lambda\sinh\lambda) - \cos\lambda\cosh\lambda - 1$ (90)

and

$$y(x,t) = \frac{A\sin\Omega t}{\Delta}\Big\{(\cos\alpha x - \cosh\alpha x)(1 + \sin\lambda\sinh\lambda + \cos\lambda\cosh\lambda + 2\mu\lambda\cos\lambda\sinh\lambda) + (\sinh\alpha x - \sin\alpha x)(\sinh\lambda\cos\lambda + \cosh\lambda\sin\lambda + 2\mu\lambda\cos\lambda\cosh\lambda) + \cos\alpha x\left[\mu\lambda(\sin\lambda\cosh\lambda - \cos\lambda\sinh\lambda) - \cos\lambda\cosh\lambda - 1\right]\Big\}. \quad \ldots\ldots (91)$$

When the imposed pulse-rate Ω is such that $\Delta = 0$, the lamina begins to resonate. This happens when Ω coincides with one of its normal free mode pulse-rates.

We require the first root of the transcendent equation (90), in which $\mu = 34$, because the mass of the quartz crystal, $M = 0.785$ g, is supported by two strips of mass $m = 11.6$ mg.

We find

$$\lambda_0 = 0.544$$

and from $\lambda = \alpha L$ and $\alpha^4 = \Omega^2\frac{\rho S}{EI}$ we can deduce the pulse-rate Ω for which the system begins to resonate:-

$$\Omega_0 = \frac{\lambda_0^2}{L^2}\left[\frac{EI}{\rho S}\right]^{\frac{1}{2}} . \quad (92)$$

We have designed a mounting analogous to the quartz crystal support (Fig 30), in which the resonator is replaced by a circle of duralumin. Since their densities are similar, the crystal dimensions can be maintained. To this circle is cemented a miniature accelerometer of very low mass (140 mg) and the whole is equal to the mass of a partial quartz crystal 5, that is to say 0.785 g. The accelerometer is a pietzite which gives a load variation at the amplifier input. An automatic sweep of the excitation frequency is made and a recording is made of the output voltage corresponding to the response of the element under study as a function of frequency. The system is shown, schematically, in Fig 31.

As a numerical example, let:-

$$\lambda_0 = 0.544$$
$$L = 14 \times 10^{-3} \text{ m}$$
$$E = 2 \times 10^{11} \text{ N/m}^2$$
$$I_a = \frac{10^{-13}}{12} \text{ m}^4$$
$$\rho = 8.9 \times 10^3 \text{ kg/m}^3$$
$$S = 10^{-7} \text{ m}^2$$
$$I_b = \frac{10^{-15}}{12} \text{ m}^4 \quad .$$

I_a and I_b are the moments of inertia corresponding to positions (a) and (b), respectively, of Fig 29.

For position (a) we have, by applying equation (92):-

$$\frac{\Omega a}{2\pi} = 329 \text{ Hz} \quad .$$

Fig 32 shows the response curve for such a case and indicates the presence of the main resonance peak at 281 Hz. This is confirmed by experiment. The difference between the two values is easily explained by the choice of an analytical model which is not an exact counterpart of the real case.

For position (b), $\frac{\Omega b}{2\pi} = 33$ Hz. This is the position which offers the smallest moment of inertia to flexing. Referring to Fig 27, we see that for 30 Hz, the disturbance A_Ω/A_0 has the greatest value. This shows the direct action of the support in such a case.

The solution $y(x,t)$ also enables us to find the pulse-rate for which the displacement of the mass is zero, by solving the equation $y(L,t) = 0$. We shall not do this, here, as it is only of limited interest.

4.II Symmetrical vibrations of an arched beam

The assembly of two supports and the crystal forms an arched beam. We have studied its symmetrical vibrations whilst neglecting the longitudinal and transverse vibrations of the strips. Also, the model used is that of an arched beam with its load distributed over its horizontal part (Fig 33).

The method is to find the static deformations of the beams and to introduce these into the system energy.

Consider O_2J (Fig 34a).

To find the static deflexion δ in J we superimpose a fictional force F on the distributed load q .

At H_2 , the flexing moment is:-

$$M_{H_2}(x) = C - \frac{q}{2}(L - x)^2 - F(L - x) \quad .$$

The deformation energy W_2 is given by:-

$$W_2 = \frac{1}{2E_2I_2}\int_0^L M_{H_2}^2(x)dx$$

$$W_2 = \frac{1}{2E_2I_2}\left[C^2L - CFL^2 + \frac{F^2 - qC}{3}L^3 + \frac{q}{4}FL^4 + \frac{q^2L^5}{20}\right] \quad . \qquad (93)$$

Considering O_1O_2 of Fig 34b, let C_1 be the couple resulting from the action of O_2J at O_2 .

$$M_{H_2}(0) = C_1$$

and

$$C_1 = C - \frac{q}{2}L^2 - FL$$

$$M_{H_1}(x) = C - L\left(\frac{qL}{2} + F\right) - \phi(L_1 - x)$$

and

$$W_1 = \frac{1}{2E_1I_1}\int_0^{L_1} M_{H_1}^2(x)dx$$

$$W_1 = \frac{1}{2E_1I_1}\left[\left\{C^2 + \left(\frac{qL}{2} + F\right)\left[L^2\left(\frac{qL}{2} + F\right) - 2CL\right]\right\}L_1 + \left\{L\left(\frac{qL}{2} + F\right) - C\right\}\phi L_1^2 + \frac{\phi^2}{3}L_1^3\right]$$

LT
1897

..... (94)

Let $W = W_1 + W_2$ where W is the total deformation energy of the system. The deformation of $0_2 0_3$ is symmetrical with respect to J. Hence at the deformation there is a horizontal tangent J. This is expressed as $\alpha = \frac{\partial W}{\partial C} = 0$, where α represents the angle of rotation of the tangent to J. Likewise, the horizontal displacement of J is zero, from which we have $h = \frac{\partial W}{\partial \phi} = 0$.

Thus we obtain the following system:-

$$\left.\begin{aligned} &\frac{1}{2E_1I_1}\left\{\left[2C - 2L\left(\frac{qL}{2} + F\right)\right]L_1 - \phi L_1^2\right\} + \frac{1}{2E_2I_2}\left\{2CL - FL^2 - \frac{q}{3}L^3\right\} = 0 \\ &\frac{1}{2E_1I_1}\left\{\left[L\left(\frac{qL}{2} + F\right) - C\right]L_1^2 + \frac{2}{3}\phi L_1^3\right\} = 0 \end{aligned}\right\} \quad (95)$$

which allows the calculation of C and ϕ in terms of F. Now F is fictional, and hence equal to zero:-

$$C = \frac{qL^2}{6}\left(\frac{4E_1I_1L + 3L_1E_2I_2}{E_2I_2L_1 + 4E_1J_1L}\right) - \frac{qL^2}{6}B \quad (96)$$

$$\phi = \frac{2qL^2}{L_1}\left(\frac{E_1I_1L}{E_2I_2L_1 + 4E_1I_1L}\right) - \frac{2qL^2}{L_2}B\,. \quad (97)$$

We can also determine $\delta_J - \frac{\delta W}{\delta F}$:-

Translator's note This equation cannot be read from the copy supplied for translation at the bottom of page 38. (98)

We now calculate the beam deflections:

For $0_1 0_2$:-

$$E_1I_1y_1''(x) = -M_{H_1}(x)$$

and

$$E_1I_1y_1(x) = \frac{qL^2}{12}(3 - B - 12D)x^2 + q\frac{L^2}{3L_1}Dx^3\,.$$

For 0_2J :-

$$E_2 I_2 y_2''(x) = - M_{H_2}(x)$$

and

$$E_2 I_2 y_2(x) = q\frac{x^4}{24} - \frac{qL}{6}x^3 + \frac{qL^2}{12}(3 - B)x^2 + \frac{qL^3}{6}(B - 1)x \quad .$$

In order to study the vibrations of the arched beam we put:-

$$\begin{cases} y_1(x) = \delta f_1(x) & \text{with} \quad \dfrac{dy_1}{dt} = \delta f_1(x) \\ y_2(x) = \delta f_2(x) & \dfrac{dy_2}{dt} = \delta f_2(x) \ . \end{cases}$$

The kinetic energy of a section of the beam of length dx is:-

$$\frac{1}{2} S\rho dx \left(\frac{dy}{dt}\right)^2$$

and the total kinetic energy of the whole arched beam will be:-

$$T = \frac{\delta}{2} S\rho \left[2 \int_0^L f_2^2(x)dx + 2 \int_0^{L_1} f_1^2(x)dx \right] . \qquad (99)$$

The sum of the total deformation energy $W = W_1 + W_2$ and the total kinetic energy T is constant, since the system is not dissipating.

Hence $W + T$ = constant and we shall calculate $f_1(x)$ and $f_2(x)$.

$$f_1(x) = \frac{8E_2 I_2}{AE_1 I_1 L^2}\left[\frac{3 - B - 12D}{4}x^2 + \frac{D}{L_1}x^3\right]$$

$$f_2(x) = \frac{4E_2 I_2}{AE_1 I_1 L^4}\left[\frac{x^4}{4} - Lx^3 + 2L^3 x\right] \quad .$$

On order to calculate the coefficients A, B and D we shall use the following numerical values:-

$$I_1 = \frac{10^{-15}}{12}\ m^4\ , \qquad E_1 = 2 \times 10^{11}\ N/m^2\ , \qquad L_1 = 1.4 \times 10^{-2}\ m\ ,$$

$$I_2 = 5.61 \times 10^{-12}\ m^4\ , \quad E_2 = 6.64 \times 10^{10}\ N/m^2\ , \quad L = 7.5 \times 10^{-3}\ m\ ,$$

from which we obtain:-

$$\begin{aligned} A &= 4.999 = 5 \\ B &= 2.999 = 3 \\ D &= 3.355 \times 10^{-5}\ . \end{aligned}$$

Thus we obtain:-

$$\int_0^{L_1} f_1^2(x)dx = 4.756\ \frac{L_1^5}{L^4}$$

$$\int_0^{L_2} f_2^2(x)dx = 4.284 \times 10^8 L$$

and:-

$$T = S\rho\delta^2\left[4.756\ \frac{L_1^5}{L^4} + 4.284 \times 10^8 L\right] = \beta\delta^2\ .$$

Similarly:-

$$W_1 = 1.25\ \frac{q^2 L^4 L_1}{2E_1 I_1}$$

$$W_2 = 0.3\ \frac{q^2 L^5}{2E_2 I_2}\ . \qquad (100)$$

By replacing δ by its value in W_1 and W_2 we have:-

$$W = 11.5 \left(\frac{0.3L}{E_2 I_2} + \frac{1.25 L_1}{E_1 I_1} \right) \left(\frac{E_2 I_2}{L^2} \right)^2 \delta^2 = \alpha \delta^2 \quad .$$

and since $W + T = \text{constant}$ we find:-

$$\delta + \frac{\alpha}{\beta} \delta = 0 \quad , \qquad \text{where } \Omega^2 = \frac{\alpha}{\beta} \quad . \qquad (101)$$

Hence:-

$$\Omega^2 = \frac{11.5 \left(\frac{0.3L}{E_2 I_2} + \frac{1.25 L_1}{E_1 I_1} \right) \left(\frac{E_2 I_2}{L^2} \right)^2}{S\rho \left(4.284 \times 10^8 L + 4.756 \frac{L_1^5}{L^4} \right)} \quad .$$

Calculation gives

$$\frac{\Omega}{2\pi} = 2166 \text{ Hz} \quad .$$

Consequently, if the arched beam is excited at this frequency it will start to resonate. We have checked this by experiment on a model which was dynamically similar to the resonator (Fig 35).

The main resonance appears at about 2000 Hz as shown in Fig 36.

The method used to obtain this frequency is based on the hypothesis of a small, static deformation, which is justified here. On the other hand, the hypothesis of a purely-solid fixing for the strips is much more difficult to satisfy in practice. This would explain the differences between the theoretical and experimental values.

In the two cases studied, the overpressure due to the resonance vibration of the supports is in excess of 25 dB, giving a coefficient of 18 which multiplies the acceleration of the applied vibration. For a small acceleration, 2 g for example, some 36 g are obtained at resonance, which could lead to breakage or at least a high degree of degradation in both the supports and the crystal.

We have, therefore, sought to obtain a type of support for which the response shows no over-pressure in the range 20-2000 Hz.

Our choice has fallen on four supports of trapezoidal profile, held by thermo-compressed rivets (Fig 37). The ENSCMB piezoelectric laboratory have constructed several of these resonators which have withstood sinusoidal vibrations with high accelerations and have enabled the measurements to be completed.

The vibration experiments were carried-out on an analogue model (Fig 38) which gave a response which was perfectly flat over the range of frequencies being considered (Fig 39). Above 3000 Hz the exciter itself is resonating and the response from the model is false. The slope of the response curve shows a slight over-pressure, equal to 1.4, at 2000 Hz.

4.III Conclusions

The influence of the resonator supports is not negligible since they introduce natural modes of vibration which can lead to destruction of the quartz crystal. The resonator is sensitive to low-frequency vibrations and the supports themselves should not increase this effect. The choice of four supports seems capable of supplying the requirements of mechanical strength in a severe environment.

Chapter 5 Influence of 'white noise' vibration on the resonator

The study is similar to that for sinusoidal vibrations but, with 'white noise' the disturbance covers all frequencies within the chosen range. The measurement principle is the same. The disturbances applied were in the range 20 to 2000 Hz, adjustable in 80 steps, each of 25 Hz. The power spectral density of the acceleration was constant but the amplitude of the vibration varied as a function of frequency. The experimental apparatus was analogous to that used for sinusoidal vibrations as were also the methods of measurement and analysis.

The application of white noise allows us to define the law for the effect of the disturbance as a function of frequency. The 'response' of the crystal to this excitation is an overall one, whilst in the case of sinusoidal vibration it was a discrete one. We shall see that the results confirm those obtained for sinusoidal vibrations.

5.1 Experimental results

Once again we shall consider three particular positions for the quartz crystal. Fig 40 shows the spectrum for the undisturbed resonator when the white noise (2×10^{-1} g^2/Hz) vibration acts in the same direction as the natural vibration of the quartz crystal (vertical position ox') there are considerable increases in amplitudes for the very low frequencies (Fig 41). The power spectral

density of the frequency variations, $S_{\Delta f_0}$, satisfies a law in f^{-4}, which agrees well with a law for amplitude decrease as a function of frequency, in f^{-2}, as we showed for the sinusoidal vibrations. The same results are true for the vertical position oz' .

In the horizontal position, the quartz crystal is less sensitive to vibrations. On the other hand it is true to say that an increase in the vibration has less effect on the crystal in this case than in the previous positions. Fig 42 shows the frequency fluctuations for a vibration density of 4.50×10^{-1} g^2/Hz (about 30 g, effectively). It is obvious that the vibration density must be more than doubled in order to obtain an effect comparable with that of Fig 41. Again there appears to be an f^{-2} law for the variation of the modulation amplitude as a function of frequency. This accuracy is important because the slope was less significant in the case of sinusoidal vibrations.

5.II Long-term effect of 'white noise' vibration on the natural frequency of quartz

We know that the vibration causes either a frequency modulation, if the disturbance is sinusoidal, or fluctuations in the natural frequency of quartz if there are several modulating frequencies. It can be asked how the initial frequency behaves when the disturbance is applied for a long time, that is to say if there is a displacement in the initial resonant frequency during the vibration. For that, it is sufficient to close the servo loop and to use the method of measurement developed for the continuous accelerations. In fact, no precise law comes out of it to indicate how this initial frequency develops during the vibration period. It seems, then, that the conclusion can be drawn that the integral with time of the effect of sinusoidal or random disturbances on the quartz crystal is zero. In the same way, there appear to be no sensible variations in the resistance to motion of the resonator during sinusoidal or random vibrations. On the other hand, if the frequency of the sinusoidal excitation corresponds to a vibration frequency of the quartz crystal and support assembly, the voltages at the resonator terminals show very considerable fluctuations.

All the measurements carried-out for a white-noise excitation of the resonator confirms the previous results.

Conclusions from Part 1

In this first part we have studied the resonator alone, placed in a transmission mounting so that its parameters could be measured. For continuous acceleration measurements show that the frequency variation depends upon the

intensity and direction of the applied acceleration with respect to the crystallographic axes of the crystal. In the case of sinusoidal vibrations, analysis shows that their effect is to produce a low-frequency modulation of the quartz natural frequency. 'White noise' vibrations lead to fluctuations in the quartz crystal frequency whose amplitude spectrum varies as f^{-2}. The crystal position is still preponderant in the case of vibrations. A model of a crystal mounting is proposed which can withstand very large continuous accelerations (100 g) or vibrations of the order of 40 g within the range of frequencies used.

Part 2 - OSCILLATOR SUBJECTED TO ENVIRONMENTAL CONDITIONS

In this second part we go on to study the characteristics of an oscillator subjected to the same disturbances as was the resonator, previously. We note the main criteria which characterise the instability of an oscillator and the methods used in this case.

In order to carry-out the manipulations, we built an oscillator of medium quality in which all the electronics were made compact by moulding in resin.

This precaution enabled all the tests to be carried out using the same electronics and several resonators. In particular, and wherever possible, we carried out the environmental tests either on the electronics alone but associated with a resonator or on the complete oscillator.

Comparison between the results will enable us to show what an important role is played by the resonator.

Chapter 1 Notes on the characteristics of an oscillator

1.I Representation of a quasi-sinusoidal signal[17]

The voltage produced can be represented by:-

$$v(t) = \left[A_0 + a(t)\right] \cos \left[\omega_0 t + \phi t\right]$$

where $a(t)$ and $\phi(t)$ are random functions, which vary slowly with respect to $\cos \omega_0 t$, and which represent the amplitude and phase variations, respectively.

The instantaneous angular velocity is:

$$\omega(t) = \frac{d}{dt} (\omega_0 t + \phi t) = \omega_0 + \phi^{\circ}(t)$$

where $\phi^{\circ}(t)$ represent the fluctuations of the angular velocity about ω_0.

The effects of the amplitude fluctuations are negligible, for an ultra-stable oscillator, in comparison with the phase fluctuations and so we can write:-

$$v(t) = A_0 \cos [\omega_0 t + \phi(t)] \quad .$$

The stability of a quasi-sinusoidal signal will be studied in the spectral region (purity) and in the time field (instability I(t)).

I.II Stability in the spectral region

This is characterised by the radio frequency, phase and frequency spectra.

Thus we define the power spectral density of the frequency variations S_ϕ° of the random process $\phi(t)$ by the Fourier transform of its autocorrelation function $R_\phi^\circ(\tau)$:-

$$S_\phi^\circ(f) = \int_{-\infty}^{\infty} R_\phi^\circ(\tau) e^{-i2\pi/\tau} d\tau$$

where $R_\phi^\circ(\tau) = \overline{\phi^\circ(t)\phi^\circ(t-\tau)}$, with the bar indicating a mean value in time.

The physical spectral density $S_{\phi\ physical}^\circ(f)$, with only positive values, can be written:-

$$S_{\phi_p}^\circ(f) = \int_0^{\infty} R_\phi^\circ(\tau) \cos 2\pi f\tau \, d\tau \quad .$$

The stationary phase fluctuations can also be written as:-

$$S_\phi(f) = \int_{-\infty}^{\infty} R_\phi(\tau) e^{-i2\pi f\tau} d\tau \quad .$$

The phase and frequency spectra are related by

$$S_\phi^\circ(f) = 4\pi^2 f^2 S_\phi(f) \quad .$$

It is possible to introduce the reduced variable

$$y(t) = \frac{\phi^{\circ}(t)}{\omega_0} \quad \text{and define} \quad S_y(f) = \frac{S^{\circ}_{\phi}(f)}{\omega_0^2} \ .$$

From the experimental point of view, the phase spectrum $S_{\phi}(f)$ is obtained by analysis of the output voltage from an ideal phasemeter whose input is the signal under study.

The spectrum $S_{\phi}(f)$ arises by analysis of the output voltage from a perfect frequency discriminator to whose input is applied the signal under study.

Radio-frequency spectrum

The power spectral density $S_v(f)$ of the signal $v(t)$ gives the power distribution in the spectral region. This spectrum is obtained by direct analysis of the signal from the oscillator:

$$S_v(f) = \int_{-\infty}^{\infty} R_v(\tau) e^{-i2\pi\tau} d\tau \ .$$

For ultra-stable oscillators, the phase and radio-frequency spectra are related by the following equation when the approximation to a small modulation index is satisfied:

$$S_v(f) \doteq \frac{P}{2}\left[S_{\phi}(f + f_0) + S_{\phi}(f - f_0)\right] \ .$$

I.III Stability in the time field

The instability in the relative frequency $I(\tau)$ is characterised by the standard deviation of the frequency variations $\phi^{\circ}(t)$ measured over a period τ.

$$I(\tau) = \frac{\sigma\left[\langle \phi^{\circ} \rangle_{t,\tau}\right]}{\omega_0}$$

where $\langle \phi^{\circ} \rangle_{t,\tau}$ is a stationary, random variable which represents the mean value of the oscillator pulse rate over a period of observation τ, and hence:-

$$\langle \phi^{\circ} \rangle_{t,\tau} = \frac{1}{\tau} \int_{t-\frac{\tau}{2}}^{t+\frac{\tau}{2}} \phi^{\circ}(t')dt' = \frac{\phi\left(t + \frac{\tau}{2}\right) - \phi\left(t - \frac{\tau}{2}\right)}{\tau} \quad .$$

The variance measures the dispersion of the different values of $\langle \phi^{\circ} \rangle_{t,\tau}$ about its mean value:-

$$\sigma^2[\langle \phi^{\circ} \rangle_{t,\tau}] = \overline{[\langle \phi^{\circ} \rangle_{t,\tau} - \langle \phi^{\circ} \rangle_{t,\tau}]^2} \quad .$$

Now

$$\sigma^2[\langle \phi^{\circ} \rangle_{t,\tau}] = \overline{\langle \phi^{\circ} \rangle^2_{t,\tau}} \quad \text{since } \overline{\langle \phi^{\circ} \rangle_{t,\tau}} = 0 \quad .$$

$I(\tau)$ can be written in the form:-

$$I(\tau) = \frac{\sigma[\langle \phi^{\circ} \rangle_{t,\tau}]}{\omega_0} = \frac{\sqrt{\overline{\langle \phi^{\circ} \rangle^2_{t,\tau}}}}{\omega_0}$$

$$= \frac{\sqrt{\overline{\left[\phi\left(t + \frac{\tau}{2}\right) - \phi\left(t - \frac{\tau}{2}\right)\right]^2}}}{\omega_0 \tau} \quad .$$

1.IV Relationship between the time field and the frequency field

The variance and power spectral density of a random variable are related by the autocorrelation function.

We have:-

$$\sigma^2[\langle \phi^{\circ} \rangle_{t,\tau}] = \frac{2}{\tau^2}[R_{\phi}(0) - R\phi(\tau)] \quad .$$

Now:-

$$R_{\phi}(\tau) = \frac{1}{\pi} \int_{c}^{\infty} S_{\phi}(\omega) \cos \omega\tau \, d\omega$$

and

$$S_{\phi}^{\circ}(\omega) = \omega^2 S_{\phi}(\omega)$$

and we obtain:-

$$\frac{\sigma[\langle \phi^{\circ} \rangle t, \tau]}{\omega_0} = \frac{1}{\omega_0}\left[\frac{1}{2\pi}\int_{-\infty}^{\infty} S_{\phi}^{\circ}(\omega)\left(\frac{\sin\frac{\omega\tau}{2}}{\frac{\omega\tau}{2}}\right)^2 d\omega\right]^{\frac{1}{2}} .$$

The importance of $S_{\phi}^{\circ}(\omega)$ shows up in this equation since the instability $I(\tau)$ can be determined from $S_{\phi}^{\circ}(\omega)$.

This equation allows us to change from the representation of the stability in the spectral region to the representation in the time field.

In practice, estimations of $I(\tau)$ can only be made from a large number of measurements, independent of the frequency, over a time period τ. The characteristics in the time field are easily obtained by using time or frequency counters. This possibility has led, in addition, to theoretical justifications by recommending the use of the Allan variance.

Allan variance

If we have a system of N measurements of the relative frequency, each of duration τ :-

$$\overline{y_k} = \frac{1}{\tau}\int_{t_k}^{t_k+\tau} y(\theta)\, d\theta$$

where $k = 1, \ldots . N$

$t_{k+1} = t_k + T$,

where T is the period between the start of two successive measurements, τ is the measurement period.

The variance of this system of measurements is:-

$$\sigma_y^2(N,T,\tau) = \frac{1}{N}\sum_{n=1}^{N}\left(\bar{y}_n - \frac{1}{N}\sum_{k=1}^{N}\bar{y}_k\right)^2$$

LT
1897

which is a random variable which can be defined by its mean $\langle \sigma^2(N,T,\tau) \rangle$. Under the best case, $\langle \sigma^2(N,T,\tau) \rangle$ is very slowly convergent when $N \to \infty$. Very often $\langle \sigma^2(N,T,\tau) \rangle$ diverges (when $N \to \infty$) and in practice it is very difficult to allow N to increase indefinitely. Thus N has to be limited and adjacent measurements have to be made. The Allan variance currently used is defined by:-

$$\sigma_y^2(2,\tau,\tau) \qquad \text{denoted} \quad \sigma_y^2(\tau)$$

and corresponds to the ideal variance calculated from an infinite number of pairs of measurements.

The experimental estimate gives:-

$$\sigma_y^2(\tau) \triangleq \frac{1}{M} \sum_{k=1}^{M} \frac{(\bar{y}_{k+1} - \bar{y}_k)^2}{2} \quad .$$

This variance has the advantage that it converges for the types of noise applied, here, to the oscillators.

I.V Noise in the oscillators

Fig 43 is a schematic diagram of the oscillator. The noise arising inside the oscillation loop is called 'internal'; that of the output circuits is called 'external'.

The macroscopic noise is due to temperature variations, to shocks and to variations in the supply voltage. Their effect is most noticeable in the study of the long-term stability.

The microscopic noise is due to thermal electron agitation and to noise in the semi-conductors themselves.

Internal additive thermal noise

This arises in the oscillating loop and forms the ultimate natural disturbance suffered by the oscillator. Numerous studies have led to the following equations:-

LT
1897

$$S_\phi^\circ(f) = \frac{\omega_0^2 kT}{2PQ^2}$$

$$I(\tau) = \frac{1}{Q}\sqrt{\frac{kT}{2P\tau}}$$

where k is the Boltzmann constant

T is the effective temperature of the noise source (K)

P is the power delivered to the resonator (W)

Q is the selectivity coefficient

τ is the measurement period (s).

The stability curve for $I(\tau)$ has a slope which varies at $\tau^{-\frac{1}{2}}$.

External additive thermal noise

The effects of this noise are studied by superimposing a noise voltage $e(t)$, of thermal origin, onto the signal from the loop (and supposed to be noise-free). This noise voltage arises in the circuits external to the loop.

There appears to be a component $e_q(t)$, in quadrature with the amplitude signal A_0 , which gives rise to phase variations:-

$$\phi_e(t) \triangleq \frac{e_q(t)}{A_0}$$

and to frequency instability:-

$$I_e(\tau) = \frac{1}{\omega_0\tau}\left[\frac{P_N}{P}\left(1 - e^{-\omega_e\tau}\right)\right]^{\frac{1}{2}}$$

and if $\omega_e\tau \gg 1$

$$I_e(\tau) = \frac{1}{\omega_0\tau}\sqrt{\frac{P_N}{P}}$$

where ω_c is the filter cut-off frequency

P_N is the power of the noise generated in the output circuits

$P = \frac{A_0^2}{2}$.

This noise shows a slope of τ^{-1} for the stability $I(\tau)$.

LT
189

Scintillation noise

The physical causes of frequency 'flicker' noise are the slow and random variations, of macroscopic origin, of those parameters which define the mean frequency. The result is a frequency modulation and the observance of a $1/f$ spectrum at very low frequencies. This noise causes an instability $I(\tau)$ independent of τ ($\tau \gg 1$ second), which thus produces a limit in the oscillator stability.

1.VI. Experimental method of measuring the instability $I(\tau)$

Principle (Fig 4.4)

A frequency comparator with error multiplication is used to elaborate a frequency whose fluctuations represent K times those of the oscillator being compared. This signal, of 1 MHz + $K\Delta f$ controls a 'standard time interval generator' which supplies pulses separated by an interval equal to 10^P periods of the input signal. These pulses control the starting and stopping of a very accurate chronometer, which thus counts the duration corresponding to 10^P periods. The variations in this measurement allow us to calculate the instability in the time field for a sampling period of τ_0.

Frequency comparator with error multiplication

The frequency f_0, considered as a reference, is multiplied by a factor of 10 and then mixed with the frequency f_1 multiplied by a factor of 9. Each stage elaborates this operation. The output signal $F(t)$, therefore contains the frequency fluctuations multiplied by the coefficients of four stages.

The pass-band of the comparator input circuits is about 4 kHz. However, between stages 2 and 3, and between 3 and 4, there are two quartz filters with narrow pass-bands (about 50 Hz).

The consequences of this band width can appear in the calculation of stability:- $B = \omega_H - \omega_B$

$$\left(\frac{\sigma[\langle\phi\rangle t,\tau]}{\omega_0}\right)_B = \frac{1}{\omega_0}\left[\frac{1}{\pi}\int_{\omega_B}^{\omega_H} S_\phi^\circ \left(\frac{\sin \frac{1}{2}\omega\tau}{\frac{1}{2}\omega\tau}\right)^2 d\omega\right]^{\frac{1}{2}} .$$

To obtain the natural noise of the measurement chain it is sufficient to apply the same signal to the two circuits.

This system of measurement appears to be sufficient to study oscillator drifts, but its short-term characteristics limit it to the study of medium-quality oscillators.

In the following paragraphs we shall see that another possibility exists for measuring the stability of an oscillator when the sampling time is 1 second.

Second method of measuring $I(\tau)$ when τ = 1 second - drift measurement

A second method used to measure the stability of an oscillator over 1 second, as well as to evaluate its drift, consists of dividing the reference and oscillator signals to obtain a train of 1Hz pulses. This operation is carried out using fixed dividers ($N = 5 \times 10^6$) of high quality and of high accuracy. Each train of pulses initiates the starting and stopping of a very accurate chronometer through the intermediary of a chronology control. The accuracy of this method is limited only by fluctuations in the reference (atomic clock) and the resolution of the chronometer (± 1 µs).

The chronology control ensures that orders are given to reset to zero, to place in the memory and to record. Thus, every second, we obtain the measurement of the error, θ, between the trains of pulses from the reference and from the oscillator under test (Fig 45).

Comparison chain

Fig 46 shows a block-diagram of the system. All the measurements are recorded on magnetic tape to a given format. The sampling time τ_0 determines the rhythm by which the measurements are obtained. Each measurement is labelled with the time (minute, second, tenth of second) at which it was made. We also know the time history of the measurements, and this enables the oscillator drift to be known.

Recording

Each measurement 'word' is formed from 25 characters of which two indicate the start and end of a word. The word contains the time as well as the measurement from the two chronometers used. Individual recording blocks are formed from 99 words separated by an indication of the end of the block. Each test, containing a certain number of blocks, constitutes one set of data which is distinguished by the appropriate orders.

Depending upon the sampling time, τ_0 , the time taken to record a block varies from 20 seconds to 3 minutes.

Data analysis

The recordings are analysed with a program on an IRIS 80 computer. However, between recording and data analysis there takes place an operation which transforms the original tape (7-channel EBCDIC) into one compatible with the 9-channel EBCDIC reading-head of the computer.

The calculations carried-out give both the instability $I(\tau)$, calculated from the Allan variance, and also the drift corresponding to a measurement period of one or several recorded blocks.

Chapter 2 Oscillator subjected to a continuous acceleration

We use the two methods of measurement of the instability $I(\tau)$ which we have described earlier. The first gives $I(\tau)$ for values of τ between 1 ms and 1 second, and the second allows the oscillator drift to be found.

2.I Measurement of instability, $I(\tau)$

Analysis of the operation of the error multiplication comparator[18] shows that the instantaneous frequency which it gives out is equal to:-

$$F(t) = f_0 + K\dot{\phi}(t)$$

where f_0 is the nominal output frequency
and K is the multiplication coefficient.

From this the total phase of the signal $F(t)$ can be deduced,

$$\phi(t) = \omega_0 t + K\phi(t) \quad .$$

The phase variation during the time interval $(t, t + \tau)$ is equal to:-

$$\phi(t + \tau) - \phi(t) = \omega_0 \tau + K[\phi(t + \tau) - \phi(t)]$$

and hence:-

$$\tau_0 = \tau + \frac{K}{\omega_0}[\phi(t + \tau) - \phi(t)] \quad .$$

Now the mean value of the frequency variations during the time τ_0 can be written:-

$$\langle \phi^{\circ} \rangle_{t,\tau_0} = \frac{\phi(t - \tau_0) - \phi(t)}{\tau_0}$$

from which we have

$$\frac{\langle \phi^{\circ} \rangle t,\tau_0}{\omega_0} = \frac{\tau_0 - \tau}{\tau_0^K}$$

from which, by taking the standard deviation of each expression, we have:-

$$I(\tau) = \frac{\sigma_y(\tau)}{\tau_0^K}$$

where $$\sigma_y^2(2,\tau,\tau) = \frac{1}{m} \sum_{k=1}^{m} \left(\frac{\tau_{k-1} - \tau_k}{2} \right)^2 \quad . \qquad (102)$$

2.II Experimental results

We have traced the variations of $I(\tau)$ as a function of the applied acceleration when τ takes different values (Fig 47). It can be seen that the slopes of the curves diminish as τ decreases. It would appear, then, that the short-term instability is degraded less quickly by a continuous acceleration than is the medium-term instability. This confirms the results from the resonator alone which give the deviation of the frequency from the quartz crystal under the effect of an oscillation. This deviation corresponds, here, to an 'accelerated' drift of the oscillator frequency. Hence the long-term stability is degraded more quickly by the acceleration.

Fig 48 shows the shapes of the curves of $I(\tau)$ for a particular position of the quartz crystal and for different values of the acceleration.

Fig 49 shows the influence of the crystal position with respect to the acceleration. The measurement time τ = 100 ms is the same for all the curves. The increase in $I(\tau)$ as a function of acceleration is seen. The variations of $I(\tau)$ do not show the same slopes and this difference can be attributed, at least in part, to the method of mounting the crystal.

2.III Oscillator drift

The effect of the continuous acceleration is to cause a displacement in the 'phase-frequency' curve for the resonator. An 'accelerated' increase of the oscillator drift might thus be expected, due to the variations in the resonant frequency of the quartz crystal. Measurements of the error θ, made as described earlier (Fig 46), allow us to know the variation of θ over a known period as well as its sign with respect to the initial error, θ_0, corresponding to the oscillator at rest.

As far as drift is concerned, we can let

$$y(t) = C_0 + C_1 t + n(t)$$

where $y(t)$ is the instantaneous frequency deviation
C_0 is the frequency at $t = t_0$
C_1 is the slope of the drift
and $n(t)$ is the random noise in the oscillator.

For any one position of the quartz crystal and for a given acceleration, observation of the variations of θ over a period Δt allows $C_1(\Gamma)$ to be determined. The figure gives the variations in θ (observed every second over a period of 120 seconds) as a function of the acceleration. Fig 45 shows that if the oscillator frequency increases, θ decreases, and vice-versa, which leads to:-

$$C_1(\Gamma) > 0 \quad \text{if} \quad \Delta\theta < 0$$

$$C_1(\Gamma) < 0 \quad \text{if} \quad \Delta\theta > 0 \ .$$

Fig 50 summarises the results. The increases in θ for positions (1), (3) and (5) of the crystal should be noted. These correspond very well with a decrease in the resonator frequency (Fig 7) and hence of that of the oscillator.

Positions (2), (4) and (6), for which θ is negative, do, in fact, indicate an increase in the oscillator frequency and confirm the results found for the resonator alone.

We have tried to apply the acceleration to the electronics alone, whilst maintaining the operation of the oscillator. However, in order to do this the resonator must be placed at the centre of a rotating arm and the electronics at its extremity. This requires the use of long lengths of cable which create

variable, parasitic capacities and upset the oscillator frequency. It is not then possible to use the comparison chain for the measurement of $1(\tau)$.

Analysis of phase noise

Fluctuations in the oscillator phase have been analysed by a method described in the next chapter. The analysis shows that there is only a slight increase in phase noise for the low frequency components.

Chapter 3 Oscillator subjected to a sinusoidal acceleration

The same vibrations which were applied, previously, to the resonator alone were applied to the oscillator. All the measurements carried-out will enable the various results to be compared with those for the resonator. In order to determine the influence of the external sinusoidal vibration in the spectral region we have carried out an analysis of the oscillator phase noise.

3.I Measurement of phase noise S_ϕ (Fig 51)[19]

The reference oscillator (synthesiser) was servoed in phase with the oscillator under test. For that we used a mixer which gave a voltage proportional to the phase fluctuations outside the pass-band of the servo system. The time-constant (several seconds) reduced the servo system pass-band to very low frequencies. A low-pass filter (0 to 500 kHz) eliminated the possible component at the oscillator frequency. A low noise amplifier, of gain 1200, gave direct access for the analysis of the signal in the range 0 to 5000 Hz with a 10Hz filter. It was also possible to record the noise and to analyse it by means of a programmable spectral analyser. Both methods gave the same results and thus the phase spectrum S_ϕ was obtained.

3.II Experimental results

The oscillator was subjected, in succession, to the same sinusoidal vibrations as was the resonator. The very low frequencies appeared very clearly in the phase spectrum. With respect to the S_ϕ spectrum when the oscillation is not disturbed (Fig 52), it can be seen that the 80 Hz, 10 g (Fig 53) vibration not only appears, but that it increases the noise level by about 30 dB. A 380 Hz, 20 g vibration (Fig 54), shows a smaller effect on the oscillator phase noise. When the vibration frequency is increased, the disturbance peaks are again present in the oscillator phase spectrum. Figs 55, 56 and 57 show the effect of frequencies equal to 1750 Hz, 2700 Hz and 4080 Hz, respectively, all for the same 20 g excitation. For a frequency of around 4000 Hz, the natural resonance of the exciter intervenes to generate other frequencies, which explains the other peaks

close to the excitation frequency. The decrease in amplitude of these different peaks should be noted.

In order to obtain a direct and continuous measurement of the effect of the external vibration frequency we used the system shown in Fig 58.

The vibration generator was controlled in frequency by the spectrum analyser itself which displaced its analysis filter at a given velocity. There was also synchronisation between the external vibration frequency and the central analysis frequency. Hence we were able to obtain the oscillator phase noise and its response to a sinusoidal vibration in the range 20-2000 Hz (Fig 59).

The decrease in noise obeys a $1/f^3$ law. The position of the crystal *vis-a-vis* the disturbance is also critical.

It is interesting to note that the vibration frequencies appear, here, very clearly superimposed on the natural noise of the oscillator. In the study of the resonator, the analysis did not permit frequencies above 500 Hz to be detected. In the present case we see that the crystal is effectively sensitive to vibrations greater than 500 Hz and their detection is facilitated by the operation of the oscillator.

It can be stated that the oscillator, disturbed in this way, sees its frequency modulated at the frequency of the external vibration.

Chapter 4 Oscillator subjected to a pseudo-random 'white noise' vibration

The external vibration applied to the oscillator is contained within the range between 20 and 2000 Hz. The oscillator used was the same on as was used previously and the resonators used were those already studied in Part 1.

Analysis of applied noise

The vibrations were maintained at a constant power spectral density within the range of frequencies chosen. Spectral analysis of the applied noise showed a climbing of the spectrum beyond 2000 Hz and some peaks about 3500 Hz. These latter frequencies correspond to the resonance vibrations of the exciting element.

4.I Instability $I(\tau)$

Fig 60 shows a comparison of the results obtained when the oscillator is subjected, successively, to 3×10^3 g^2/Hz at 2.5 g_{eff}, 5 g_{eff} and 10 g_{eff} for the three usual positions. The arrangement which corresponds to the horizontal position of the quartz crystal has an instability curve whose slope is always in τ^{-1} and values greater than those for which the oscillator is not disturbed. The increase in the disturbance seems to enhance the stability degradation.

The two other vertical positions of the quartz crystal show a very high range of instability values whose mean slope is sensibly modified to the form $\tau^{-0.6}$.

This modification of the slope is no doubt attributable to the increase in the internal natural noise of the resonator.

On the other hand it would appear to be difficult to relate each instability value to a level of applied disturbance.

We have measured the instability of the same oscillator placed under the same vibration conditions but with the resonator screened from the disturbance. The measurements gave the instability curves shown in Fig 61, for which we see a slight increase, but, however, less than the smallest instability recorded when the resonator was also disturbed.

This instability appears, moreover, to be independent of the vibration applied to the oscillating electronics alone.

4.II Oscillator drift

Using the second method of measuring $I(\tau)$ when $\tau = 1$ second, we calculated the variation of the initial displacement as a function of time passed and applied acceleration. The results showed a drift which was always negative (the oscillator frequency increased) and the highest values were obtained for the two vertical positions of the quartz crystal.

4.III Phase spectrum of an oscillator disturbed by 'white noise'

We used the same experimental apparatus as has already been described for the sinusoidal vibrations. Fig 62 shows the phase spectrum S_ϕ for the undisturbed oscillator. When the quartz crystal was in the vertical position the spectrum S_ϕ was very clearly disturbed (Fig 63) within the frequency range 0 to 2000 Hz. The effect was slightly less for the horizontal position of the resonator. The phase noise returned to its normal level above 2000 Hz, and this phase noise was recorded for analysis by means of a program. The slope of the noise appeared very strongly (Figs 64 and 65) to be of the form $1/f^3$ and we have identified it with a frequency flicker noise. The curves have been superimposed in order to facilitate comparison between the spectra when the oscillator was undisturbed, (curves 1 of Figs 64 and 5 of Fig 65), then disturbed in the horizontal position (5 g curve 2, 10 g curve 3) and, finally, in the vertical position (5 g curve 6, 10 g curve 7).

Oscillator noise was measured when the electronics alone were subjected to vibration without the resonator. This analysis (Fig 66) shows that the vibration has a slight effect on the electronics by introducing a noise whose slope is again of the form $1/f^3$. However, the noise level is much less than when the quartz crystal was affected by the external vibration along with the oscillator.

In particular, for the oscillator alone, the phase noise returned to the normal level above 1000 Hz (with vibration applied within the range 20-2000 Hz), whilst in the case where the oscillator was complete, the applied white noise acted, effectively, over the whole range, that is to say up to 2000 Hz.

Conclusions from Part 2

A quartz oscillator disturbed by a continuous acceleration shows a long-term frequency variation which is a function of the intensity and direction of the applied acceleration. When subjected to a sinusoidal vibration, its frequency is modulated by the vibration frequency found in its phase spectrum.

The effect of 'white noise' is to produce a phase noise in the accelerator of form f^{-3}, that is to say a frequency noise flicker. Measurements of the instability, $I(\tau)$, show the variations as a function of the applied acceleration and of the position of the oscillator with respect to the direction of the disturbance.

It is interesting to note the presence of frequency flicker noise when the oscillator is excited with 'white noise'. It can be said, then, that the random vibrations are one of the origins of this noise, and are very important in the study of oscillator stability.

General conclusions

In the first part of this study we were interested in quartz resonators alone, subjected to steady-state, sinusoidal or random accelerations. From both the theoretical aspects and the experimental results we have been able to describe the behaviour of the crystal in each case. When it undergoes a steady acceleration, six positions determine the variation in the crystal resonant frequency perfectly, and show it to be linear, to a first approximation.

Sinusoidal or random vibrations modulate the natural frequency of the resonator at very low frequencies, or create fluctuations in the natural frequency whose spectral density varies as f^{-4}.

The different results arising from measurements on the oscillator, subject to the same disturbances, showed the importance of the contribution from the

resonator in the oscillator frequency fluctuations. It would appear, then, that the frequency fluctuations of a quartz oscillator, when subjected to severe environmental conditions, are essentially due to the effects of the disturbances on the quartz resonator.

In particular, random vibrations gave a phase spectrum in f^{-3}, that is to say a frequency noise flicker whose origin is shown in this paper.

These results should have a beneficial result in determining the best conditions for the production of quartz oscillators designed for aerospace applications.

The next studies should be orientated towards seeking new ways of cutting the quartz which might decrease the effects of the environmental conditions.

REFERENCES

No.	Author	Title, etc
1	P.C.Y. Lee *et al*	Elastic waves and vibrations in deformed crystal plates. 27th Annual Symposium on frequency control (1973)
2	R.N. Thurston	Wave propagation in fluids and normal solids. Physical Acoustics, Vol 1, part A, Academic Press, New York (1964)
3	J.J. Gagnepain *et al*	Influence of an acceleration or of an external force on the natural frequency of a resonator. (Influence d'une accélération ou d'une force extérieure sur la fréquence propre d'un résonateur à quartz) (In preparation)
4	J.J. Gagnepain	Private communication
5	M. Valdois *et al*	Influence of environmental conditions on a quartz resonator. 28th Annual Symposium on Frequency Control, Atlantic City, 29-31 May 1974
6	M. Bernstein	Quartz crystal units for G environment. 25th Annual Symposium on Frequency Control 1971
7	-	Force-frequency coefficient of singly rotated vibrating quartz plates. IBM Journal, January 1968
8	C. Pegeot	Principle and construction of an apparatus for measuring the parameters of an equivalent system of a quartz resonator. (Principe et réalisation d'un dispositif de mesure des paramètres du schéma équivalent d'un résonateur à quartz) Doctorate thesis, Besançon, March 1974
9	R. Besson	'Hysteresis' phenomenon in the piexoelectric deformation of quartz. (Phénomène "d'hystérésis" dans la déformation piézo-électrique du quartz) C.R. Acad. Sci. Paris, Vol 273, p 1078 (1971)
10	W.G. Cady	Piezoelectricity. McGraw-Hill Book Company Inc., London 1946

REFERENCES (concluded)

No.	Author	Title, etc
11	S. Butterworth	Proc. Phys. Soc. (London) Vol 27, 1915
12	Van Dyke	The elastic network equivalent of a piezoelectric resonator. Phys. Rev., Vol 40 (1932)
13	J.J. Gagnepain	Non-linear mechanisms in quartz resonators. (Mécanismes non-linéaires dans les résonateurs à quartz) Thesis, Besançon, March 1972
14	J.J. Gagnepain	Influence of a continuous electric field on the resonant frequency of a quartz crystal. (Influence d'un champ électrique continu sur la fréquence de résonance d'un cristal de quartz) C.R. Acad. Sc. Paris, Vol 276, March 1973
15	S. Timoshenko	Theory of vibrations. (Théorie des vibrations) Librairie Polytechnique, 1947
16	R. Chaleat	Course on the mechanics of vibrations. (Cours de mécanique des vibrations) Besançon (1972)
17	J.A. Barnes *et al*	Characterisation of frequency stability. IEEE Tr. Inst. Meas. Vol IM 20 - No.2, pp 105-120 (1971)
18	J. Rutman	Noise in oscillators. Application to the metrology of frequencies and wave spectroscopy. (Bruits dans les oscillateurs. Application à la métrologie des fréquences et à la spectroscopie hertzienne) Thesis, Faculty of Science, Paris VI (1972)
19	-	Specification and measurement of frequency stability. N.B.S. Report 9794

ADVANCE DISTRIBUTION:-

RMCS
ITC
DRIC 70

BAe, Hatfield
Library, NGTE

RAE

Director
DD
Weapons Library 15
Main Library

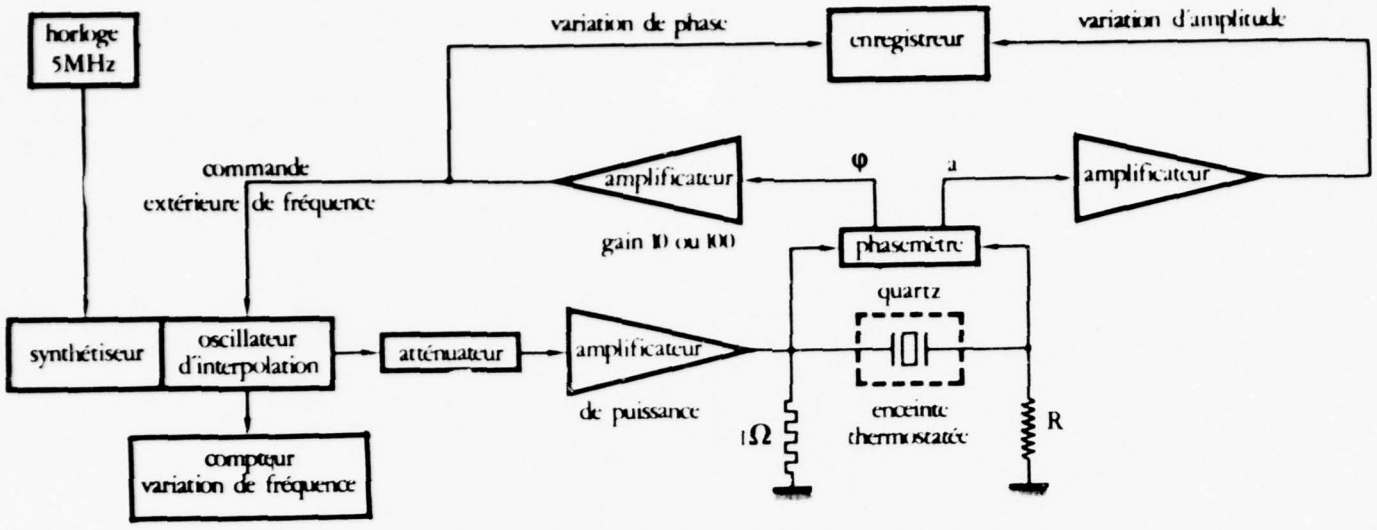

Key:

horloge 5MHz	= 5MHz clock
commande extérieure de fréquence	= external frequency control
synthétiseur	= synthesiser
oscillateur d'interpolation	= interpolation oscillator
compteur variation de fréquence	= frequency variation counter
atténuateur	= attenuator
variation de phase	= phase change
enregistreur	= recorder
variation d'amplitude	= amplitude variation
amplificateur de puissance	= power amplifier
phasemètre	= phasemeter
enceinte thermostatée	= thermostatically-controlled chamber
amplificateur	= amplifier

Fig 1 Apparatus for measuring the frequency variation of a quartz resonator

Fig 1

Figs 2-5

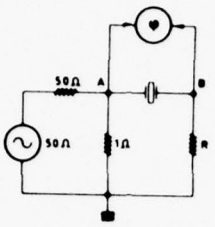

Fig 2 Layout for measuring the quartz parameters

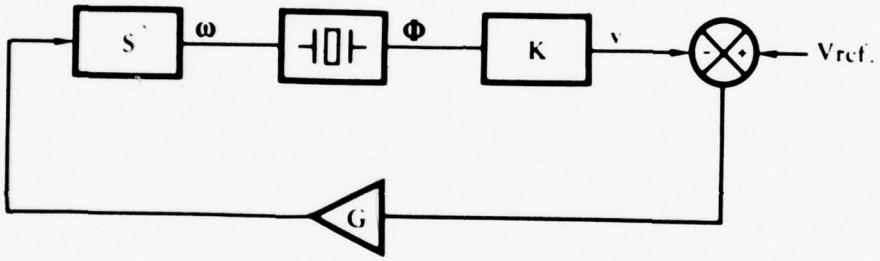

Fig 3 Servo-system

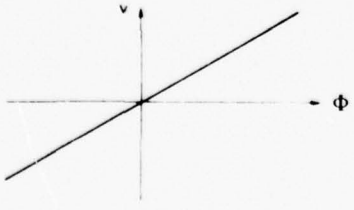

Fig 4 Phasemeter output voltage

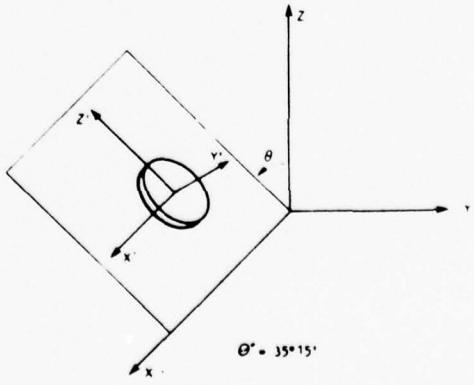

Fig 5 Quartz crystal cut along AT

LT 1897

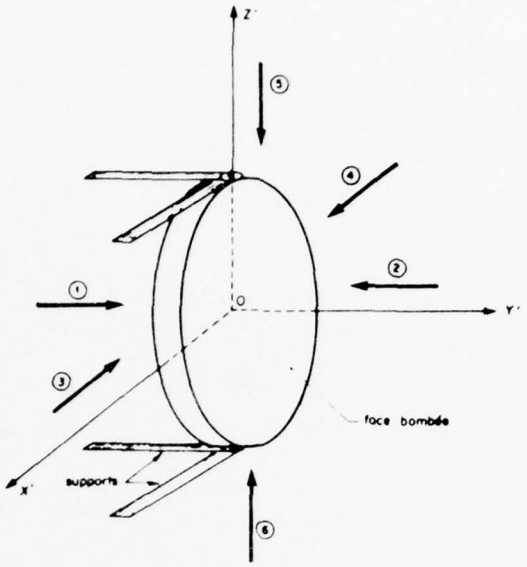

Key:
supports = supports
face bombée = convex face

Fig 6 Relative positions of the quatz crystal with respect to the directions of the acceleration

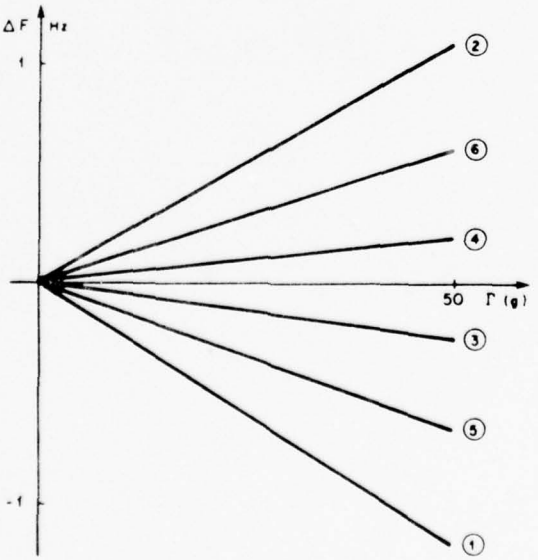

Fig 7 Frequency variations as a function of acceleration

Fig 8

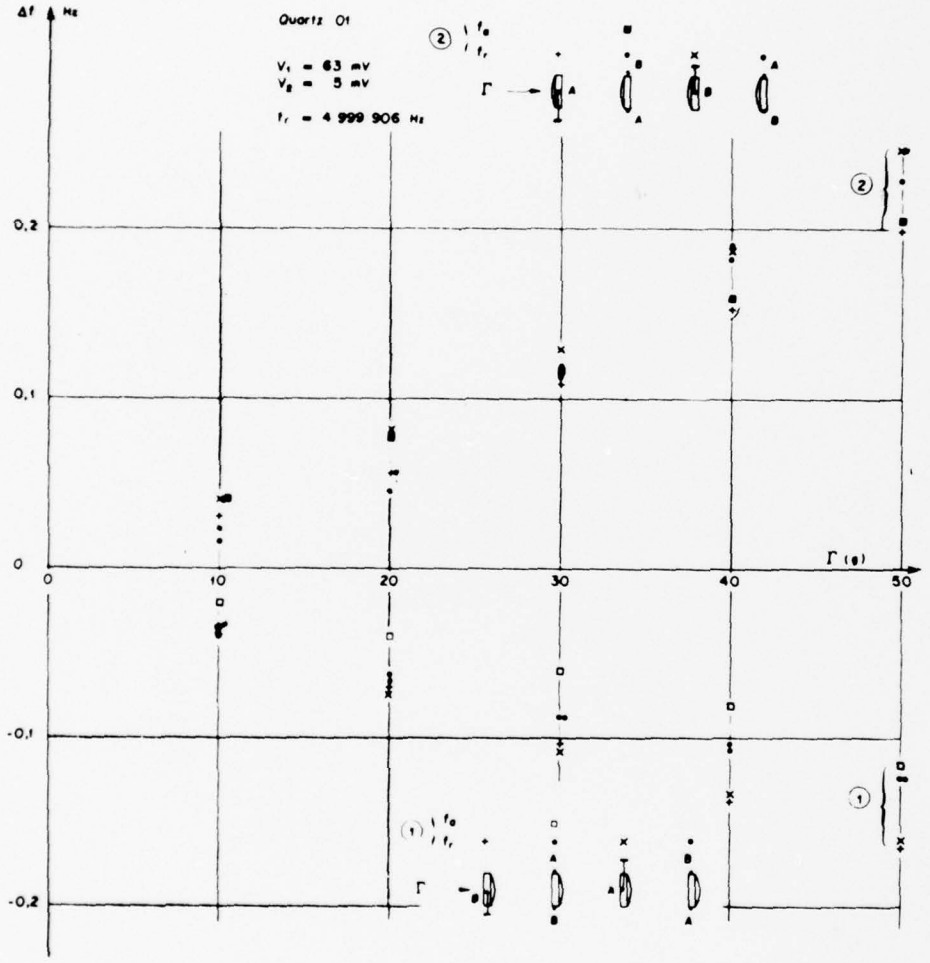

Fig 8 Variations in resonant and anti-resonant frequencies for acceleration directions (1) and (2) (*cf* Fig 6)

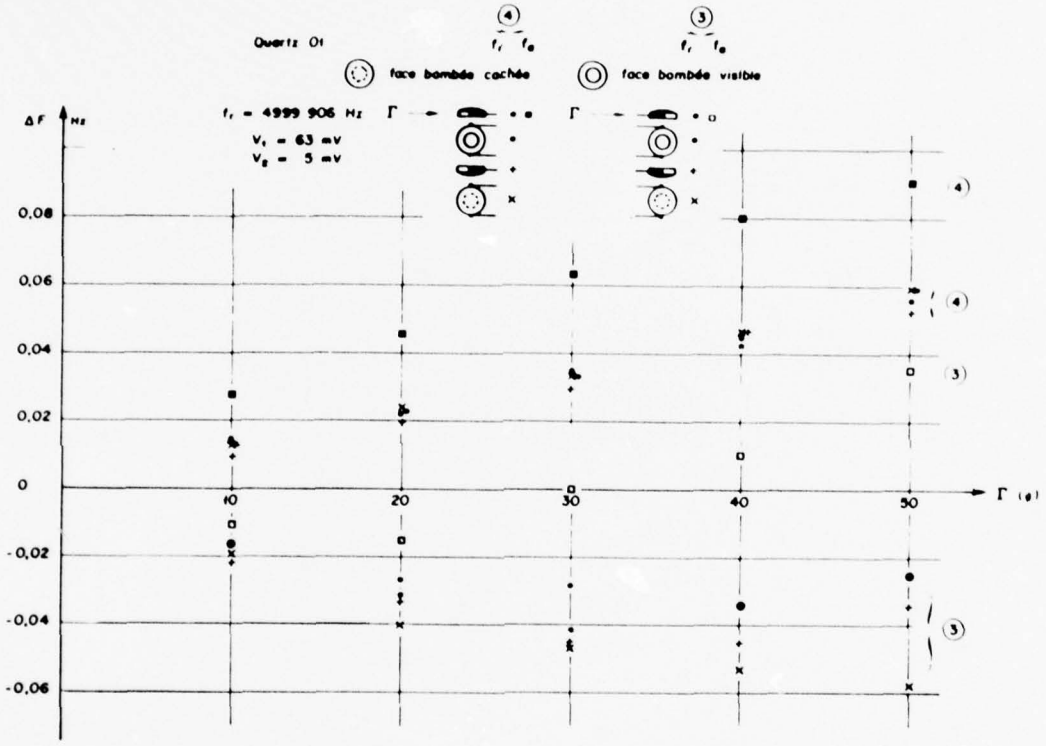

Key:
face bombée cachée = convex face hidden
face bombée visible = convex face visible

Fig 9 Variations in resonant and anti-resonant frequencies for acceleration directions (3) and (4) (*cf* Fig 6)

Fig 10

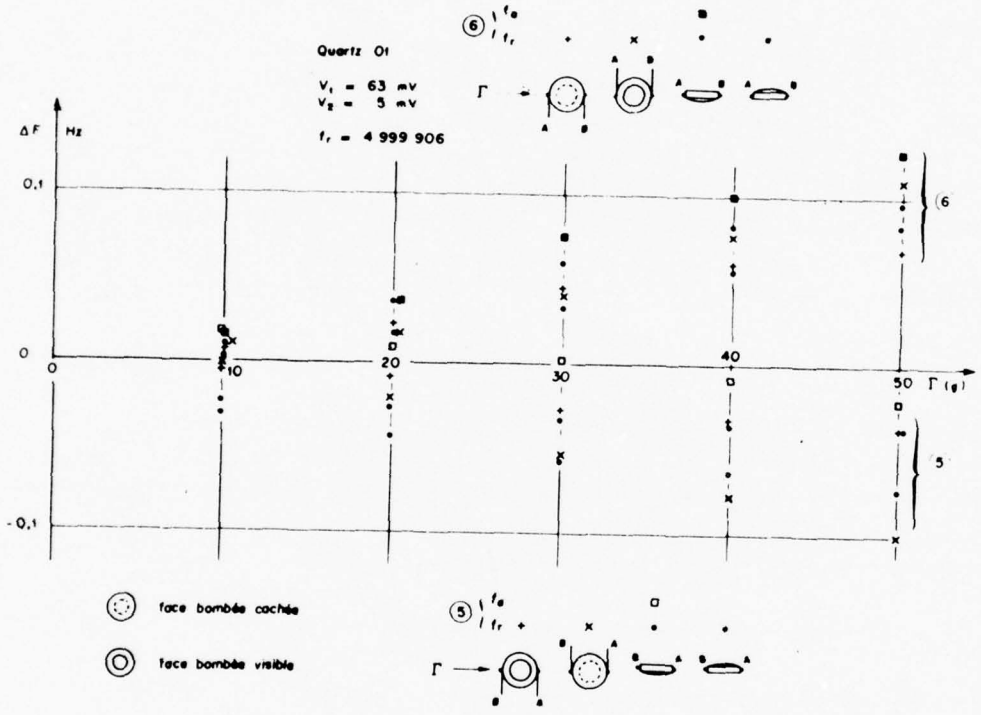

Key:

face bombée cachée = convex face hidden
face bombée visible = convex face visible

Fig 10 Variations in resonant and anti-resonant frequencies for acceleration directions (5) and (6) (*cf* Fig 6)

LT 1897

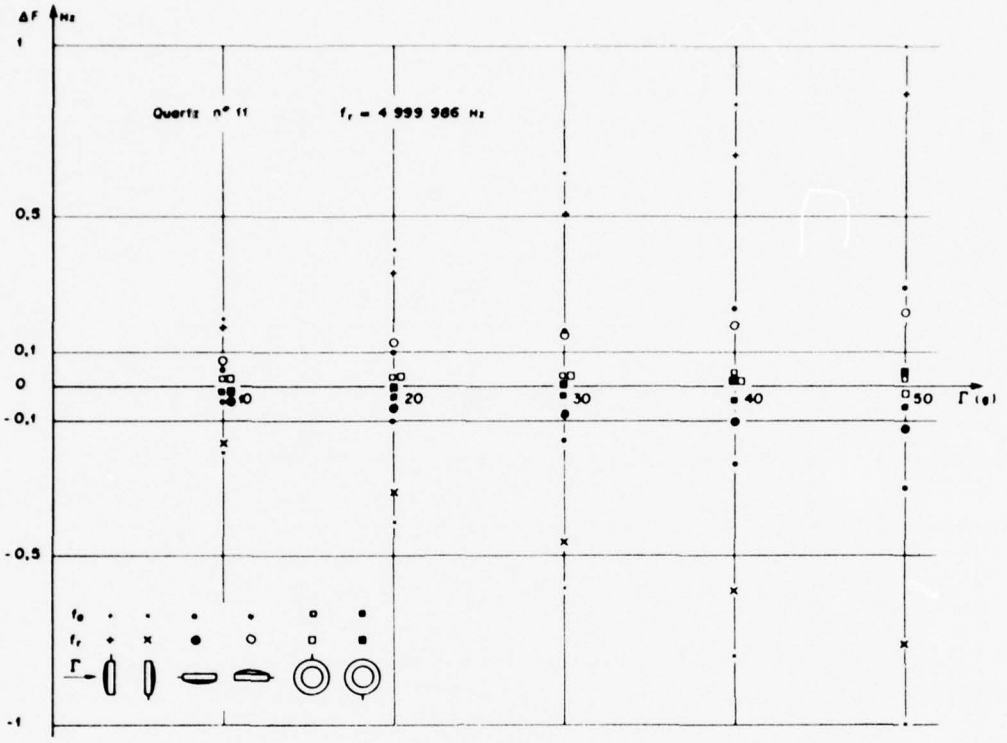

Fig 11 Frequency variation as a function of acceleration for a quartz crystal with 3 supports

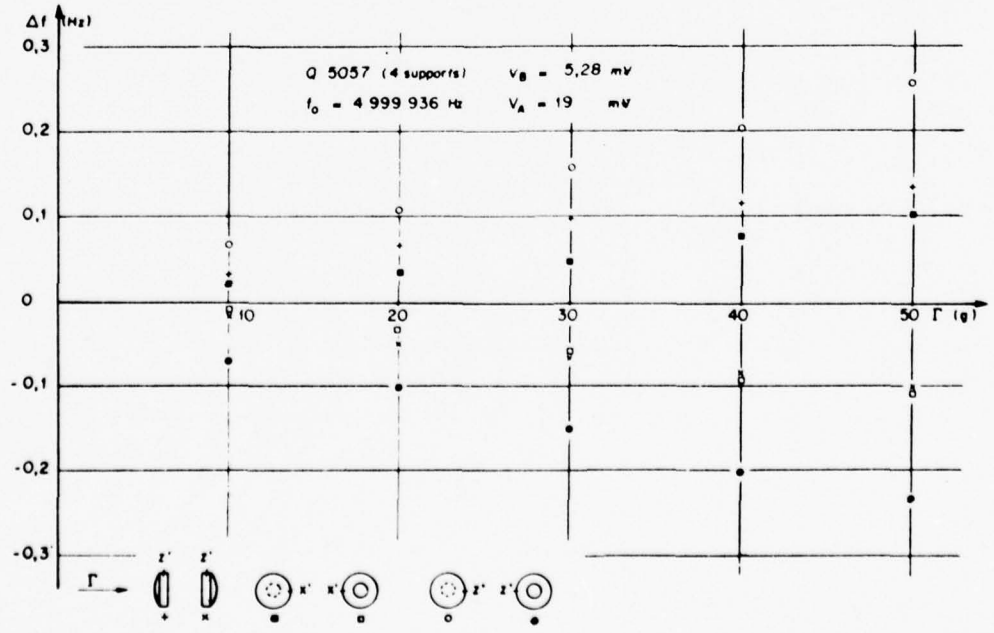

Fig 12 Frequency variation as a function of accleration for a quartz crystal with 4 supports

Figs 13&14

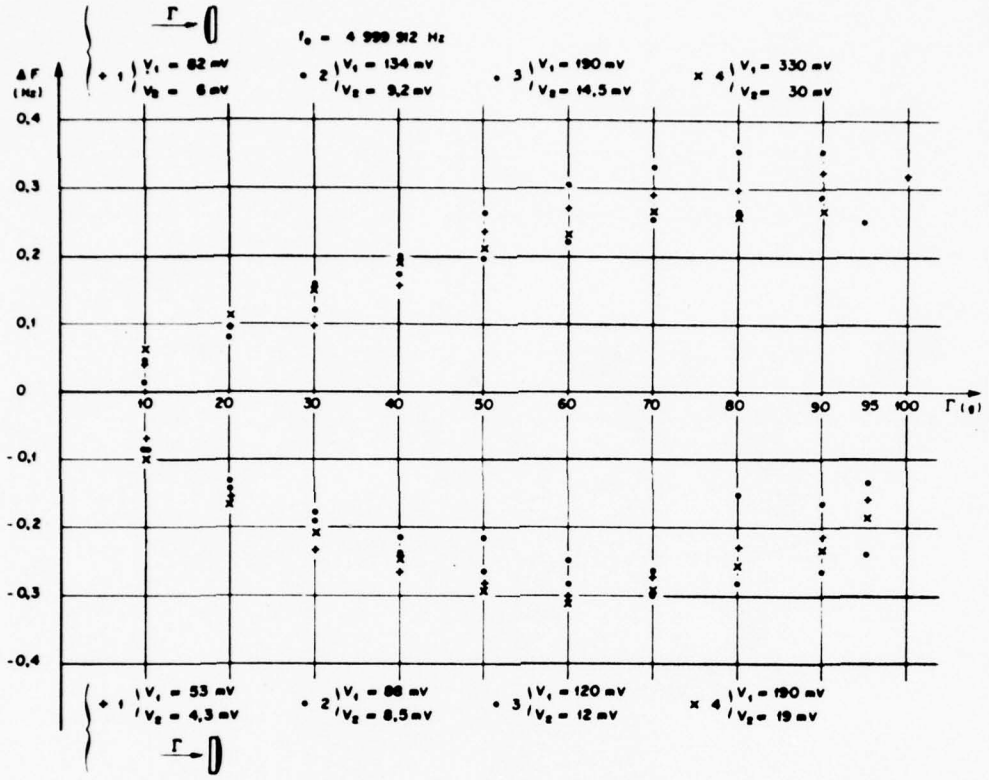

Fig 13 Effect of large accelerations on the frequency variation

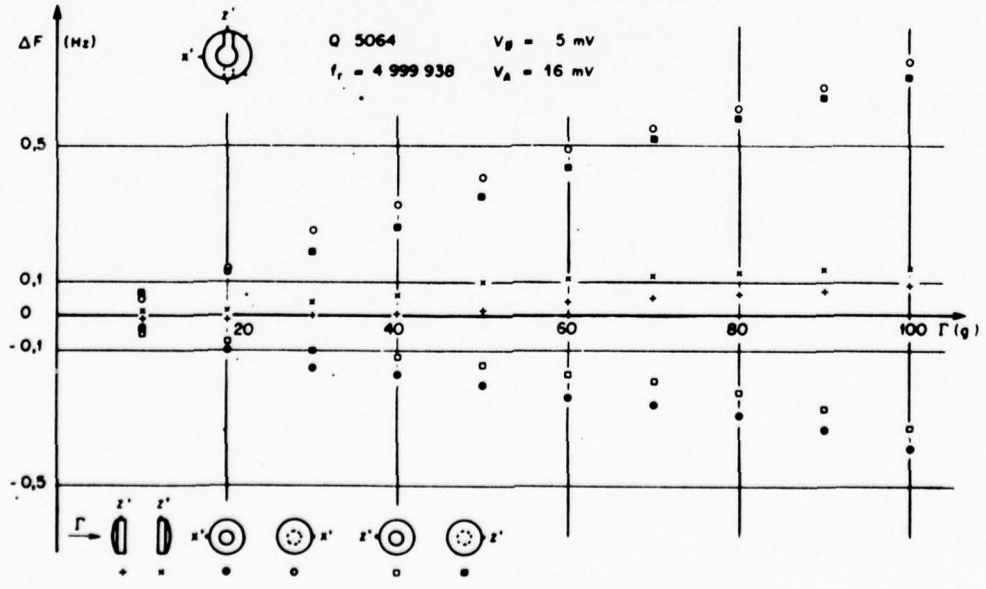

Fig 14 Influence of the support positions with respect to the quartz crystal (crystal with 5 supports)

LT 1897

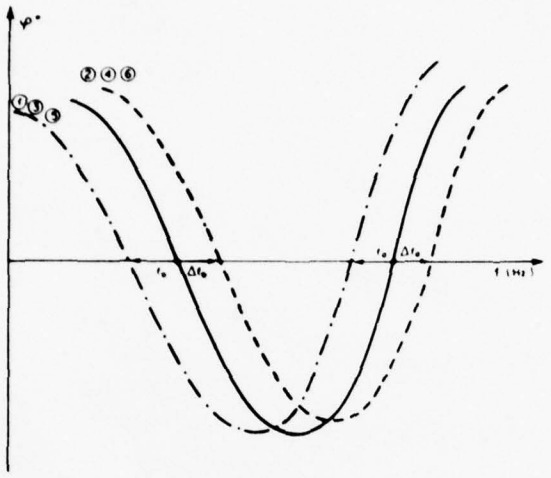

Fig 15 Displacement of the phase-frequency curve for a quartz crystal under the effect of an acceleration

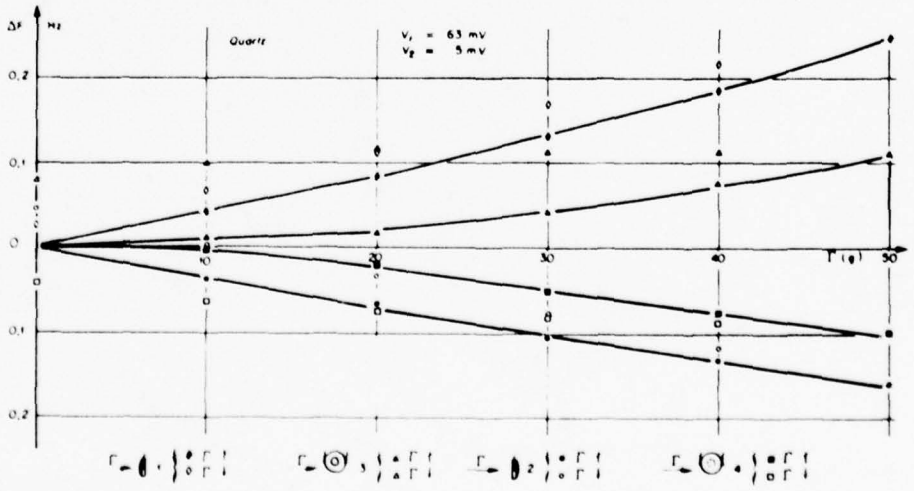

Fig 16 'Hysteresis' effect in the frequency variation

Fig 17

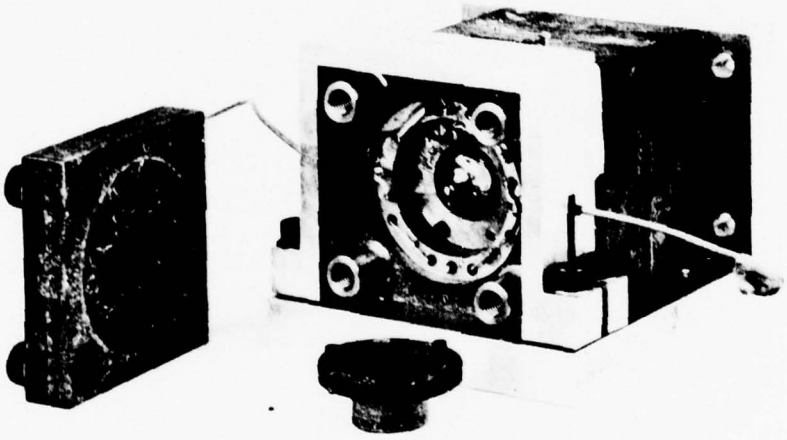

Fig 17 Thermostatically-controlled chamber for vibrations

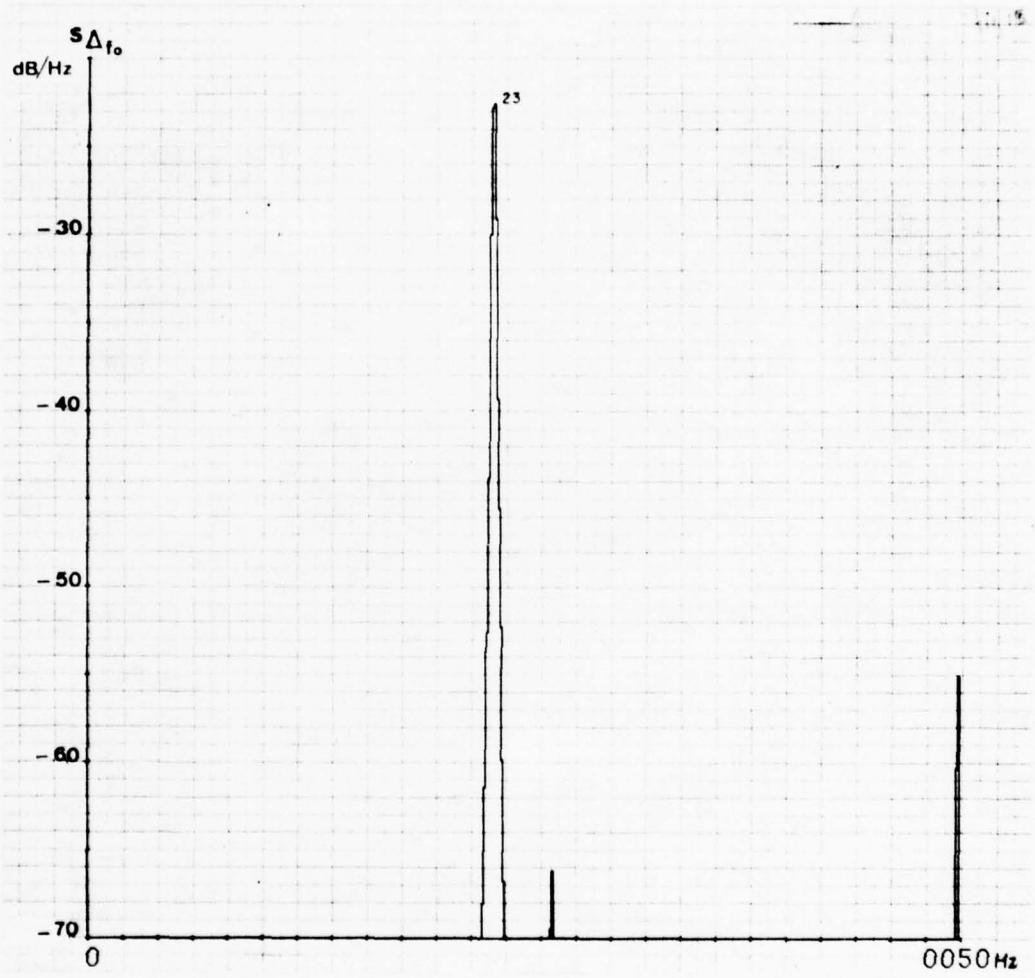

Fig 18 $S_{\Delta f_0}$ for an undisturbed quartz crystal

Fig 19

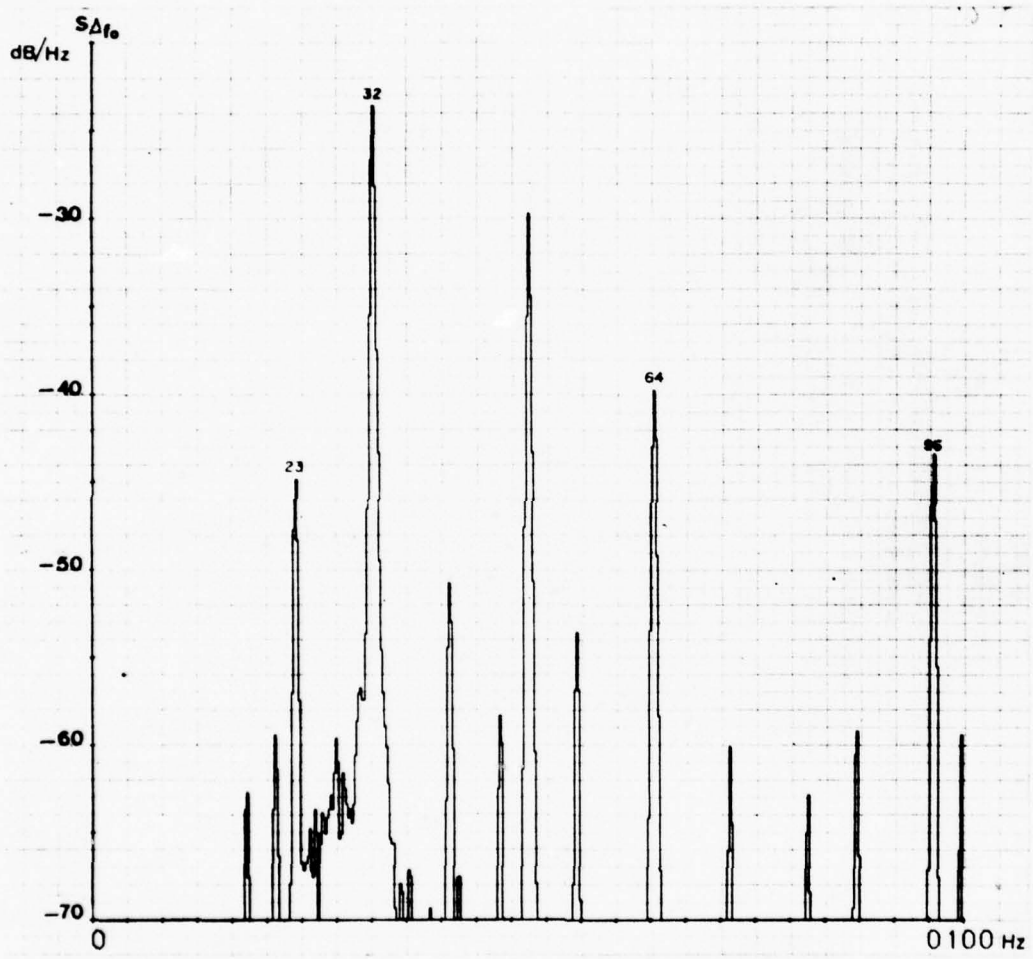

Fig 19 $S_{\Delta f_0}$ for a vibration of 32 Hz - 3 g

LT 1897

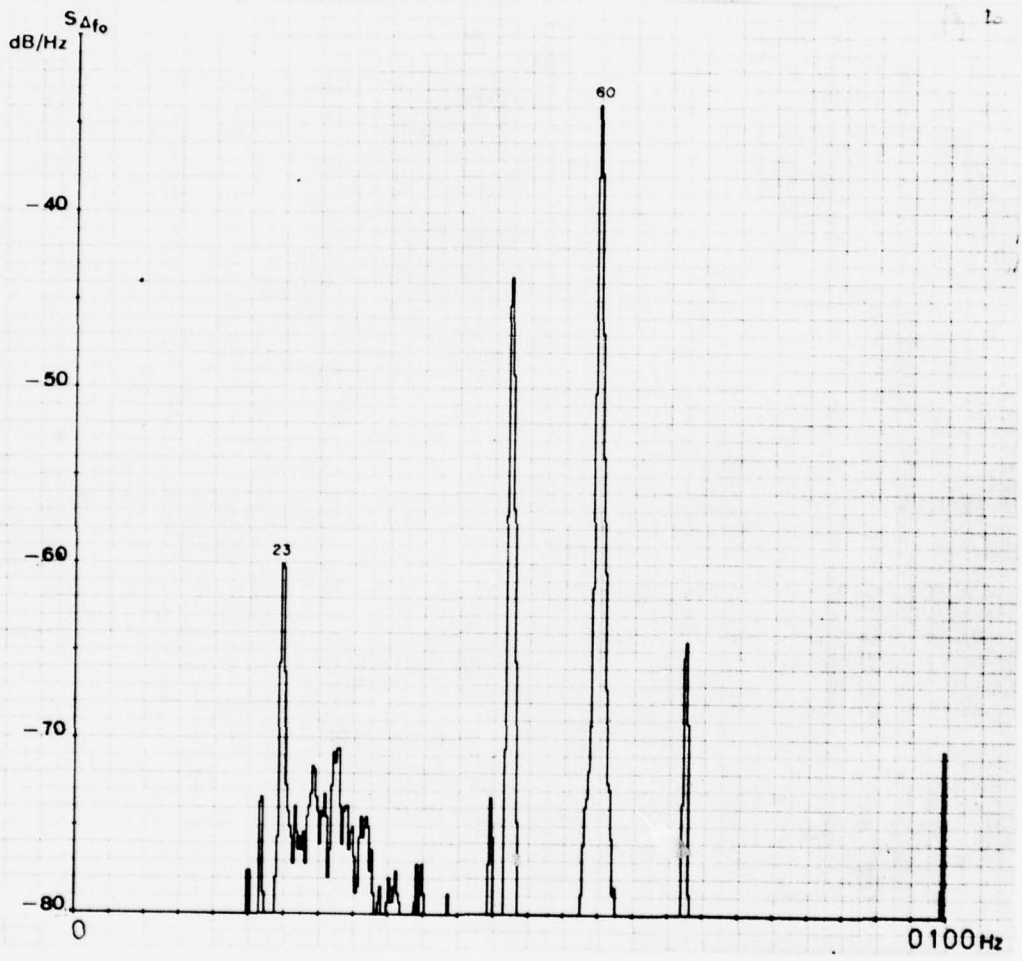

Fig 20 $S_{\Delta f_0}$ for a vibration of 60 Hz - 3 g

Fig 21

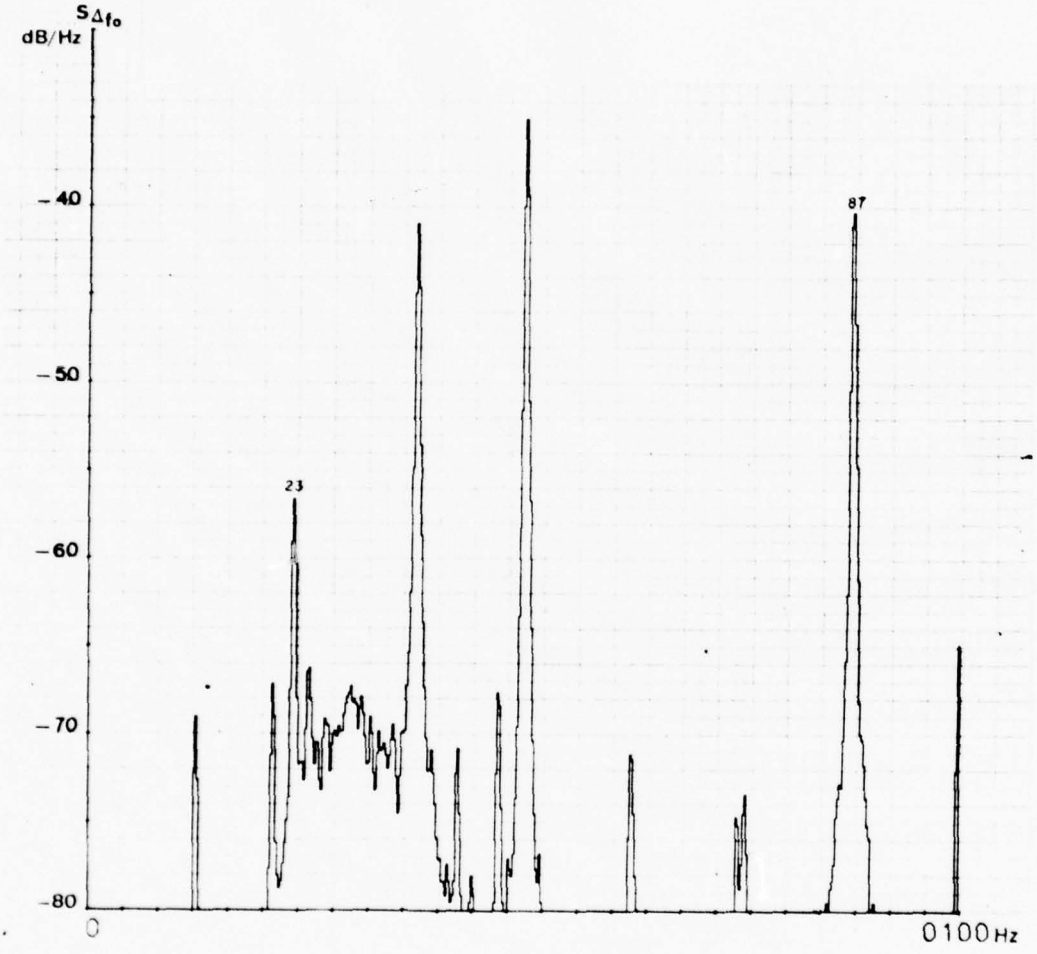

Fig 21 $S_{\Delta f_0}$ for a vibration of 87 Hz - 3 g

LT 1897

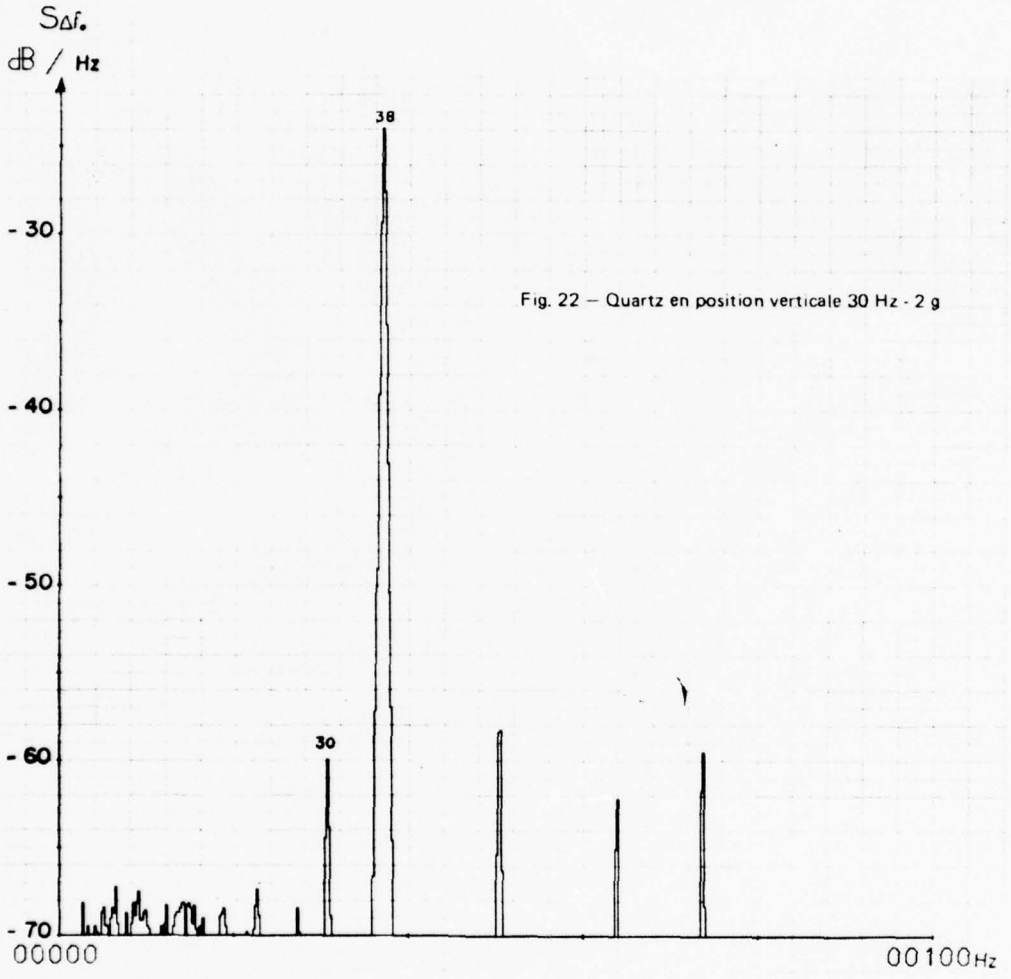

Fig. 22 — Quartz en position verticale 30 Hz - 2 g

Fig 22 Quartz crystal in the vertical position 30 Hz - 2 g

Fig 23

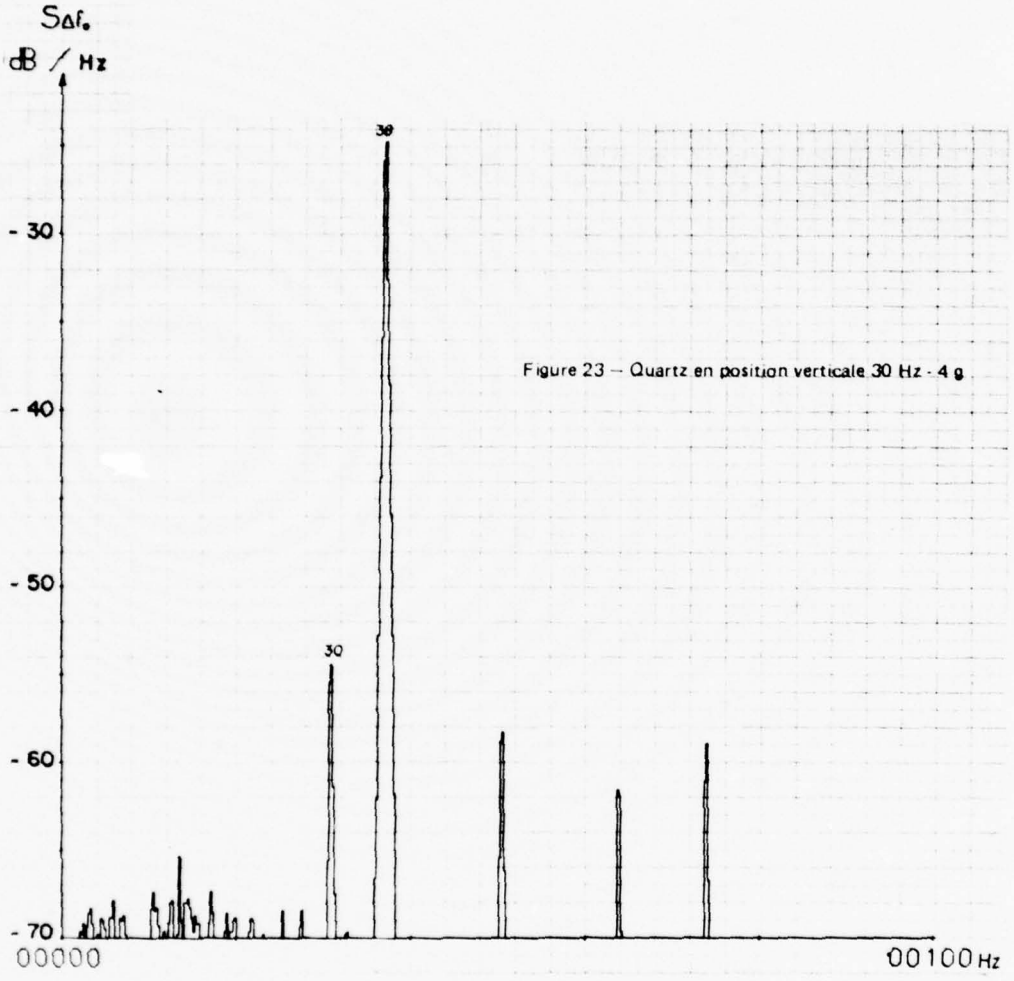

Figure 23 – Quartz en position verticale 30 Hz - 4 g

Fig 23 Quartz crystal in the vertical position 30 Hz - 4 g

LT 1897

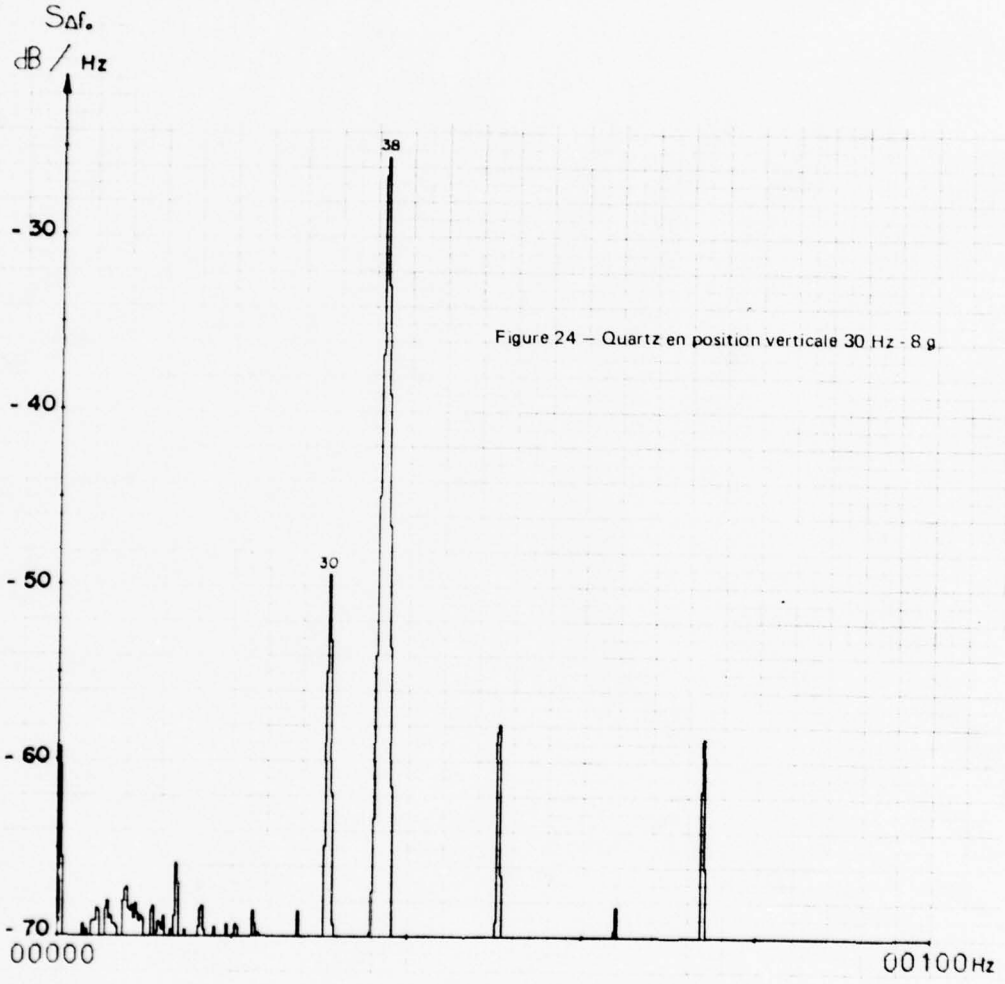

Figure 24 – Quartz en position verticale 30 Hz - 8 g

Fig 24 Quartz crystal in the vertical position 30 Hz - 8 g

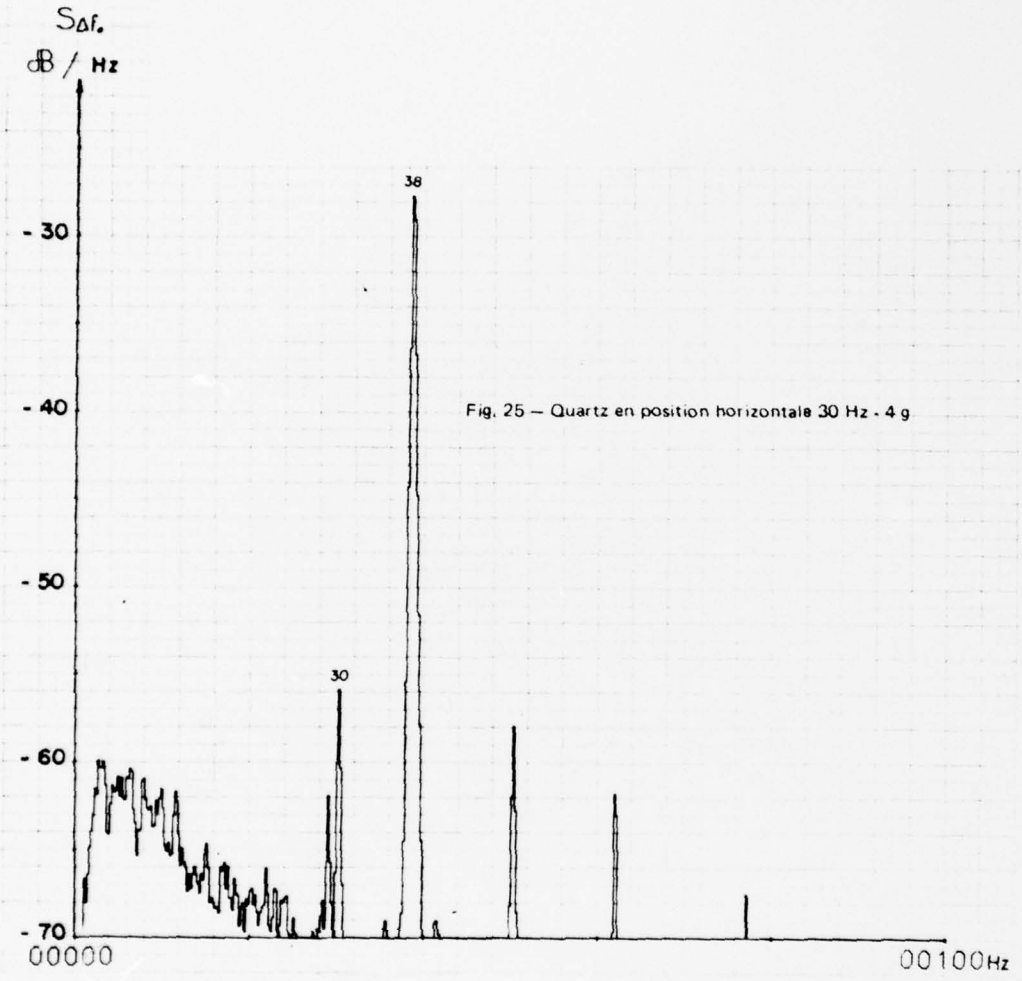

Fig. 25 — Quartz en position horizontale 30 Hz - 4 g

Fig 25 Quartz crystal in the horizontal position 30 Hz - 4 g

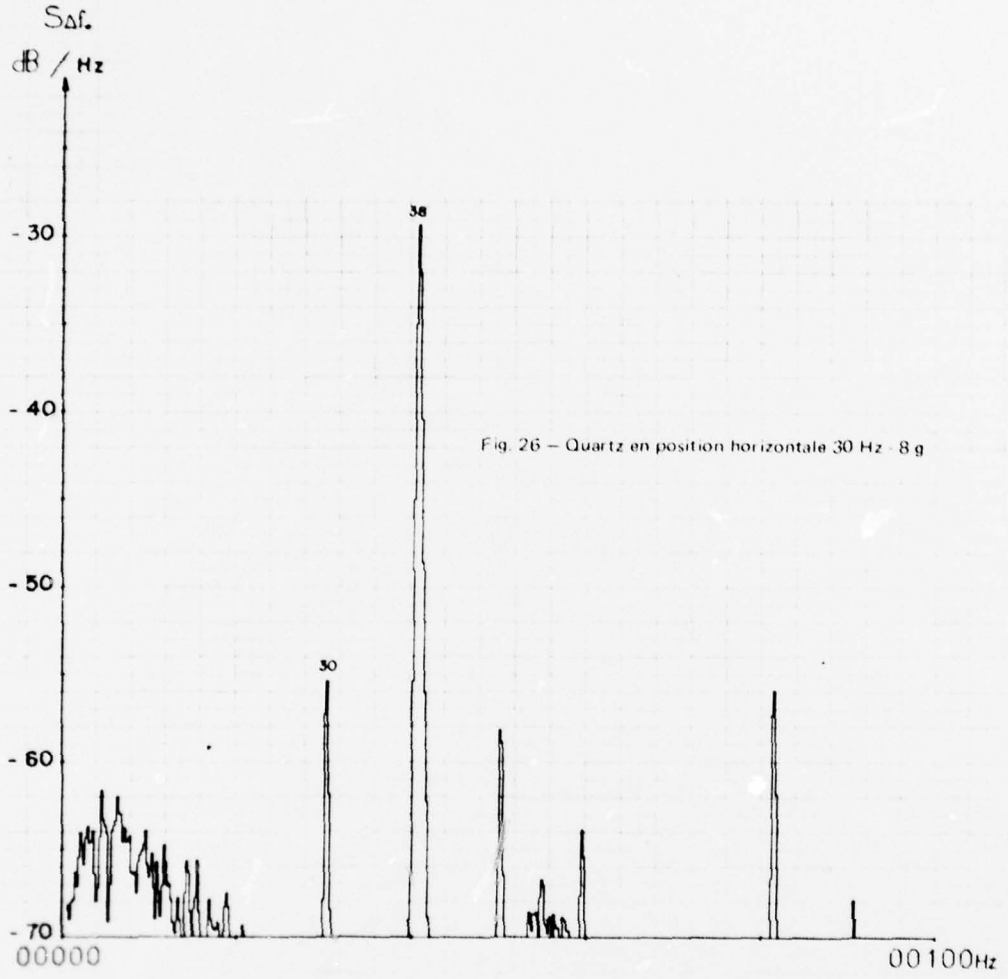

Fig. 26 – Quartz en position horizontale 30 Hz - 8 g

Fig 26 Quartz crystal in the horizontal position 30 Hz - 8 g

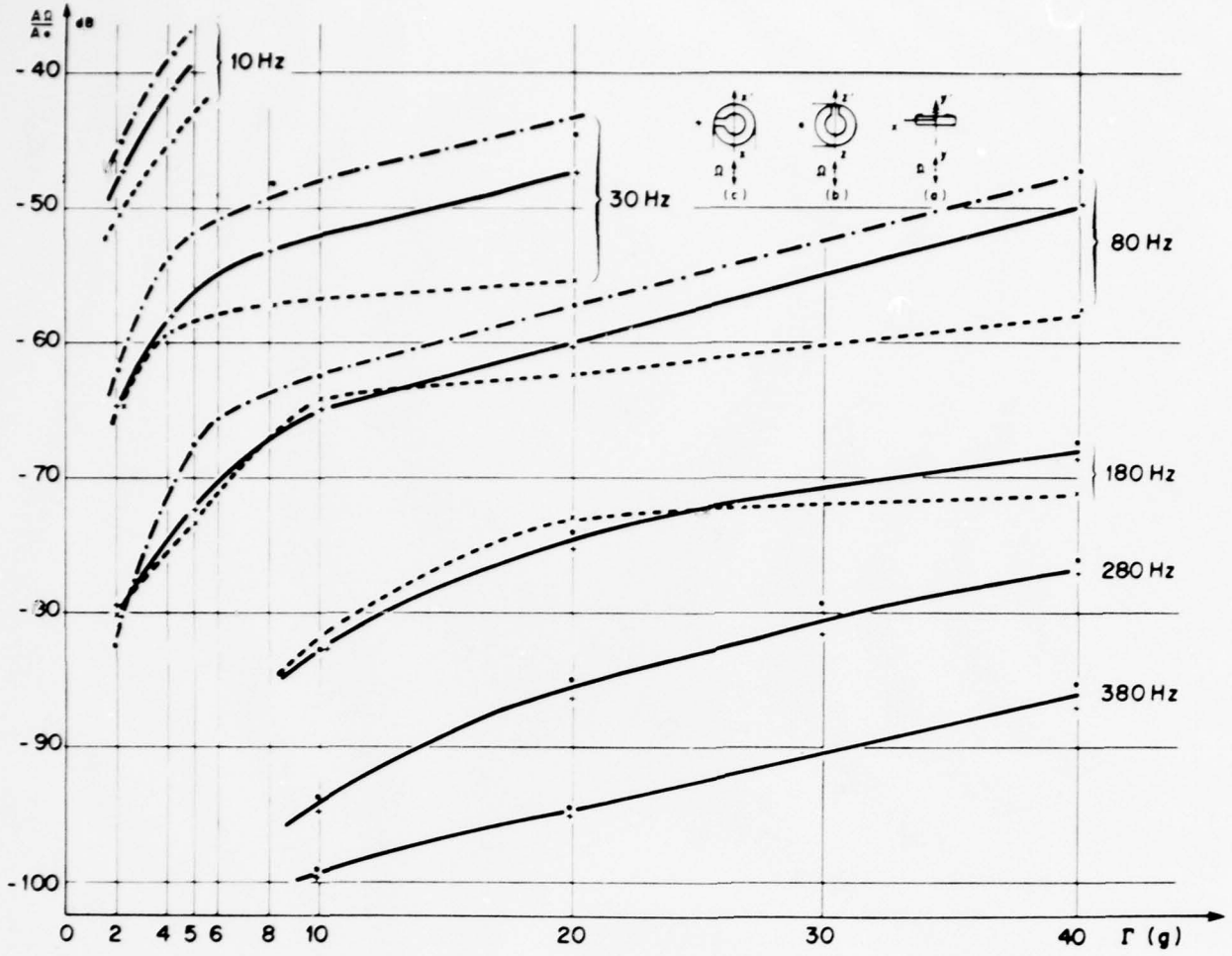

Fig 27 Effect of a vibration of frequency $\Omega/2\pi$ on the resonator in terms of the acceleration of the vibration

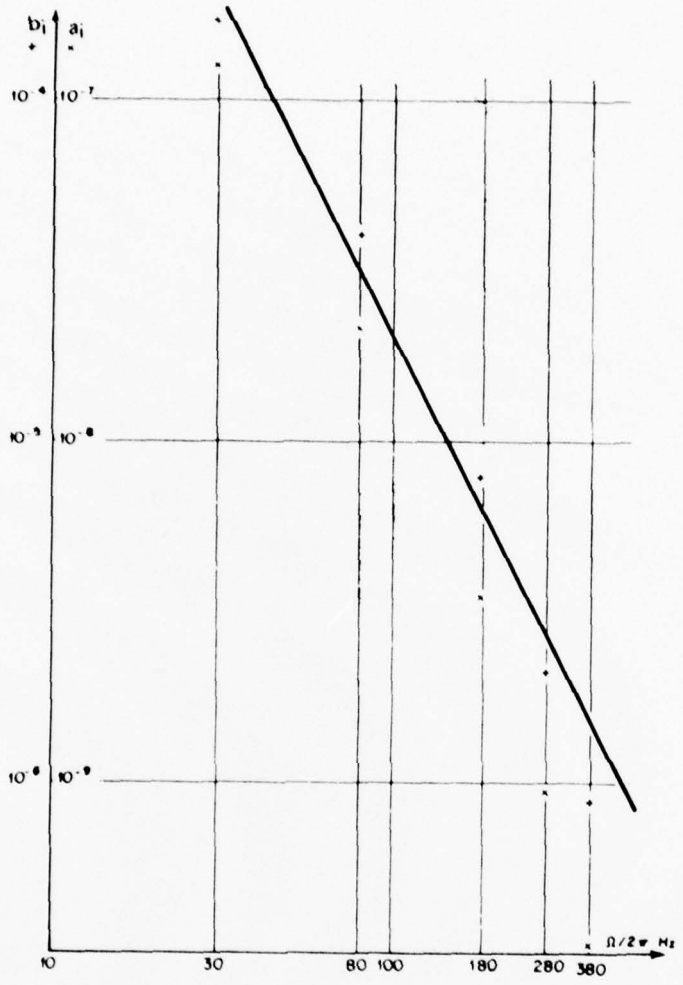

Fig 28 Coefficients a_i and b_i as functions of Ω

a

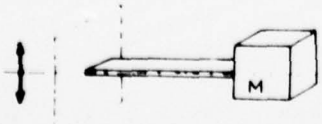

b

Fig 29 Transverse vibrations of the supports

Figs 30&31

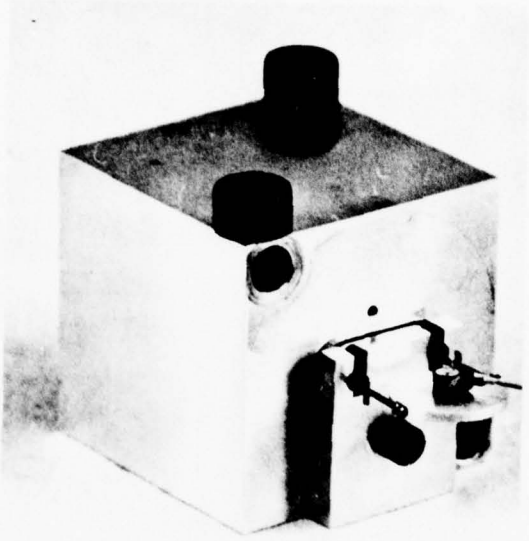

Fig 30 Mounting analogous to that of the resonator

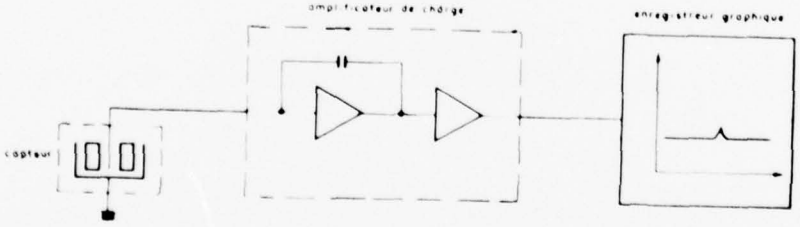

Key:

amplificateur de charge	= load amplifier
enregistreur graphique	= graph-plotter

Fig 31 Apparatus for measuring the vibrations

LT 1897

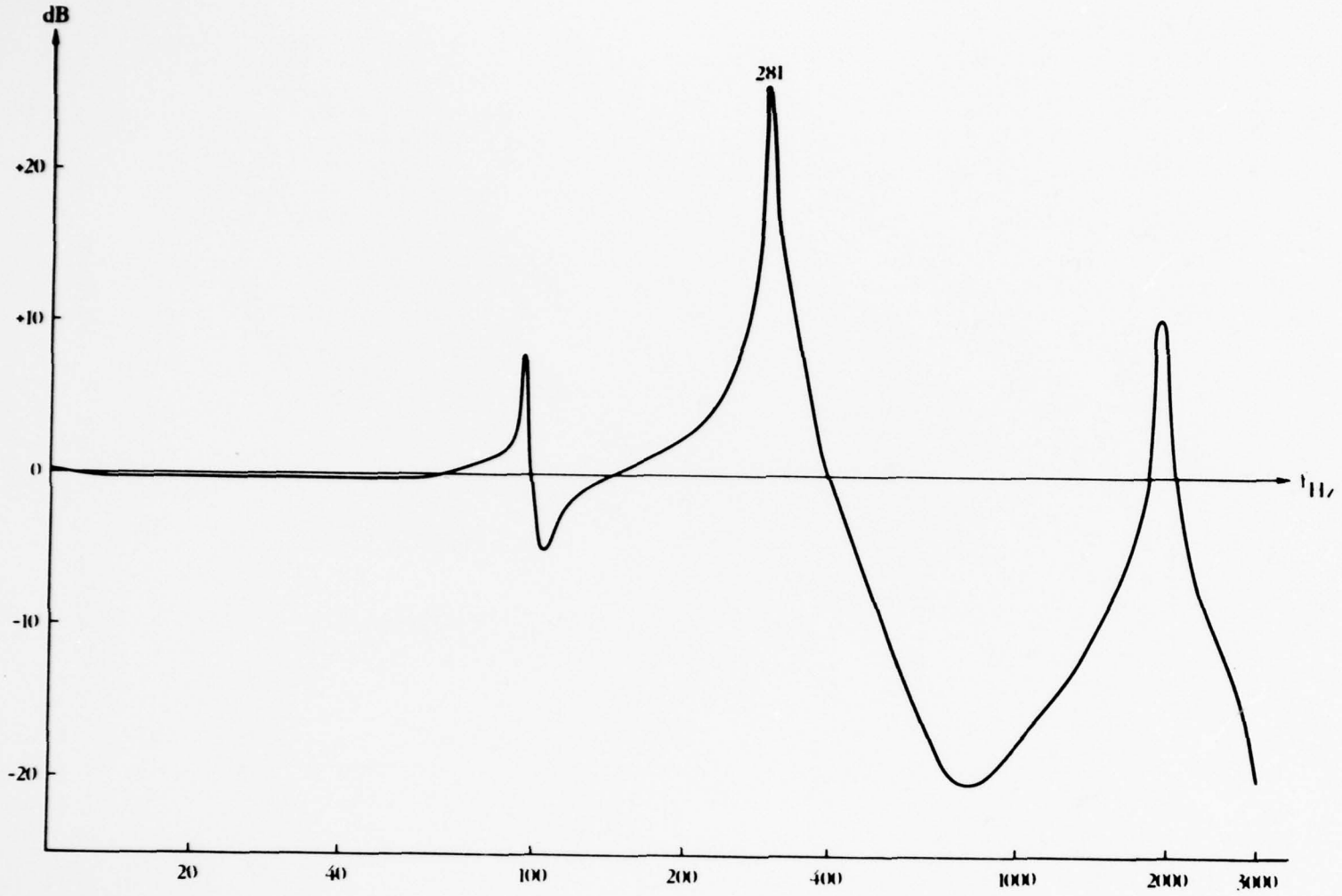

Fig 32 Response curve for the support-quartz crystal assembly to a sinusoidal excitation

Fig 32

Figs 33-35

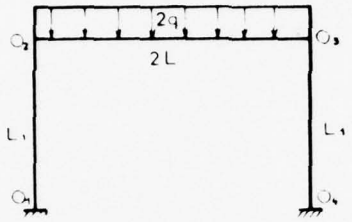

Fig 33 Symmetrical vibrations of an arched structure

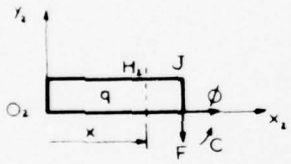

a

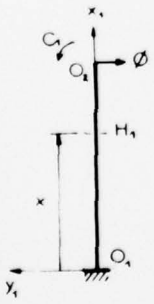

b

Fig 34 Analysis of the forces applied to the arched structure

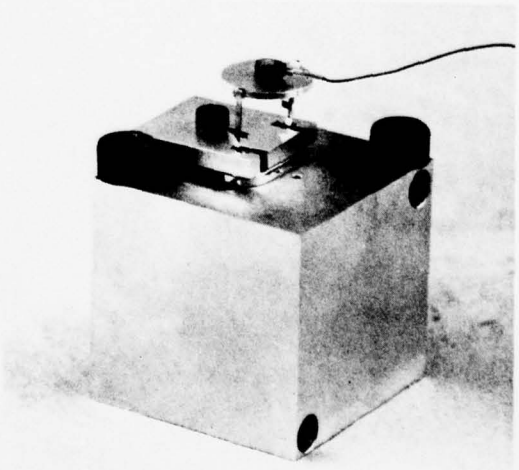

Fig 35 Mounting analogous to that of the resonator

LT 1897

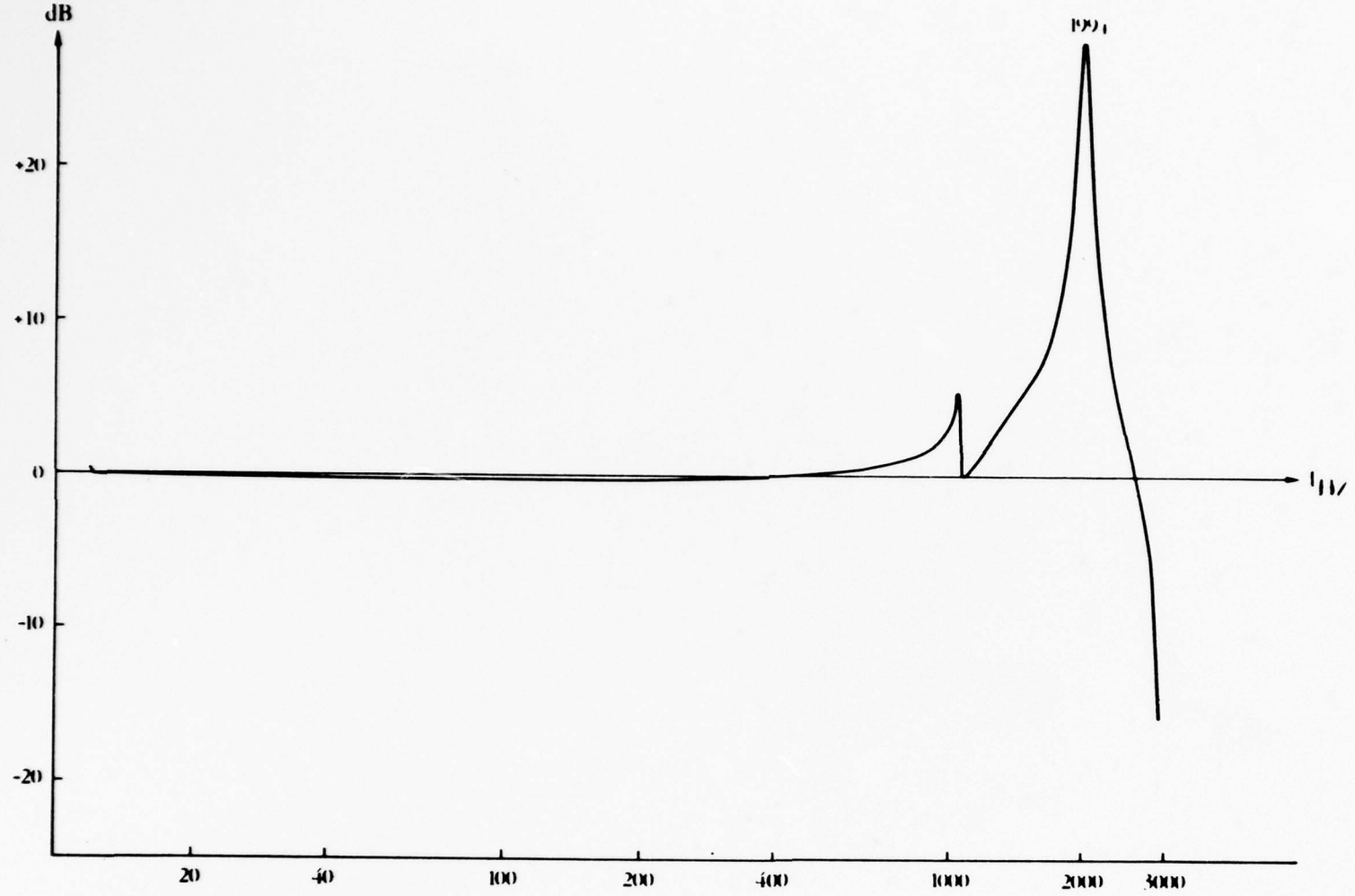

Fig 36 Response curve

Fig 36

Figs 37&38

Fig 37 Quartz crystal with 4 supports

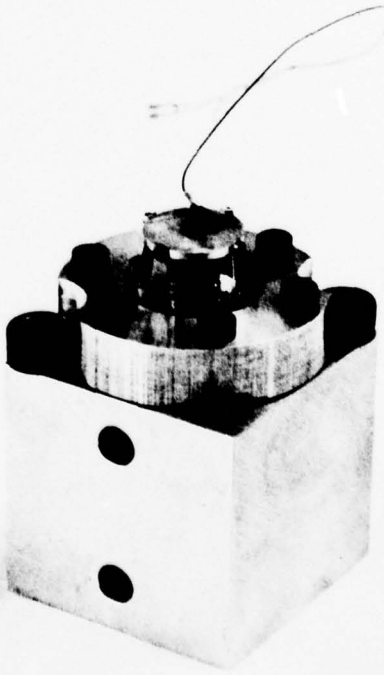

Fig 38 Mounting analogous to that of the resonator with 4 supports

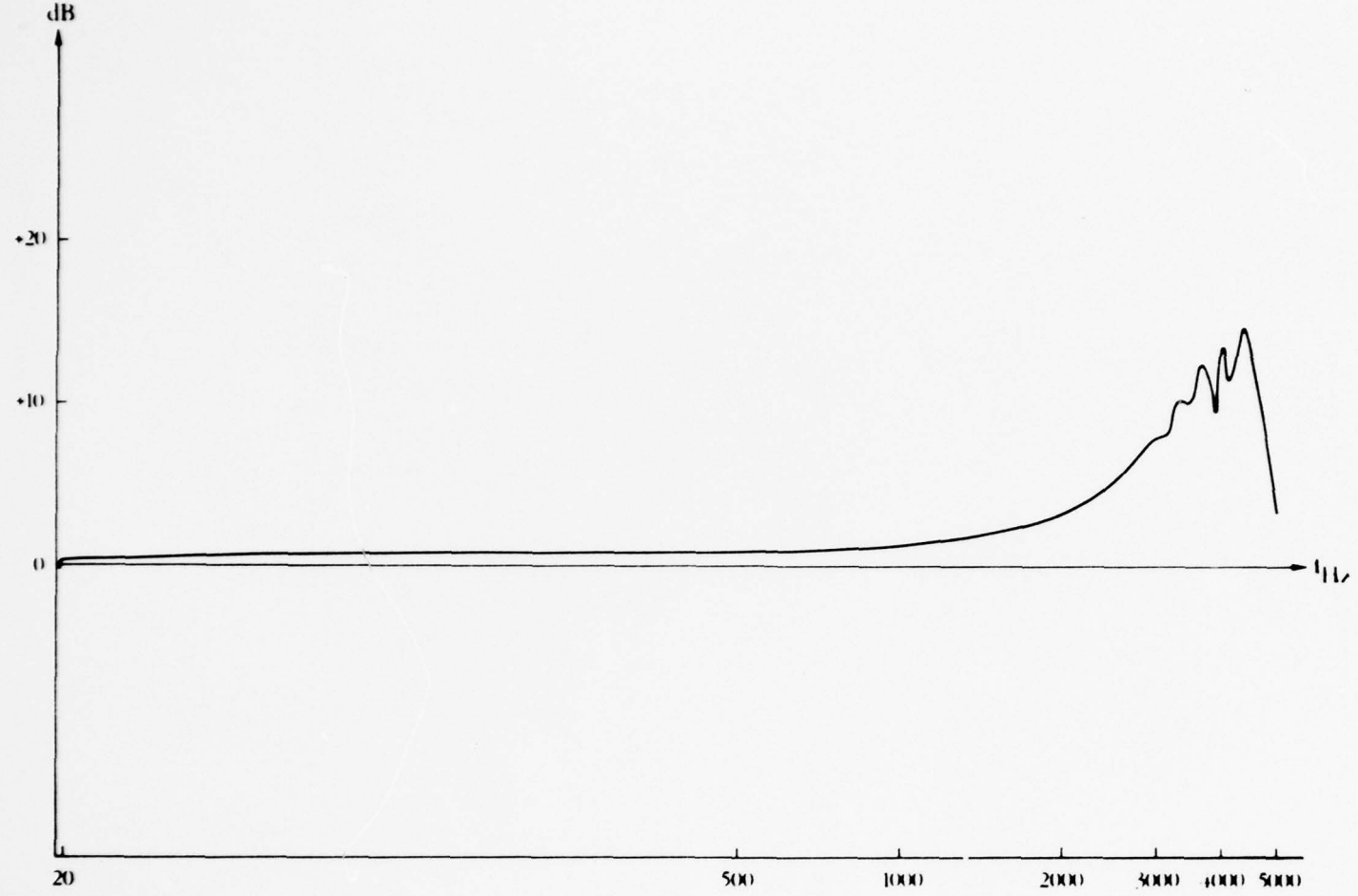

Fig 39 Response curve

Fig 39

Fig 40

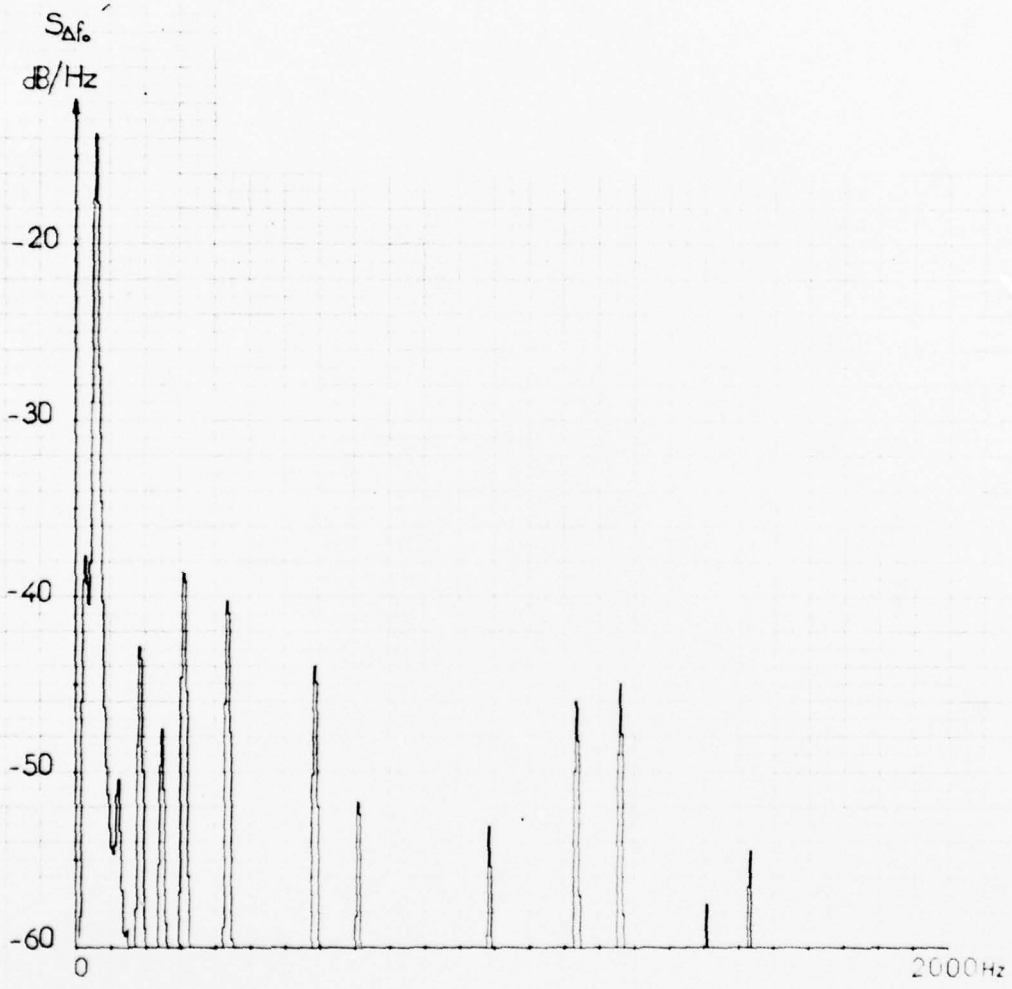

Fig 40 $S_{\Delta f_0}$ for an undisturbed quartz crystal

LT 1897

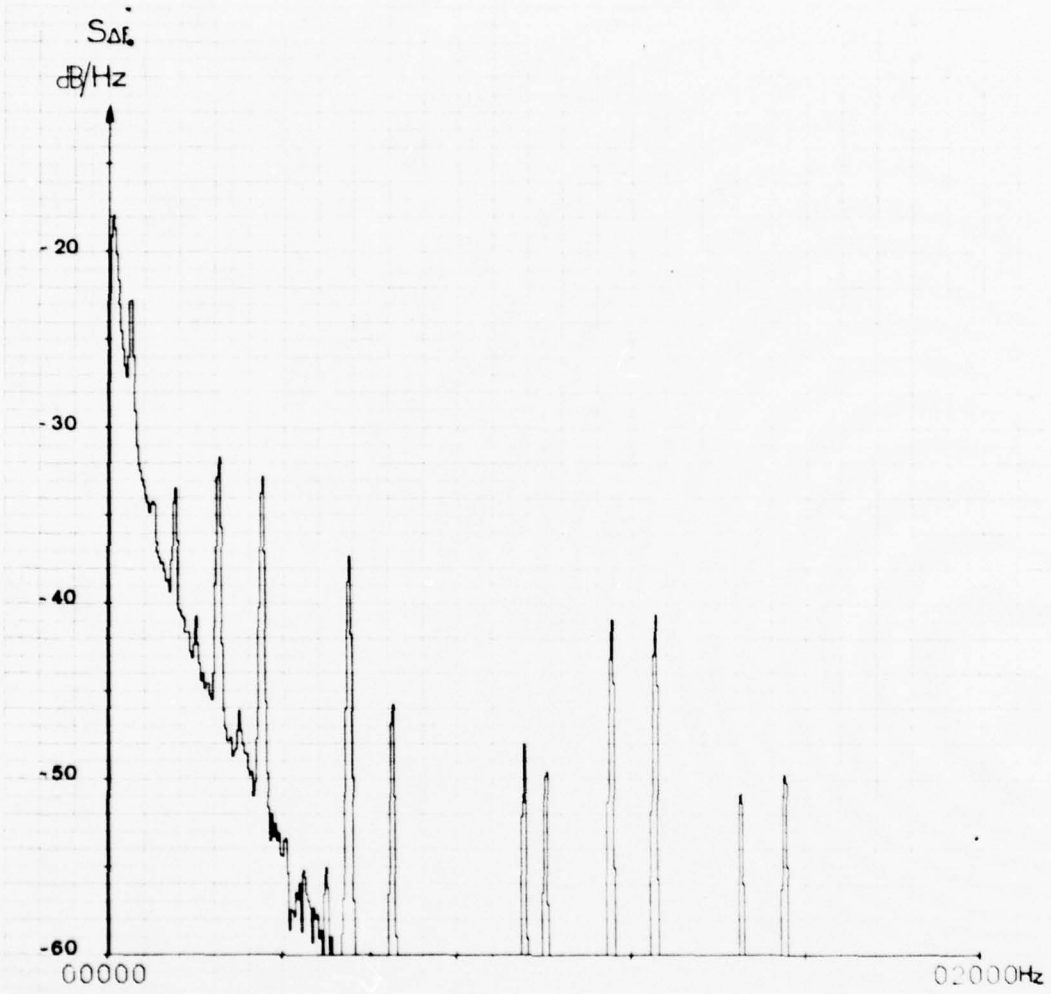

Fig 41 $S_{\Delta f_0}$ for a quartz crystal in the vertical position subjected to white noise of 2.10^{-1} g^2/Hz within the range 20-2000 Hz

Fig 42

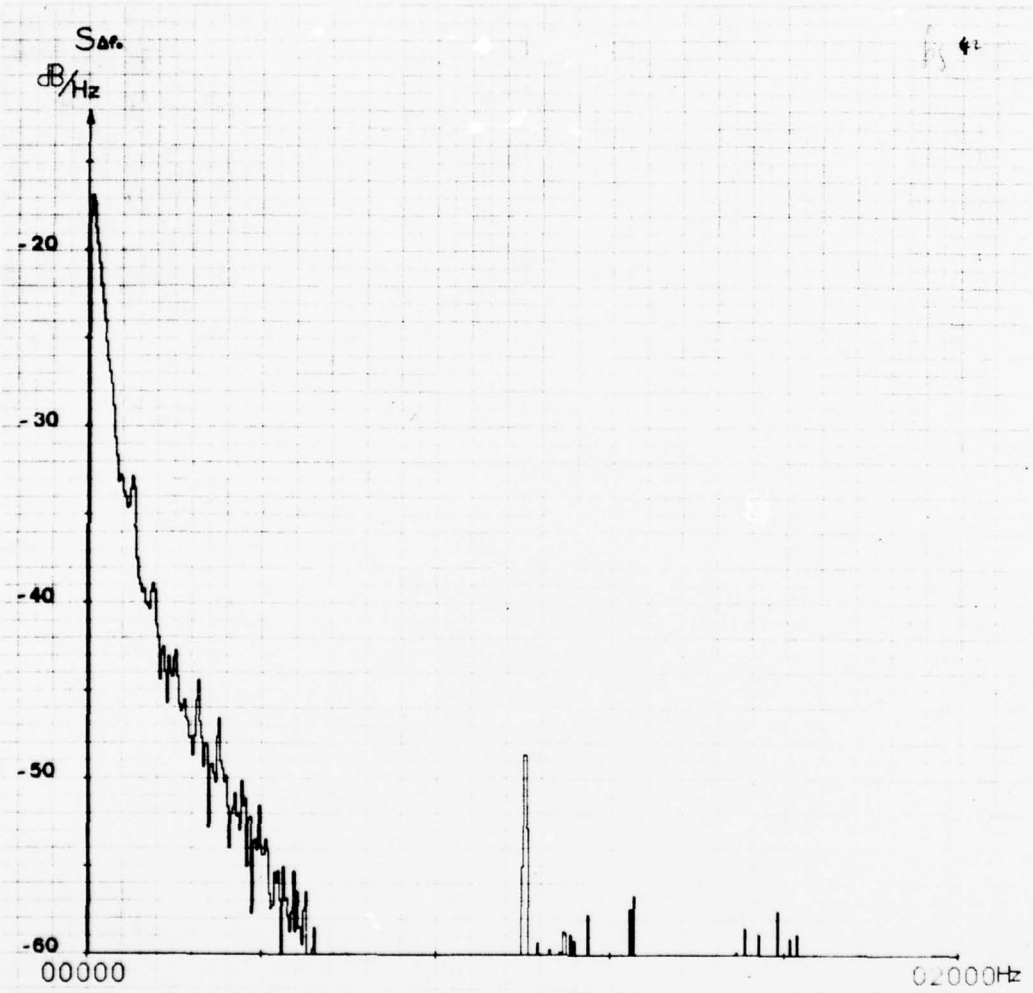

Fig 42 $S_{\Delta f_0}$ for a quartz crystal in the horizontal position subjected to white noise of 4.5×10^{-1} g^2/Hz within the range 20-2000 Hz

LT 1897

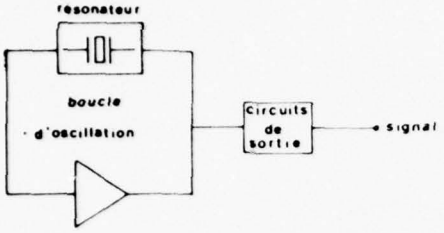

Key:

Résonateur	= resonator
Boucle d'oscillation	= oscillation loop
amplificateur	= amplifier
circuits de sortie	= output circuits

Fig 43 Schematic diagram of oscillator

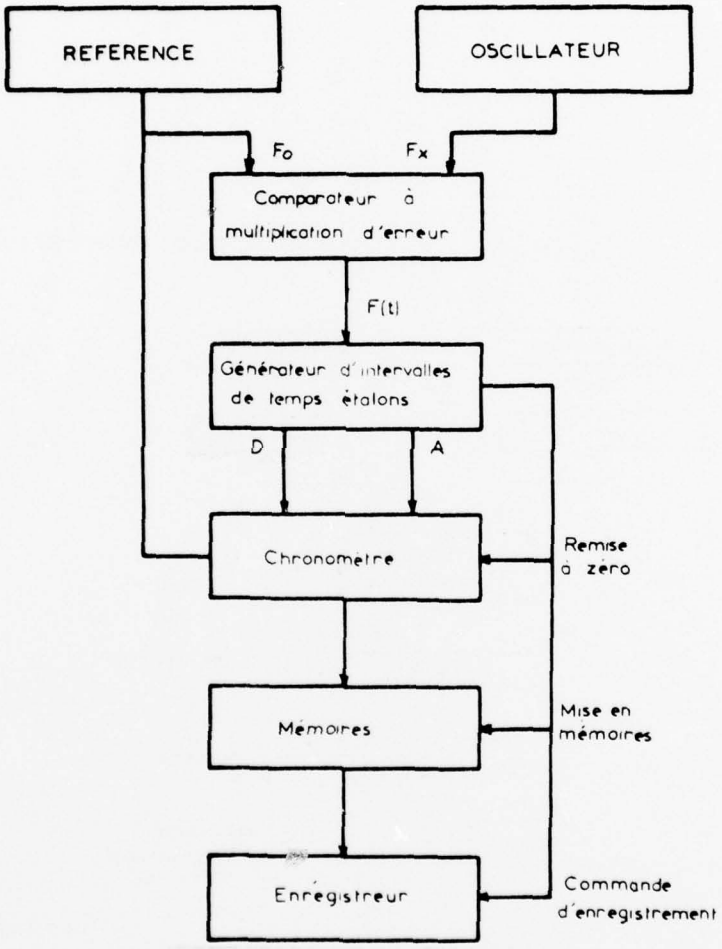

Key:

Référence	= reference
Oscillateur	= oscillator
Comparateur a multiplication d'erreur	= comparator with error multiplication
Générateur d'intervalles de temps étalons	= generator of standard time intervals
Chronomètre	= chronometer
Mémoires	= memory
Enrégistreur	= recorder
Remise à zéro	= re-set to zero
Mise en mémoires	= store in memory
Commande d'enrégistrement	= recorder control

Fig 44 Apparatus for measuring $I(\tau)$

Figs 45&46

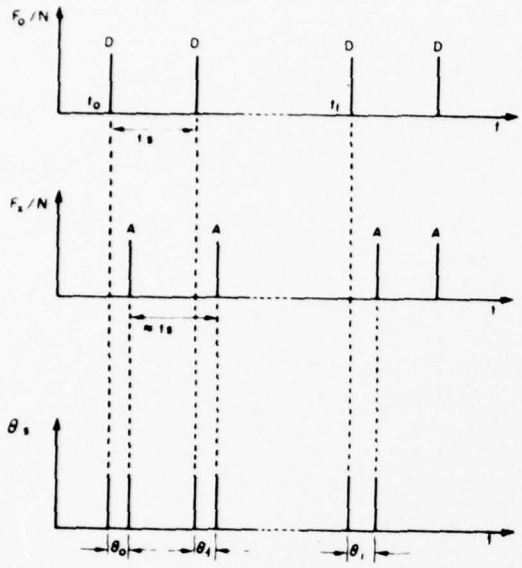

Fig 45 Measurement principle

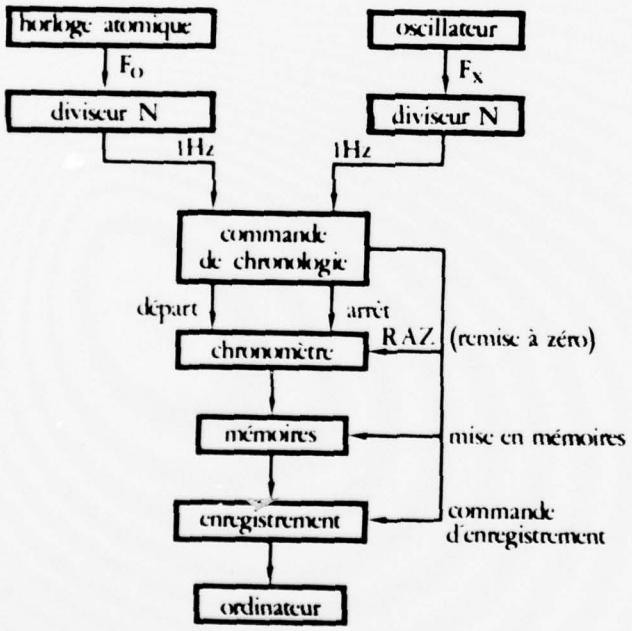

Key:

horloge atomique	= atomic clock
diviseur N	= divider N
oscillateur	= oscillator
commande de chronologie	= chronology control
départ	= start
arrêt	= stop
chronomètre	= chronometer
mémoires	= memories
enregistrement	= recording
ordinateur	= computer
remise à zéro	= re-set to zero
mise en mémoires	= store in memory
commande d'enrégistrement	= recorder control

Fig 46 Block diagram of system for drift measurement

LT 1897

AD-A078 733 ROYAL AIRCRAFT ESTABLISHMENT FARNBOROUGH (ENGLAND) F/G 9/1
INFLUENCE OF THE ENVIRONMENTAL CONDITIONS ON A QUARTZ RESONATOR--ETC(U)
MAY 78 M VALDOIS
UNCLASSIFIED RAE-LIBRARY TRANS-1897 DRIC-BR-70941 NL

2 OF 2
AD A078733

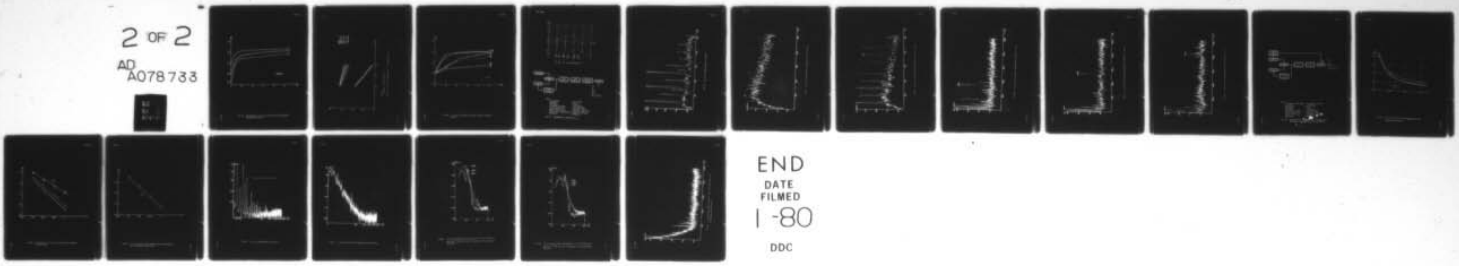

END
DATE FILMED
1-80
DDC

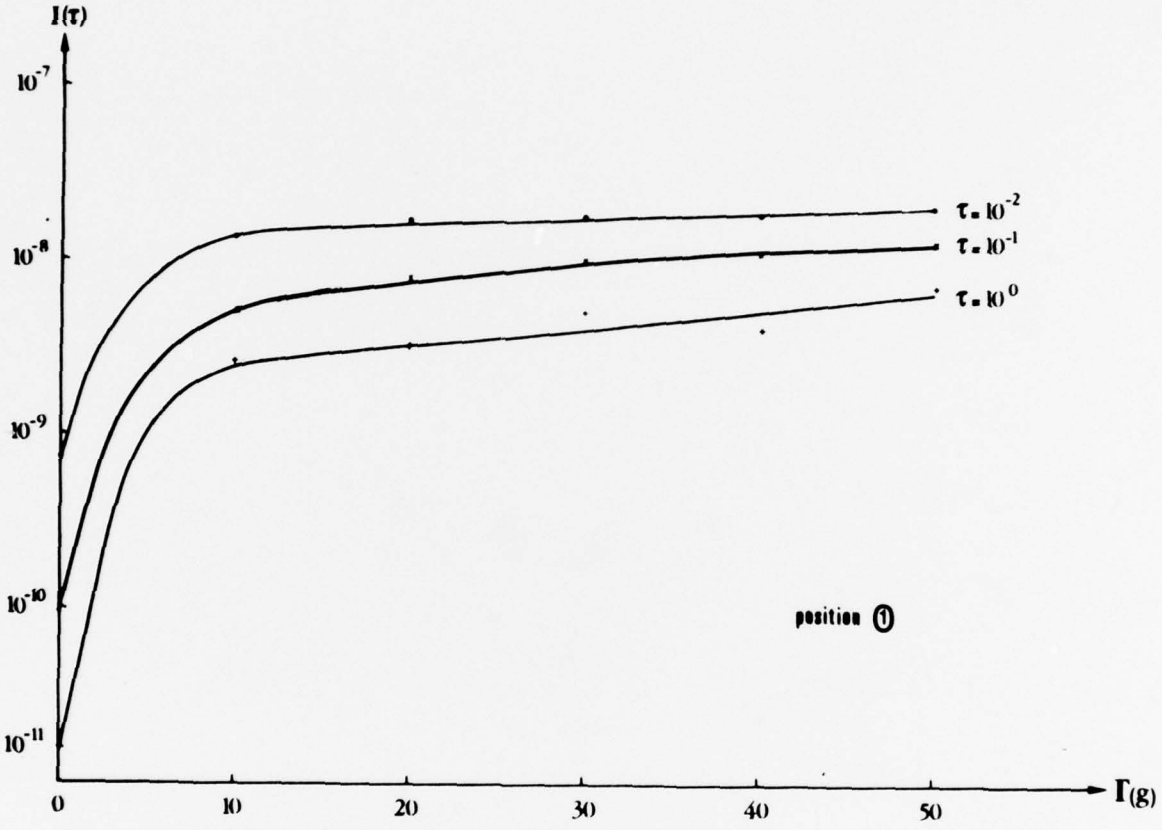

Fig 47 Variations of $I(\tau)$ as a function of the applied acceleration and of τ

LT 1897

Fig 48

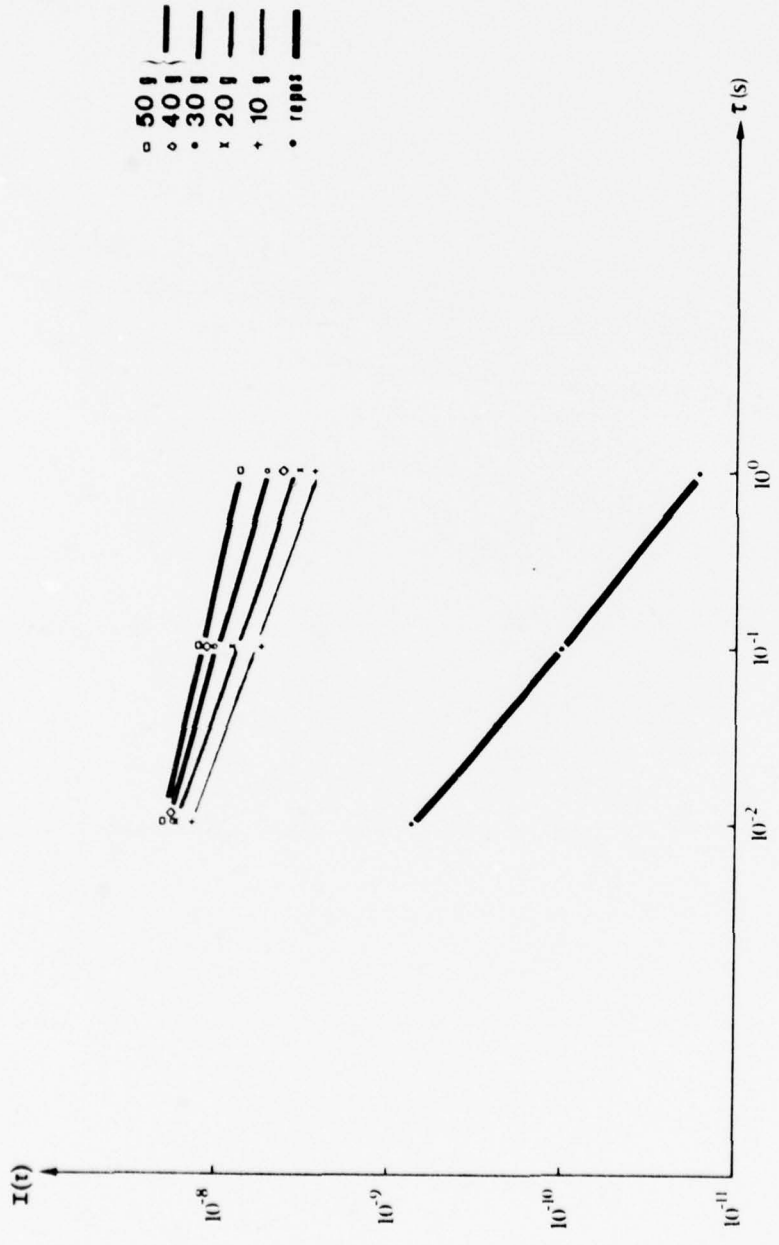

Key:
Repos = rest position

Fig 48 $I(\tau)$ as a function of τ for positon (1)

LT 1897

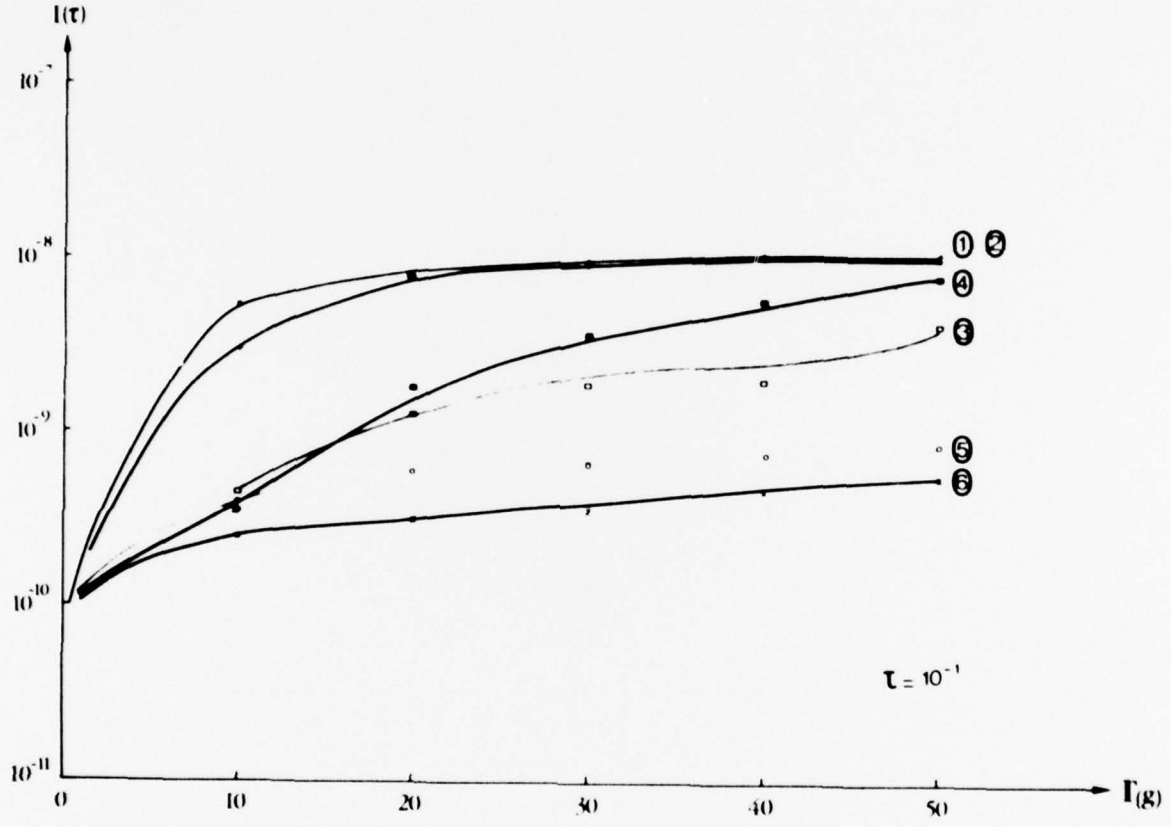

Fig 49 $I(\tau)$ as a function of quartz crystal position and of Γ

Figs 50&51

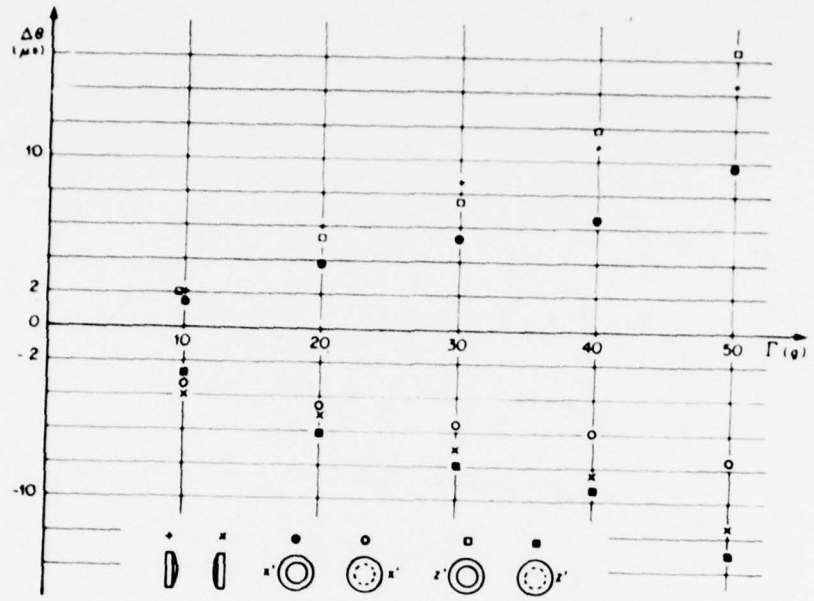

Fig 50 $\Delta\theta$ as a function of Γ

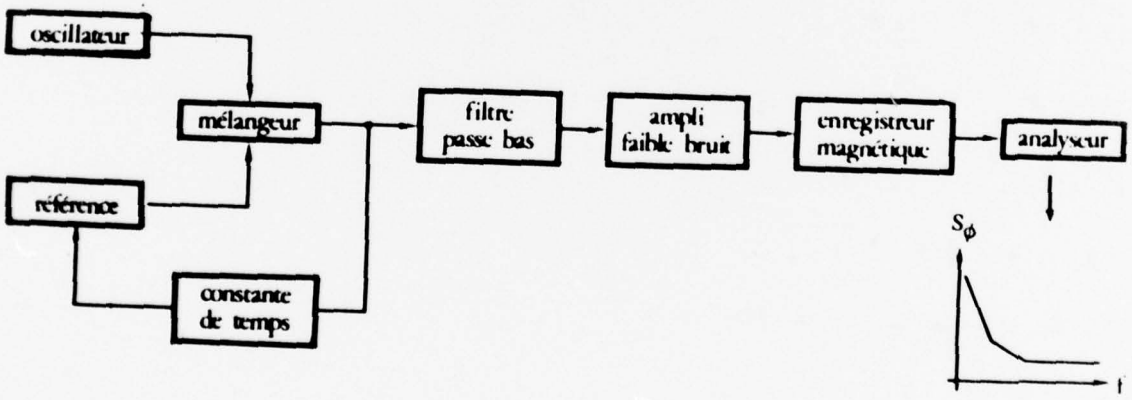

Key:

oscillateur	= oscillator
mélangeur	= mixer
référence	= reference
constante de temps	= time constant
filtre passe bas	= low-pass filter
ampli faible bruit	= low-noise amplifier
enrégistreur magnétique	= magnetic recorder
analyseur	= analyser

Fig 51 Equipment for measuring S_ϕ

LT 1897

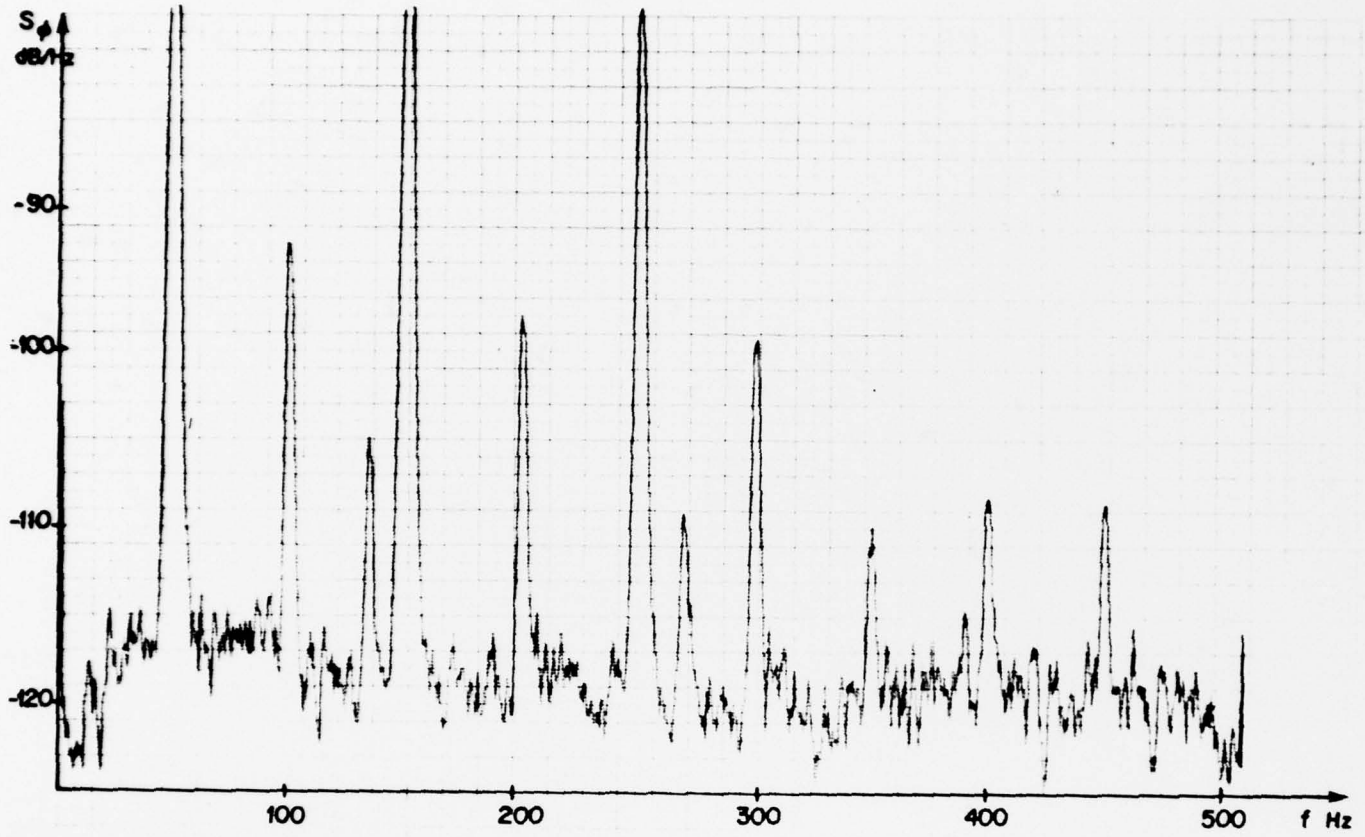

Fig 52 S_ϕ for an undisturbed oscillator

Fig 52

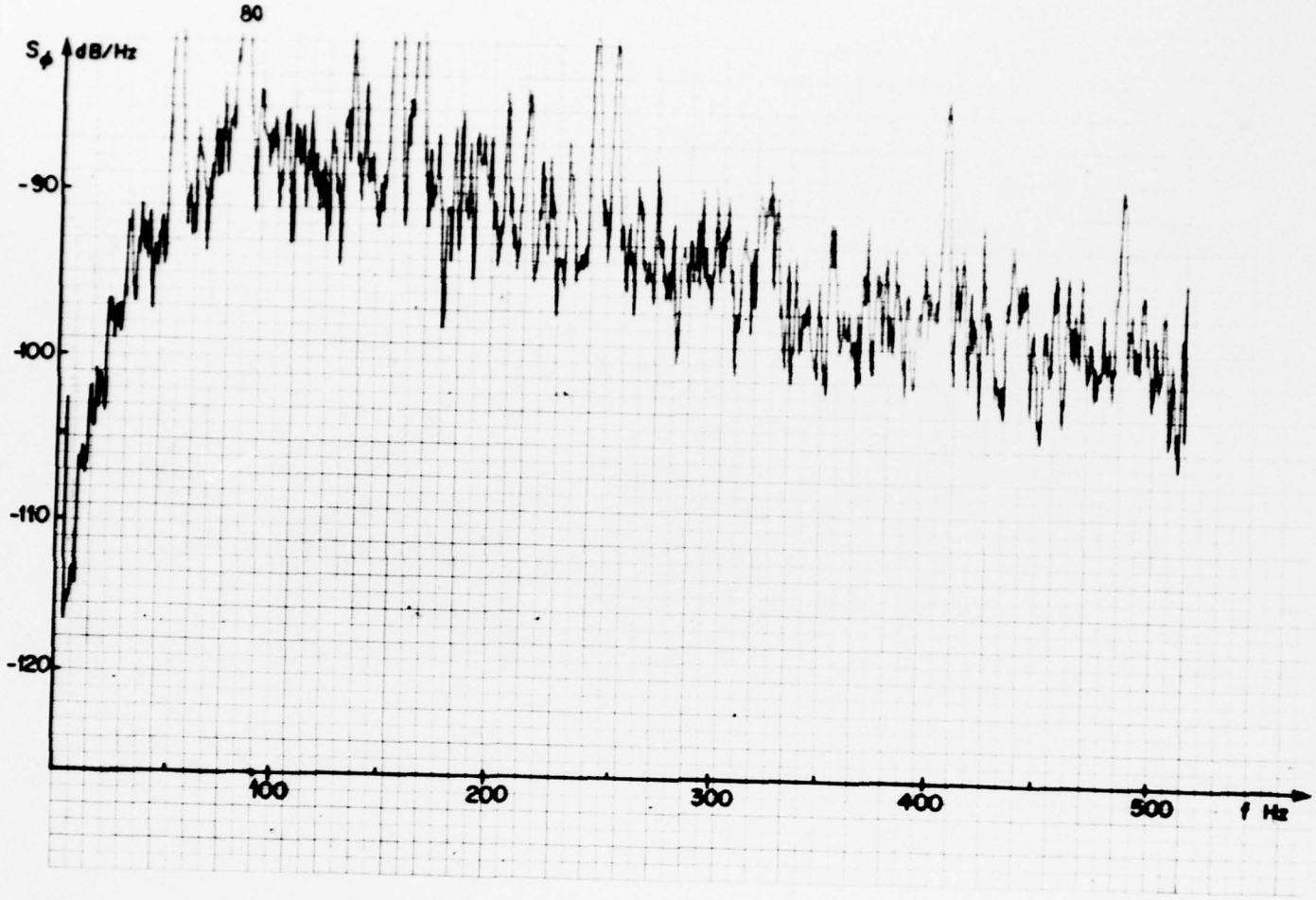

Fig 53 S_ϕ for an oscillator subjected to 80 Hz -10 g

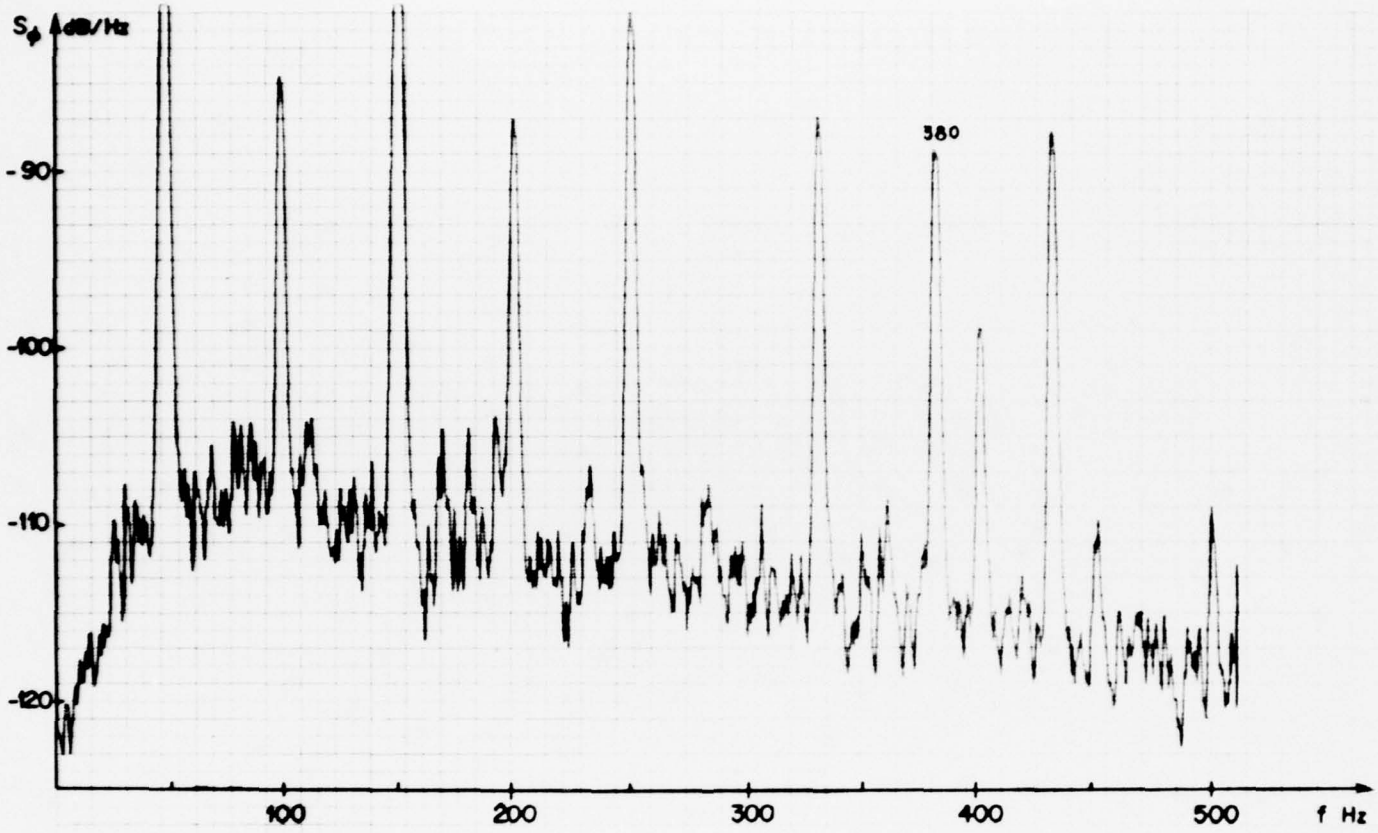

Fig 54 S_ϕ for an oscillator subjected to 380 Hz - 20 g

Fig 54

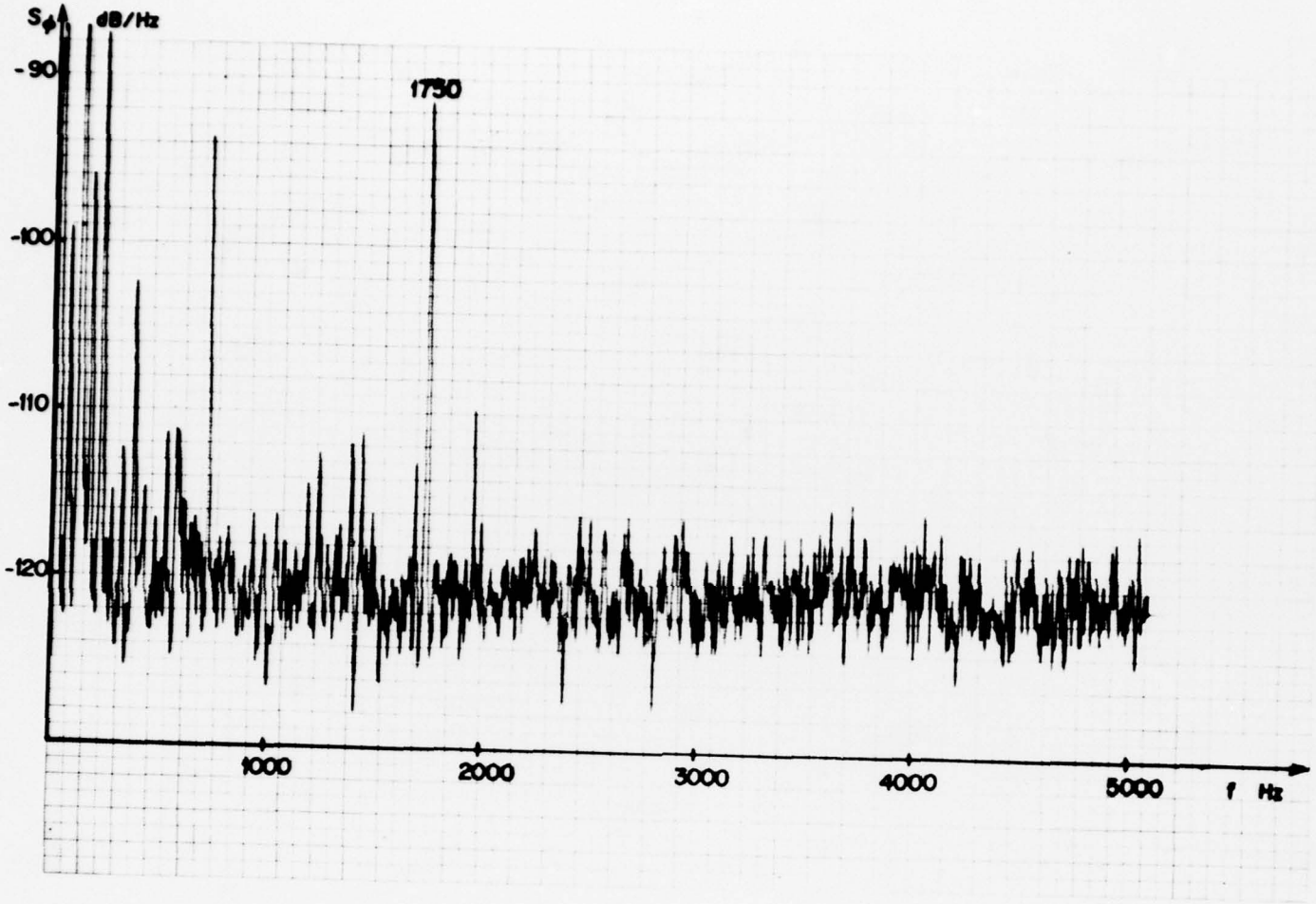

Fig 55 S_ϕ for an oscillator subjected to 1750 Hz - 20 g

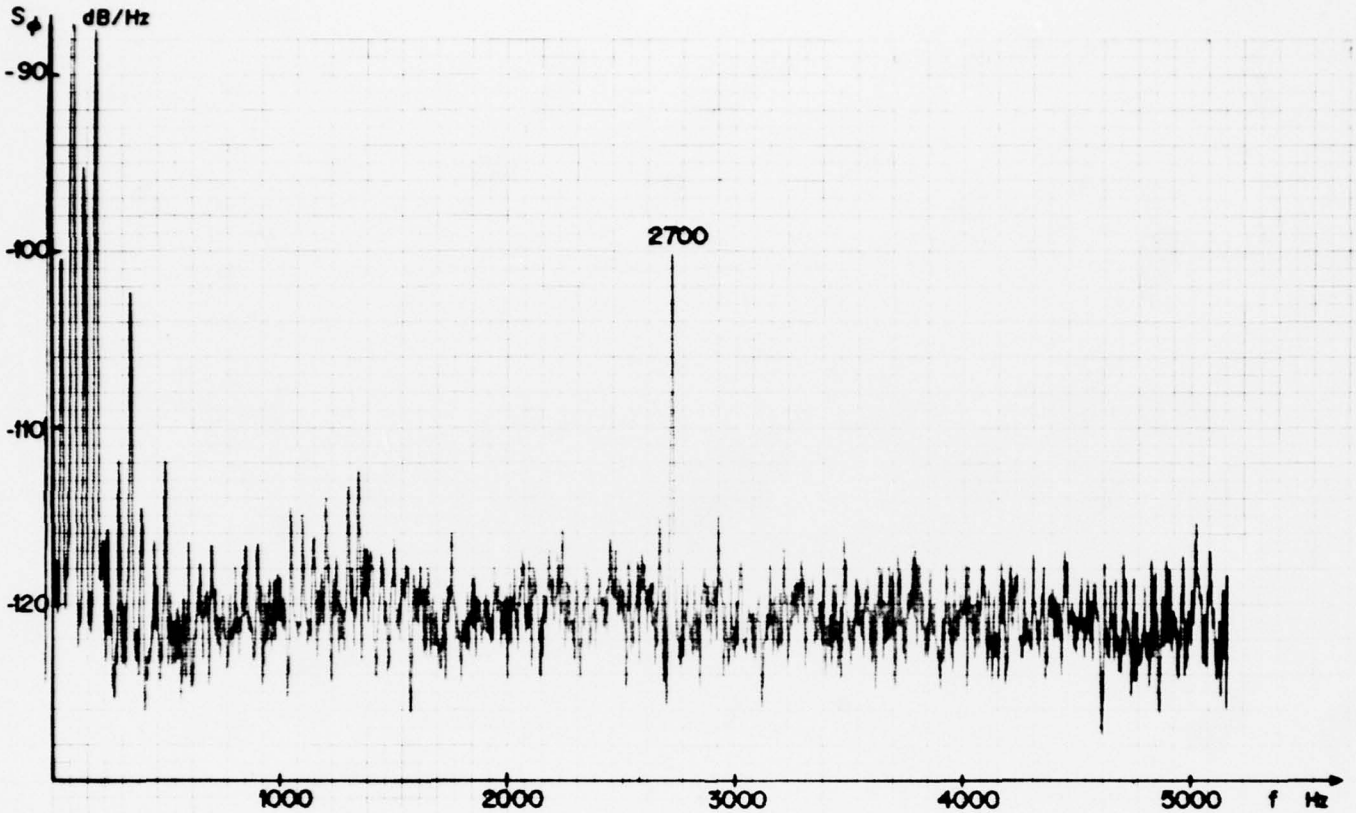

Fig 56 S_ϕ for an oscillator subjected to 2700 Hz - 20 g

Fig 56

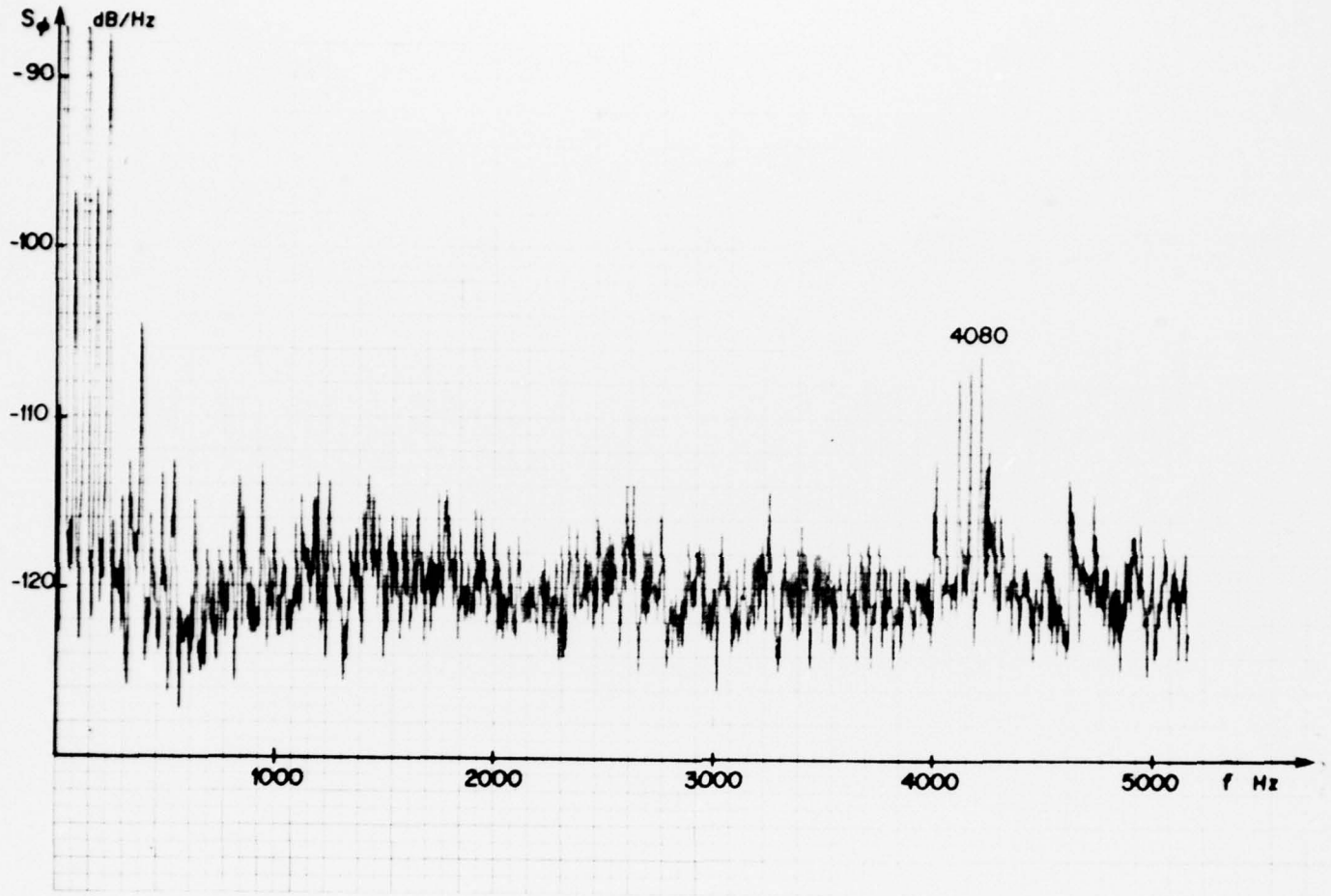

Fig 57 S_ϕ for an oscillator subjected to 4080 Hz - 20 g

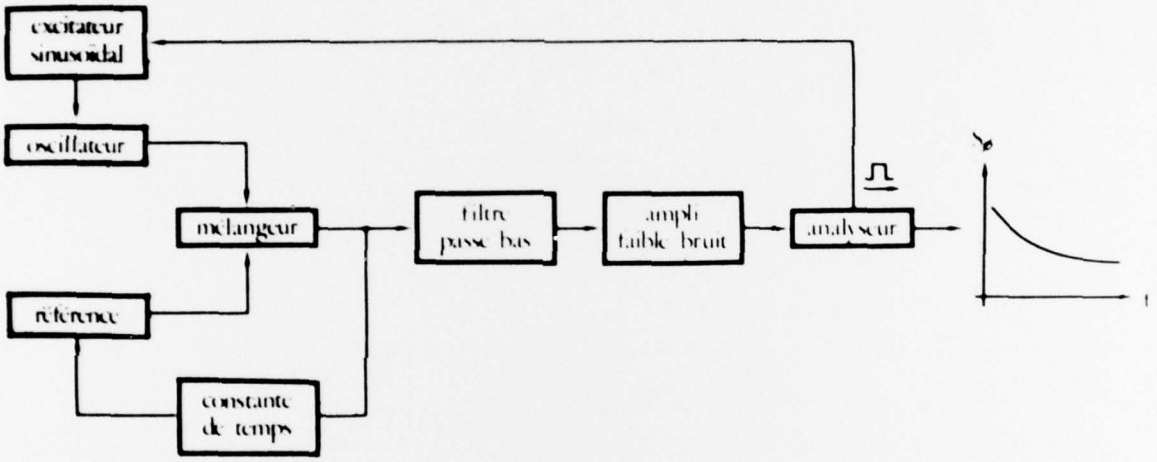

Key:

excitateur sinusoidal	= sinusoidal exciter
oscillateur	= oscillator
mélangeur	= mixer
référence	= reference
constante de temps	= time constant
filtre passe bas	= low-pass filter
ampli faible bruit	= low-noise amplifier
analyseur	= analyser

Fig 58 Equipment for measuring the influence of a sinusoidal disturbance on the oscillator

Fig 59

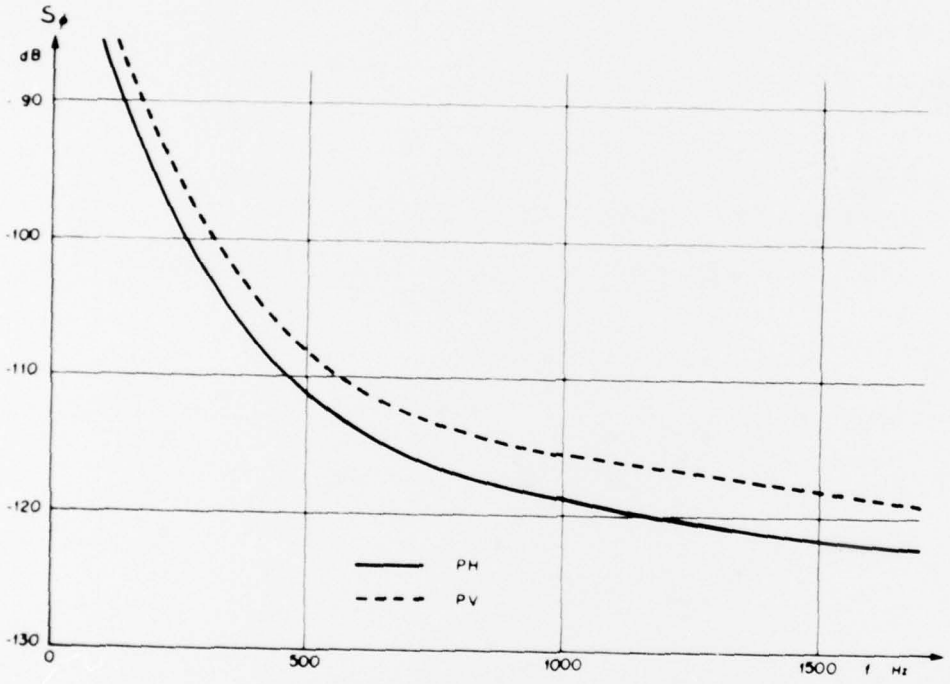

Fig 59 S_ϕ as a function of the frequency of the sinusoidal vibration

LT 1897

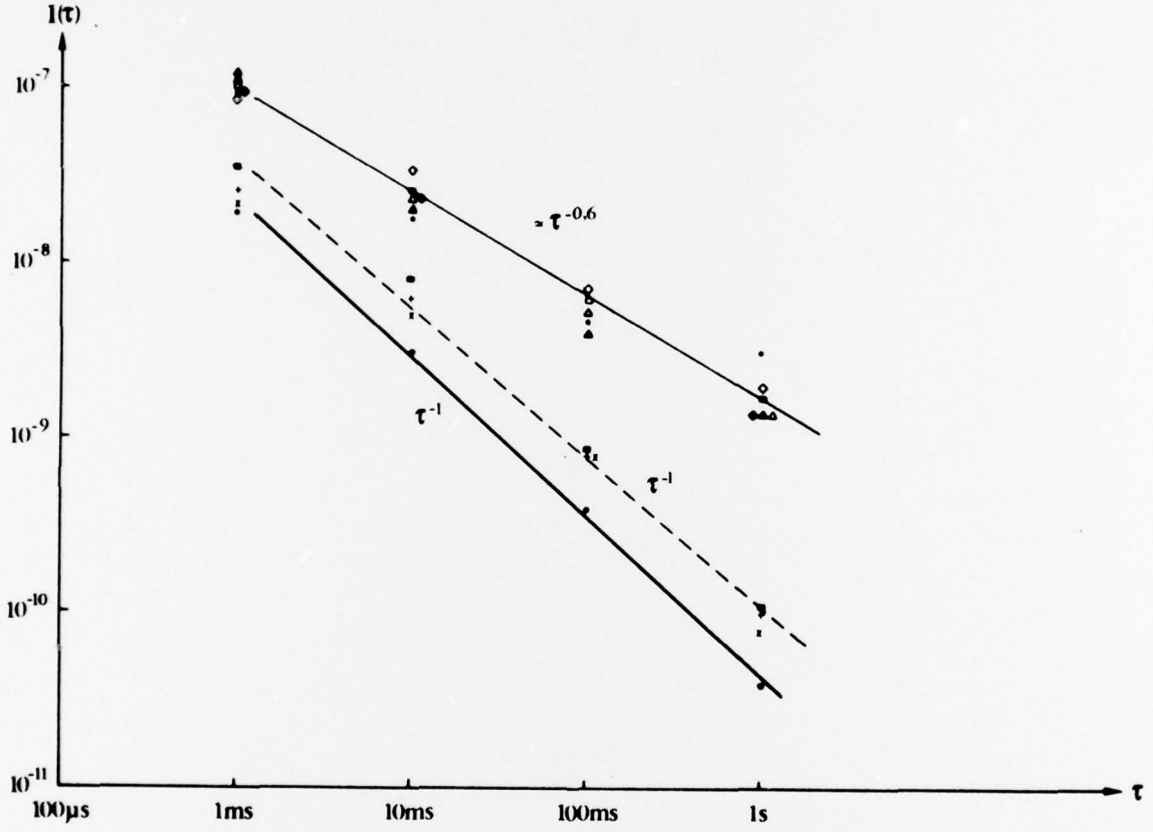

Fig 60 Variations of $I(\tau)$ for an oscillator subjected to white noise

Fig 61

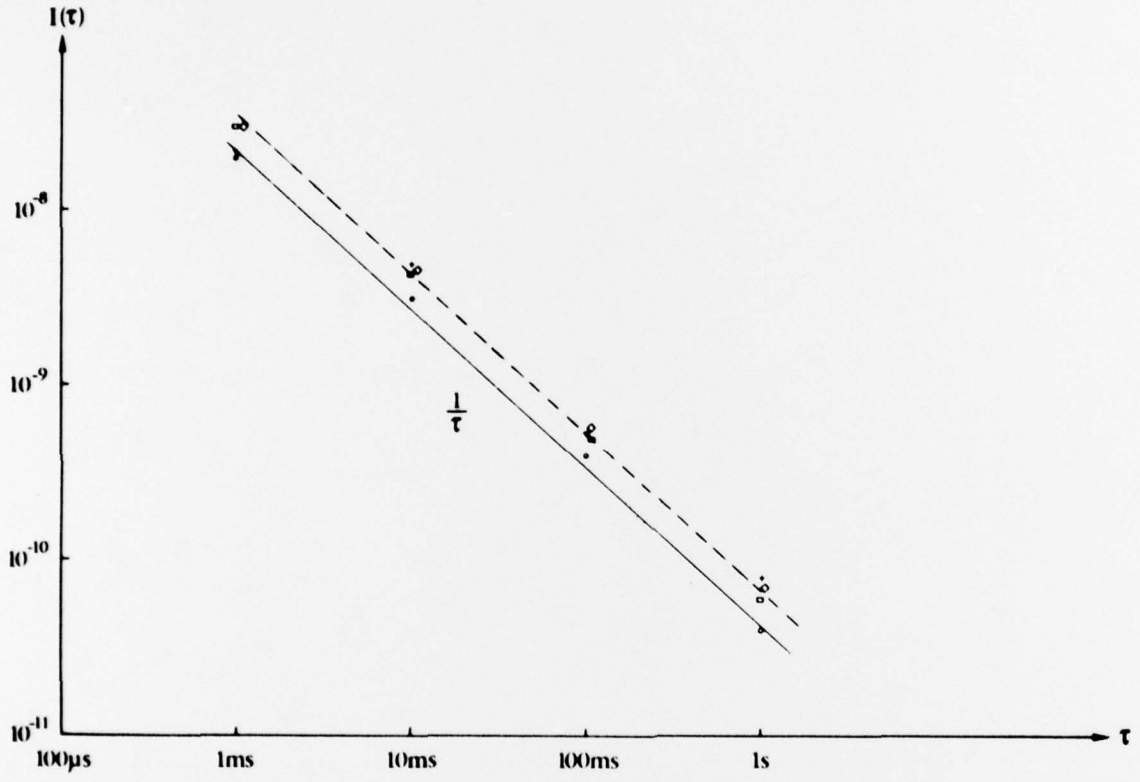

Fig 61 $I(\tau)$ for an oscillator where only the electronics are disturbed by white noise

LT 1897

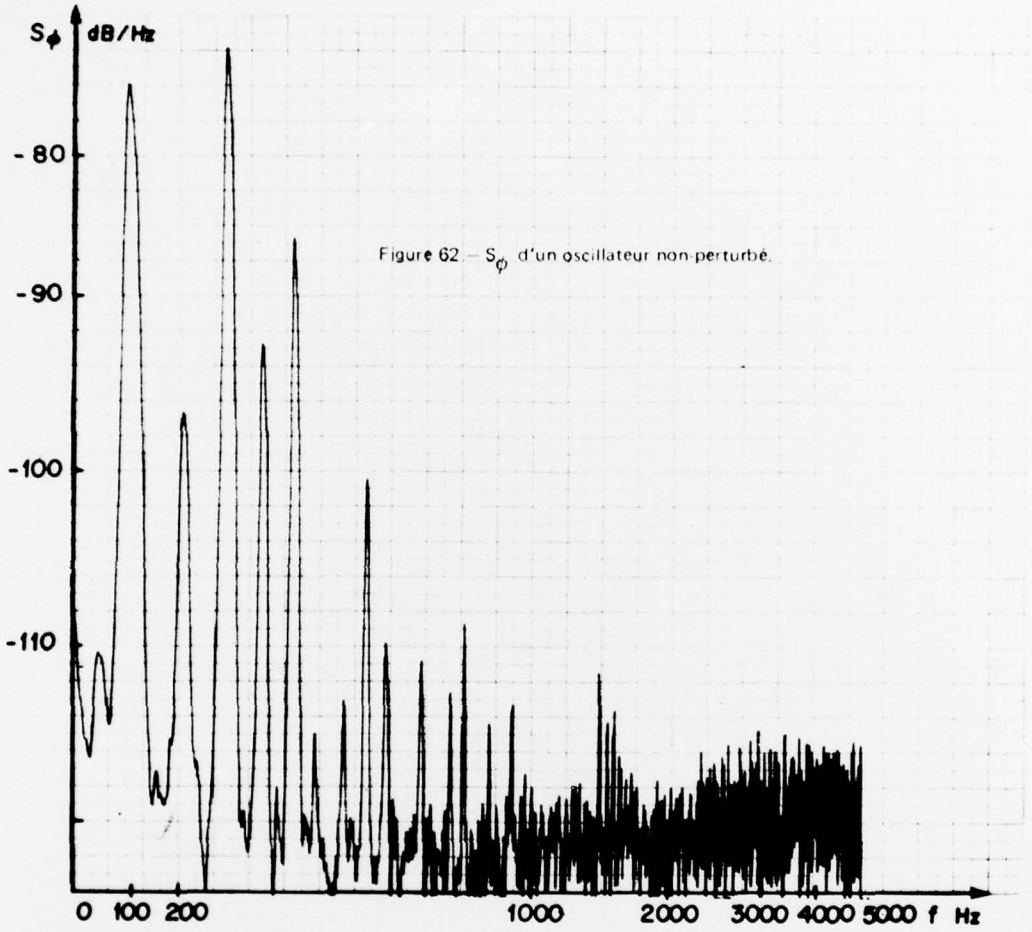

Figure 62 — S_ϕ d'un oscillateur non-perturbé.

Fig 62 S_ϕ for an undisturbed oscillator

Fig 63

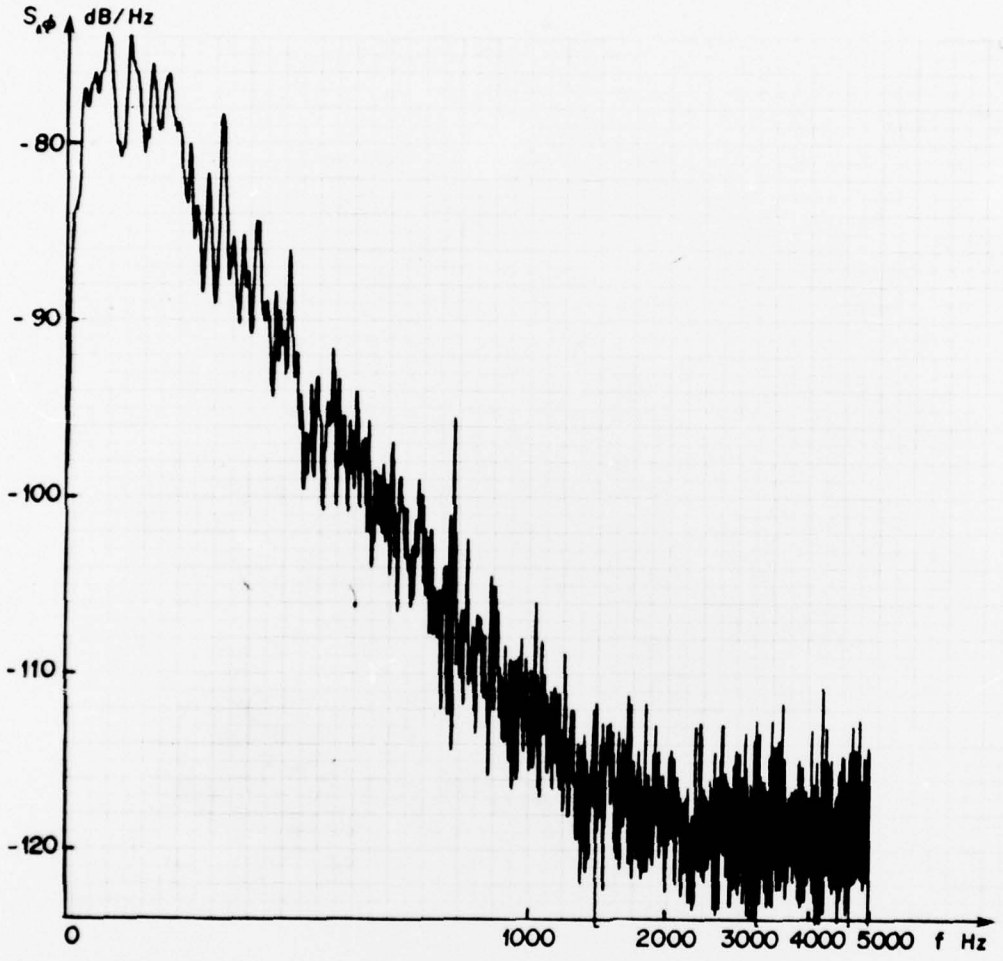

Fig 63 S_{ϕ} for an oscillator subjected to white noise

LT 1897

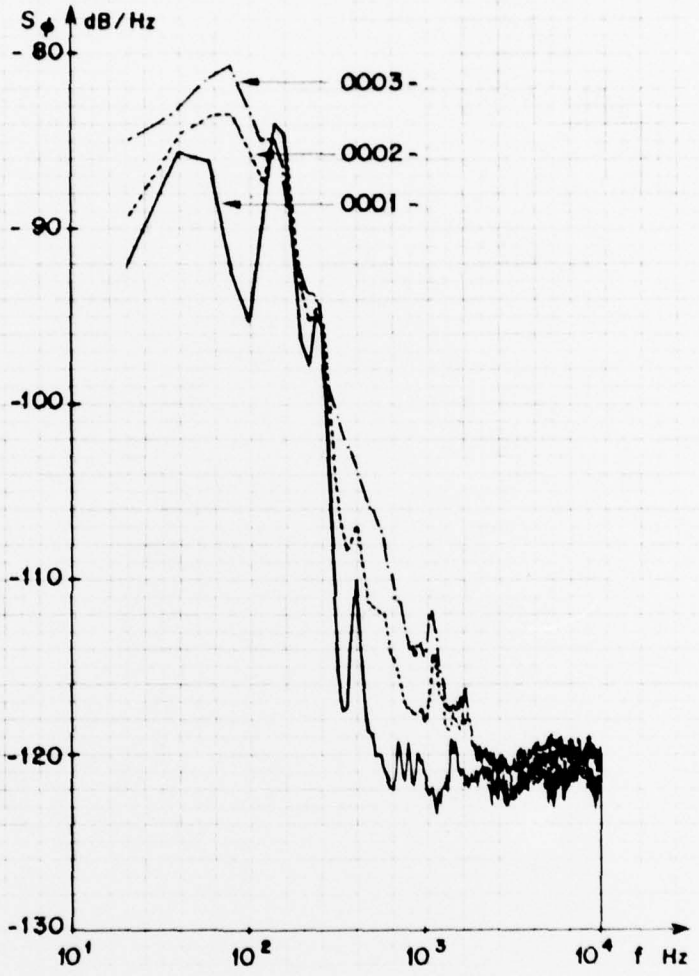

Fig 64 S_ϕ for an oscillator subjected to $1.25\ 10^{-2}\ g^2/Hz$ (2) and $5.10^{-2}\ g^2/Hz$ (3) for a resonator in the vertical position

Fig 65

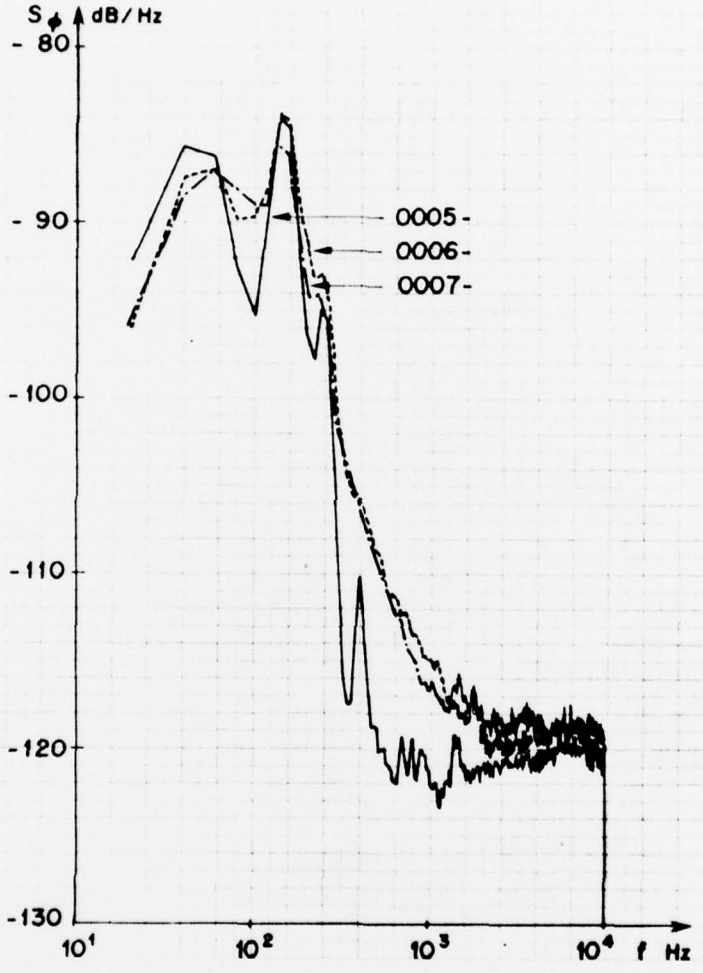

Fig 65 S_ϕ for an oscillator subjected to 1.25 10^{-2} g^2/Hz (6) and 5.10^{-2} g^2/Hz (7) for a resonator in the horizontal position

LT 1897

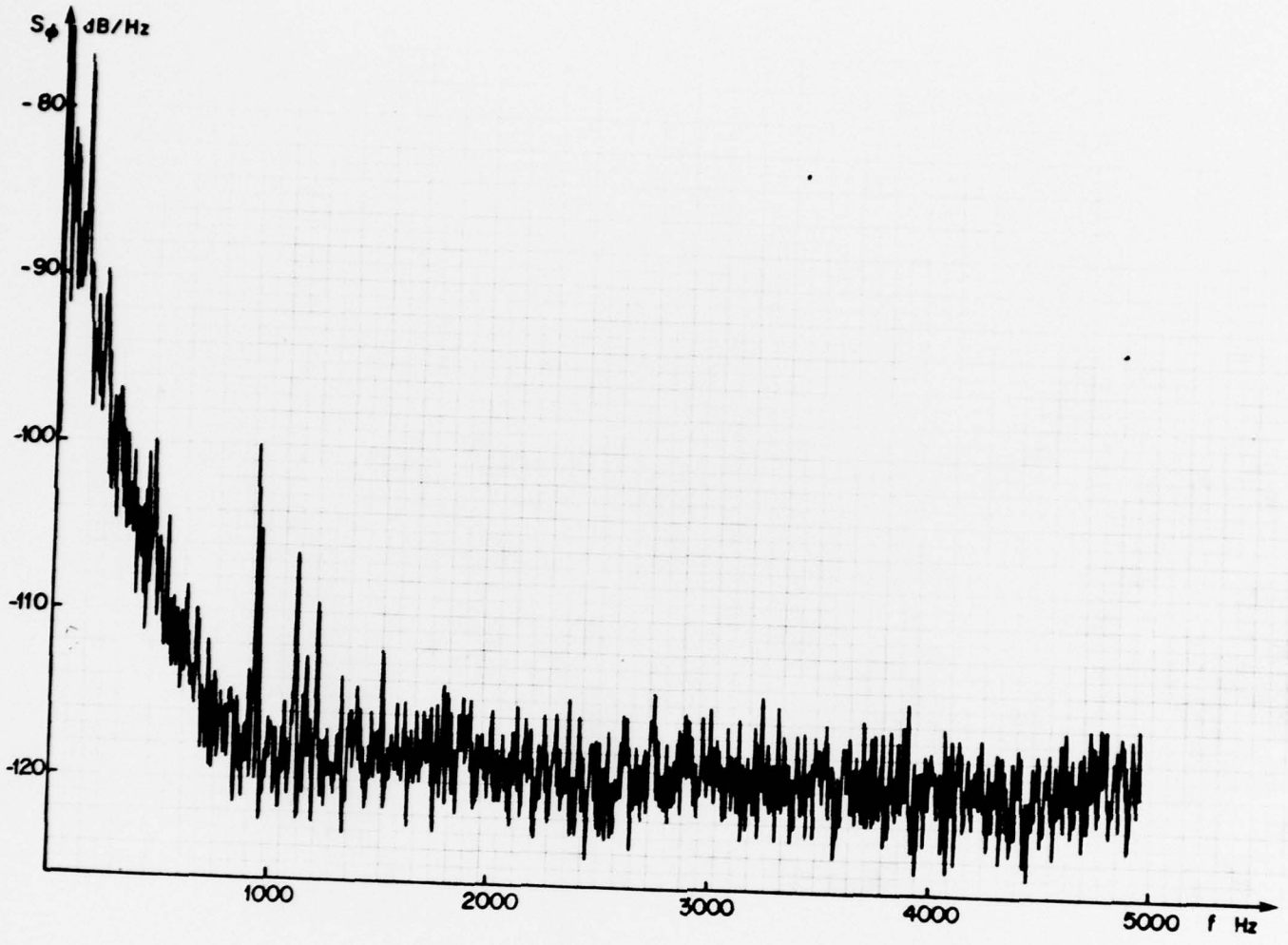

Fig 66 S_ϕ for an oscillator of which only the electronics are disturbed by white noise

Fig 66